UPPSALA
UNIVERSITET

Digital Comprehensive Summaries of Uppsala Dissertations from the Faculty of Science and Technology 205

Resonant Inelastic X-ray Scattering of Rare-Earth and Copper Systems

KRISTINA KVASHNINA

ACTA
UNIVERSITATIS
UPSALIENSIS
UPPSALA
2006

ISSN 1651-6214
ISBN 91-554-6625-7
urn:nbn:se:uu:diva-7094

Dissertation presented at Uppsala University to be publicly examined in Häggsalen, Ångström Laboratory, Uppsala, Friday, September 22, 2006 at 10:15 for the degree of Doctor of Philosophy. The examination will be conducted in English.

Abstract

Kvashnina, K. 2006. Resonant Inelastic X-ray Scattering of Rare-Earth and Copper Systems. Acta Universitatis Upsaliensis. *Digital Comprehensive Summaries of Uppsala Dissertations from the Faculty of Science and Technology* 205. 52 pp. Uppsala. ISBN 91-554-6625-7.

Rare earths and copper systems were studied using X-ray absorption spectroscopy (XAS) and resonant inelastic X-ray scattering (RIXS). The use of monochromased synchrotron radiation and improved energy resolution for RIXS made possible to obtain valuable information on the electronic structure in 4f, 5f and 3d systems. Experimental results for rare-earths (Ho, Gd, Cm,U, Np, Pu) were analyzed by atomic multiplet theory based on the Hartree-Fock calculations.

The inelastic scattering structures in RIXS spectra at 5d edge of actinides found to be sensitive to actinide oxidation states in different systems. Comparison of experimental and calculated Cm 5d RIXS spectra gave direct information about valency of the 248-curium isotope in oxide.

Scientific understanding of processes that control chemical changes of radioactive species from spent fuel is improved by studying interactions of actinide ions (U, Np, Pu) with corroded iron surfaces. RIXS measurements at the actinide 5d edge indicate the reduction of U(VI), Np (V) and Pu (VI) to U(IV), Np(IV) and Pu (IV) by presence of iron ions.

This thesis is also addressed to the study of changes in the electronic structure of copper films during interaction with synthetic groundwater solutions. The surface modifications induced by chemical reactions of oxidized 100Å Cu films with Cl^-, SO_4^{2-} and HCO_3^- ions in aqueous solutions with various concentrations were studied in-situ using XAS. It was shown that the pH value, the concentration of Cl^- ion and presence of HCO_3^- ion in the solutions strongly affect the speed of the corrosion reaction. The Cu 2p RIXS was used to distinguish between the species present on the copper surface while in contact with groundwater solution.

Keywords: resonant inelastic X-ray scattering

Kristina Kvashnina, Department of Physics, Box 530, Uppsala University, SE-75121 Uppsala, Sweden

ISSN 1651-6214
ISBN 91-554-6625-7
urn:nbn:se:uu:diva-7094 (http://urn.kb.se/resolve?urn=urn:nbn:se:uu:diva-7094)

to my parents

List of Papers

This thesis is based on the following papers, which are referred to in the text by their Roman numerals.

I **Influence of Hydrogen on Properties of Rare-Earth Hydrides Studied by Resonant Inelastic X-ray Scattering spectroscopy**
K.O. Kvashnina, S. M. Butorin, B.Hjorvarsson, J.-H. Guo and J. Nordgren
AIP Conf. Proc. 837, 255 (2006)

II **Electronic Structure of Gd Hydrides Studied by Resonant Inelastic Soft X-ray Scattering**
K.O. Kvashnina, S. M. Butorin, J. Nordgren, J.-H. Guo, B.Hjorvarsson,
J. Electron. Spectrosc. Relat. Phenom. 137-140, p.487-489 837 (2004)

III **Resonant Inelastic X-ray Scattering of Curium Oxide**
K.O. Kvashnina, S. M. Butorin, D.K. Shuh, J.-H. Guo, L. Werme and J. Nordgren
Submitted to Phys. Rev. B

IV **Resonant Inelastic Soft X-ray Studies of Uranium (VI) Reduction on Iron Surfaces**
S. M. Butorin, D. K. Shuh, K.O. Kvashnina, I. Soroka, K. Ollila, K.E. Roberts, J.-H. Guo, L.Werme and J. Nordgren
Mat. Res. Soc. Symp. Proc. Vol. 807, 113-118 Material Research Society (2004)

V **Immobilization of UO_2^{2+} and NpO_2^{+} Carbonate in Groundwater through Reduction on Corroding Iron**
S. M. Butorin, D. K. Shuh, K.O. Kvashnina, K. Ollila, Y. Albinsson, J.-H. Guo, L.Werme and J. Nordgren
In manuscript

VI **Studies of Actinides Reduction on Iron Surface by means of Resonant Inelastic X-ray Scattering**

K.O. Kvashnina, S. M. Butorin, D.K. Shuh, K. Ollila, I. Soroka, J.-H. Guo, L. Werme and J. Nordgren
In manuscript

VII **Resonant Inelastic X-ray Scattering Study of Copper Compounds and Minerals at Cu L_3 edge**
K.O. Kvashnina, S. M. Butorin, A. Modin, J.-H. Guo, R. Berger, L. Werme and J. Nordgren
In manuscript

VIII **Changes in Electronic Structure of Copper Films in Aqueous Solutions**
K.O. Kvashnina, S. M. Butorin, A. Modin, I. Soroka, M. Marsellini, J.-H. Guo, L. Werme and J. Nordgren
Submitted to Phys. Rev. B

IX **Suppression of Copper Corrosion in Groundwaters Observed by In-situ X-ray Absorption Spectroscopy**
K.O. Kvashnina, S. M. Butorin, A. Modin, I. Soroka, M. Marsellini, J.-H. Guo, L. Werme and J. Nordgren
Submitted to Nature

Reprints were made with permission from the publishers.

The following publications have been omitted from the thesis due to the repetitions or character of the material.

- *Rates and mechanisms of radioactive release and retention inside a waste disposal canister. In Can Processes.*
  Y.Albinsson, A-M Jakobsson, A. Odegaard-Jensen, S. Butorin, K. Kvashnina, J. Nordgren, M Cowper, P. Macak, T. Primlov, B. Schimmelpfenning, U. Wahlgren, M. Mantynen, K. Ollila, V. Oversby, M. Snellman,
  Svensk Karnbranslehantering AB (2003)

- *X-ray absorption and emission study of hydrogenated fullerenes*
  K. O. Kvashnina, J.-H. Guo, A. V. Talyzin, A. Modin, T. Kaambre, S. M. Butorin, and J. Nordgren
  AIP Conf. Proc. 837, 230 (2006)

- *Influence of high pressure and temperature on the polymerised C_{60} preparation studied by x-ray absorption and emission spectroscopies*
  K.O. Kvashnina, A.V. Talyzin, A. Dzwilewski, J.-H. Guo, S.M. Butorin, and J. Nordgren

In manuscript

- *Electronic structure of sulfate anion $SO_4^{(2-)}$ in aqueous solution probed by means of resonant X-ray emission spectroscopy.*
  S. Kashtanov, K. Kvashnina, J. Andersson, J-H Guo, Y. Luo, S. Butorin and J. Nordgren
  In manuscript

- *Characterization of Cu_3N films using soft x-ray spectroscopy*
  A. Modin, K. Kvashnina, S. Arapan, S.M. Butorin, J. Nordgren, A. Fallgren, M. Ottosson
  In manuscript

Contents

Introduction

The rare earth elements have unique and important impact on technology. The unfilled *f* shell of rare earth elements gives them special properties, which are used to develop many new materials such as phosphors, magnetic and magnetostrictive materials and hydrogen storage materials. The rare earth materials represent a very big field of research that has undergone a rapid growth with the application of several experimental techniques and important theoretical aspects.

Rontgen's discovery of X-rays in 1895 became central to the development of modern physics. It has subsequently influenced fields as chemical physics, nuclear physics, biophysics and led the development of techniques such as Auger, Raman, X-ray photoelectron spectroscopy, X-ray diffraction, Protein Crystallography, X-ray lithography.

From spectroscopic studies of the light emitted or absorbed by atoms, it gradually became clear that the particular wavelength of light associated with atoms of a given element is characteristic of that element. Spectral information must therefore provide clues to the internal structure of the atoms.

In this thesis we present a study of properties some of the rare-earth elements, such as Holmium, Gadolinium, Curium, Uranium, Neptunium and Plutonium. The study uses advances in experimental technique, synchrotron radiation and theoretical calculations.

Actinides such as uranium, neptunium and plutonium are the major contributors to the long-term radioactivity of nuclear waste. In the Swedish disposal concept, the waste package consists of a canister with an outer copper shell, as a corrosion resistant barrier and the inner cast of iron, in order to add strength to the canister. Scientific understanding of processes that control chemical changes of radioactive species from spent fuel can be achieved by studying interactions of actinide ions (U, Np, Pu) with corroded iron surfaces.

The corrosion of copper canister in the repository controlled by the availability of corrosive groundwater components circulating around the canister. Therefore, the monitoring of in-situ corrosion processes becomes an important topic, which is necessary to study by different methods.

This thesis is organized in the following way. In chapter I the general background of RIXS, XAS and XES is explained, including theoretical calculations and experimental details. The results are presented and discussed in Chapter II.

1. X-ray Absorption and Emission Spectroscopies

This chapter gives an introduction to the basic mechanism of the absorption and emission processes, including theoretical calculations and experimental details.

1.1 Basic Aspects

Spectroscopy is defined as the study of the interaction between the light and matter. In the past time, spectroscopy referred to a different branches of a science in which visible light was used for studies on the structure of matter. Recently, the definition has broadened as new techniques have been developed that utilized not only visible light, but many other forms of radiation: microwaves, radiowaves, X-rays and others. Spectroscopy is often used for the identification of substances through the spectrum emitted or absorbed by them.

One type of the spectroscopy, X-ray absorption spectroscopy (XAS) is based on the absorption of quanta of X-ray light by a chemical substance due to the promotion of electrons from one atomic orbital to another. The wavelength of the incident photon will determine the energy level of excitation according to the Plank's law: $E=\hbar\nu$. By analyzing the XAS, information about unoccupied valence levels can be obtained. This is done by studying what radiation energy is needed to lift a core level electron to an unoccupied valence level (Fig. 1.1). A core hole state is very unstable and very quickly a valence electron will fill the hole. The excess energy is carried away from a system by another electron, called Auger electron or by an X-ray photon. The absorption can be measured indirectly by detecting the Auger electrons or, more commonly, by detecting electrons from multiple secondary processes, called total electron yield (TEY). X-ray Emission Spectroscopy (XES), on the other hand, is a method for studying the occupied valence levels. XES measures the X-ray photons emitted when valence electrons jump to fill core holes (Fig. 1.1). XAS and XES are complementary methods, providing information about the unoccupied and occupied valence states.

If electromagnetic radiation interacts with electrons, the interaction Hamiltonian can be written as

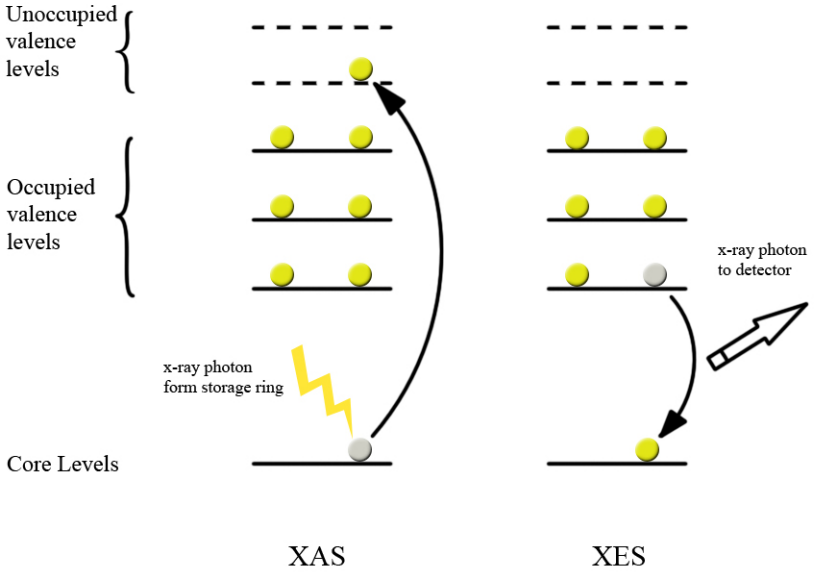

Figure 1.1: Illustration of the X-ray absorption and emission processes

$$H_{int(1)} = \frac{e}{mc} p \cdot A + \frac{e}{2mc} \sigma \cdot \nabla \times A \tag{1.1}$$

The first term describes the interaction vector field A on the momentum operator p of an electron, or in other words the electric field E acting on the electron moments. The second term describes the magnetic field $B(=\nabla \times A)$ acting on the electron spin σ. Using second order perturbation theory one finds the term

$$H_{int(2)} = \frac{e^2}{2mc^2} p \cdot A^2 \tag{1.2}$$

The Golden rule states that the transition probability W between a system in its initial state Φ_i and final state Φ_f is given by

$$W_{fi} = \frac{2\pi}{\hbar} |\langle \Phi_f | T | \Phi_i \rangle|^2 \delta_{E_f - E_i - \hbar\omega} \tag{1.3}$$

The initial and final state wave functions Φ_i and Φ_f are built from an electron part and a photon part, but in the following we will not include the photon part explicitly in the discussion. The delta function takes care of the energy

conservation and a transition takes place if the energy of the final state equals the energy of the initial state plus the X-ray energy. The squared matrix element gives the transition rates. The transition operator T is related to the interaction Hamiltonian H_{int} with the Lippmann-Schwinger equation

$$T = H_{int} + H_{int} \frac{1}{E_i - H + i\Gamma/2} T \tag{1.4}$$

Γ is the life-time broadening of an excited state and H is the Hamiltonian of the unperturbed system. The Lippmann- Schwinger equation is solved iteratively and in first order T_1=$H_{int(1)}$, which describes one-photon transitions, as X-ray absorption and X-ray emission. The transition rates of these processes are found by calculating the matrix elements of the transition operator T_1, which could be done by the first order perturbation term of the interaction Hamiltonian $p \cdot A$. Omitting the polarization degrees of freedom, the interaction Hamiltonian is found by inserting the vector field into $H_{int(1)}$

$$T_1 = \sum_k \frac{e}{m} \sqrt{\frac{2\pi\hbar}{V\omega_k}} [a_k(\hat{e}_k \cdot p) e^{ikr} + \frac{\hbar}{2} a_k(\hat{e}_k \cdot \sigma \times k) e^{ikr}] \tag{1.5}$$

The equation can be rewritten using a Taylor expansion of $e^{ikr} = 1 + ikr + ...$ Limiting the equation to the first two terms for the dipole and only to the first term for the spin interaction, the transition operator is

$$T_1 = \sum_k a_k \frac{e}{m} \sqrt{\frac{2\pi\hbar}{V\omega_k}} [(\hat{e}_k \cdot p) + i(\hat{e}_k \cdot p)(k \cdot r) + \frac{\hbar}{2}(\hat{e}_k \cdot \sigma \times k)(k \cdot r)] \tag{1.6}$$

The three terms of T_1 are the electronic dipole transition E_1, the electronic quadrupole transitions E_2 and the magnetic dipole transitions M_1 respectively. The electric quadrupole and magnetic dipole transitions both contain a factor $k \cdot r$. The transition probability is equal to the matrix element squared, hence the E_2 and M_1 terms are small and they can be neglected. This is the dipole approximation. The electric dipole transition E_1 is given by

$$T_1(E_1) = \sum_k a_k \frac{e}{m} \sqrt{\frac{2\pi\hbar}{V\omega_k}} [(\hat{e}_k \cdot p)] \tag{1.7}$$

Omitting the summation over k and using the commutation law between the position operator r and the atomic Hamiltonian, one obtains the familiar form of the X-ray absorption transition operator

$$T_1(E_1) = e\sqrt{\frac{2\pi\hbar\omega}{V}} \hat{e} \cdot r \tag{1.8}$$

Because X-ray absorption is in essentially all cases not measured with absolute intensity, one can simplify this equation to the transition operator T_1 being equal to $\hat{e} \cdot r$ or the equivalent $\hat{e} \cdot p$.

The X-ray absorption spectral shape is described with a the Fermi Golden rule

$$I_{XAS} \sim |\langle \Phi_f | \hat{e} \cdot r | \Phi_i \rangle|^2 \delta_{E_f - E_i - \hbar\omega} \tag{1.9}$$

It can be described as the initial state with a continuum electron (ε) added and a core electron is removed

$$\Phi_f = c\varepsilon\Phi_i \tag{1.10}$$

$$I_{XAS} \sim |\langle \Phi_i c\varepsilon | \hat{e} \cdot r | \Phi_i \rangle|^2 \delta_{E_f - E_i - \hbar\omega} \tag{1.11}$$

In case of $4d$ X-ray absorption for rare-earth systems, the core hole and free electron of equation (1.11) are rewritten to a $4d$ core hole and a $4f$ electron. All valence electrons except the $4f$ electrons are omitted and the intensity of XAS could be written as equation (1.13), which is the starting point of all calculation.

$$I_{XAS} \sim |\langle \Phi_i 4d4f | \hat{e} \cdot r | \Phi_i \rangle|^2 \delta_{E_f - E_i - \hbar\omega} \tag{1.12}$$

$$I_{XAS} \sim |\langle 4d4f^{N+1} | \hat{e} \cdot r | 4f^N \rangle|^2 \delta_{E_f - E_i - \hbar\omega} \tag{1.13}$$

The problem is to find the best way to treat the XAS. The successful analysis method has been developed based on the ligand-field multiplet model. In the following section some aspects of atomic multiplet theory [1] that are important for the analysis of XAS and XES will be discussed.

1.2 Atomic Multiplet Theory

Theoretical treatment of an atom containing N electrons requires first of all knowledge of a suitable Hamiltonian operator.

An appropriate operator may be obtained by summing the one-electron operator

$$H = -\frac{\hbar^2}{2m}\nabla^2 + V(r) =$$

$$= -\nabla^2 + V - \frac{\alpha^2}{4}(E-V)^2 - \frac{\alpha^2}{4}\frac{dV}{dr}\frac{\partial}{\partial r} + \frac{\alpha^2}{2}\frac{1}{r}\frac{dV}{dr}(l\cdot s) \quad (1.14)$$

where

$$\alpha = \frac{e^2}{\hbar c} = \frac{\hbar}{mca_0} = \frac{1}{137.036} \quad (1.15)$$

and angular momentum operator

$$j = l + s \quad (1.16)$$

By summing (1.14) over all N electrons, and adding a term for the electrostatic Coulomb interactions among electrons we have

$$H = H_{kin} + H_{elec-nucl} + H_{elec-elec} + H_{s-o}$$

$$= -\sum_i \nabla_i^2 - \sum_i \frac{2Z}{r_i} + \sum_{i>j}\sum \frac{2}{r_{ij}} + \sum_i \xi(i)(r_i)(l_i \cdot s_i) \quad (1.17)$$

where H_{s-o} is the spin-orbit interaction term which in (1.14) was obtained by a consideration of relativistic corrections to the non-relativistic Hamiltonian. Here r_i=$|r_i|$ is the distance of the i^{th} electron from the nucleus, r_{ij}=$|r_i - r_j|$ is the distance between i^{th} and j^{th} electrons, and the summation over $i > j$ is over all pairs of electrons.

The kinetic energy and the interaction with the nucleus are the same for all electrons in a certain atomic configuration. They define the average energy of a certain state. This leaves the electron-electron repulsion and the spin-orbit coupling as the important interactions.

1.2.1 Term Symbols

As was mentioned before, electronic symmetry configurations are indicated with their orbital moment L, spin moment S and the total moment J. Together, these three quantum numbers indicate a certain state and determine its specific energy. A specific configuration is indicated with a so-called term symbol ${}^{2S+1}L_J$

It is relatively easy to calculate the term symbol for the ground state of an atom. A $4f^{10}$ configuration (as outer shell for Ho^{3+} ion) corresponds to the quantum number $l = 3$. There are 7 orbitals ($m_l = 3,2,1,0,-1,-2,-3$) that can hold up to $2\cdot(2l+1) = 14$ electrons. The first 7 electrons can take $m_s = 1/2$ but the Pauli exclusion principle forces the next electrons 3 electrons

to have $m_s = -1/2$ because they go to already occupied orbitals. Spin quantum number for holmium can be calculated as

$$S = 7 \times 1/2 - 3 \times 1/2 = 2 \tag{1.18}$$

$$L = 3+2+1+0-1-2-3+3+2+1 = 6 \tag{1.19}$$

$L = 6$, which is I in spectroscopic notation. And the total angular momentum quantum number J=$L+S$=8 and ground state term symbol is then ${}^{2S+1}L_J = {}^5I_8$.

The number of possible microstates N for a given electron configuration can be written as

$$N = \frac{t!}{n!(t-n)!} \tag{1.20}$$

where t is the total number of electrons $t = 2(2l+1)$.

One of the transitions investigating in this thesis is 4d→4f excitation process. Crucial for its understanding are the configuration of $4d^9 4f^n$ final states. The term symbols of the $4d^9 4f^n$ states are found by multiplying the configuration of $4f^n$ with a ${}^2P$ term symbol (corresponding to the $4d^9$ configuration). The general formula to determine the total number N for a $4d^9 4f^n$ configuration is

$$N = 10 \times \frac{14!}{n!(14-n)!} \tag{1.21}$$

For example, $4d^9 4f^{11}$ configuration for Ho^{3+} ion has 3640 states. After applying Dipole Selection Rule: $\triangle$J = -1,0 +1, reduced number of states which can be reached from ground state are found. There are 61 dipole allowed transitions from the ground to the final states for Ho^{3+} ion. The next question is calculate the matrix elements of these states.

1.2.2 The Matrix Method

The approximation method was first developed by Slater, and later extended by Condon and Shortley; it is commonly known as the Slater-Condon theory.

The basic procedure consists of expanding the unknown wavefunction Ψ^k in terms of a set of known basis functions Ψ_b in the Schrodinger equation

$$H\Psi^k = E^k\Psi^k, \tag{1.22}$$

$$\Psi^k = \sum_b y_b^k \Psi_b \tag{1.23}$$

Now we assume that a set of M suitable basis functions has been chosen $(1 \leq b \leq M)$.

Substitution of (1.22) into the Schrodinger equation (1.23) gives

$$\sum H y_{b'}^k \Psi_{b'} = E^k \sum y_{b'}^k \Psi_{b'} \tag{1.24}$$

Multiplying this form by anyone of the basis functions Ψ_b, and integrating over all $3N$ space coordinates, and summing over both possible directions of each of the N spins, we obtain

$$\sum_{b'=1}^{M} H_{bb'} y_{b'}^k = E^k \sum_{b'=1}^{M} y_{b'}^k \langle \Psi_b | \Psi_{b'} \rangle = E^k y_b^k, \tag{1.25}$$

where

$$H_{bb'} \equiv \langle \Psi_b | H | \Psi_{b'} \rangle \tag{1.26}$$

is the matrix element of the Hamiltonian operator H (1.17) between the basis functions b and b' .

For large M, the only practical procedure is to numerically diagonalize the Hamiltonian matrix $H \equiv (H_{bb'})$. It is if we write the set of expansion coefficients in the form of column vector Y^k then equation (1.25) may be written as a single matrix equation

$$HY^k = E^k Y^k \tag{1.27}$$

and the problem is to find the M eigenvalues E^k of the matrix H, together with the corresponding eigenvectors Y^k. This is accomplished by supplying numerical values of the matrix elements $H_{bb'}$ to a computer and finding by standard techniques, wich will be explained in the next section.

Once we have computed the Hamiltonian matrix elements $H_{bb'}$, the calculation of the energy levels and eigenfunctions of the atom is more simple - all we have to do is find the eigenvalues of the matrix H.

So, the approximate solution to the Schrodinger equation can be written in the form

$$\Psi_{nlm_l m_s} = \frac{1}{r} P_{nl}(r) \cdot Y_{lm_l}(\theta, \phi) \cdot \sigma_{m_s}(s_z) \tag{1.28}$$

In the equation the radial and angular parts are separated, implying that the radial and angular matrix elements can be calculated separately. At this stage the energy level is characterized by the quantum numbers nl. The radial wave functions are calculated with standard Hartree-Fock codes.

1.2.3 Hartree-Fock Equations

It is convenient to be able to describe the energy of a configuration in terms of

$$E_{av} = \langle b|H|b\rangle_{av} \tag{1.29}$$

where the average is to be carried out over all basis functions b belonging to the configuration.

The appropriate form of this average is

$$E_{av} = \frac{\sum_b \langle b|H|b\rangle}{n_{bf}} \tag{1.30}$$

where n_{bf} is number of basis functions.

The Hamiltonian operator in the approximation that we shall use, is given by equation (1.17). We now derive the expression for the configuration - average energy of an electron in an orbital $n_i l_i$ in essentially classical terms

$$E^i = E^i_k + E^i_n + \sum_{j\neq i} E^{ij} \tag{1.31}$$

and the average total energy of all N electrons may be written as

$$E_{av} = \sum_i E^i_k + \sum_i E^i_n + \sum\sum_{i>j} E^{ij} \tag{1.32}$$

The average total energy of the atom is the sum of all kinetic and electron-nuclear energies plus the averaged electron-electron Coulomb interactions summed over all electron pairs.

The kinetic energy is given by

$$E^i_k \equiv \int_0^\infty P^*_{n_i l_i}(r)[-\frac{d^2}{dr^2} + \frac{l_i(l_i+l)}{r^2}]P_{n_i l_i}(r)dr \tag{1.33}$$

Since the Hamiltonian operator is a function of r only, the angular integration and summation over spins can be carried out immediately and electron-nuclear energy is obtained by

$$E_n^i \equiv \int_0^\infty (-2Z/r)|P_i(r)|^2 dr \tag{1.34}$$

The electron-electron Coulomb energy is

$$E^{ij} \equiv F_{(ij)}^{(0)} - \frac{1}{2}\sum_k \begin{vmatrix} l_i & k & l_j \\ 0 & 0 & 0 \end{vmatrix} G^k(ij) \tag{1.35}$$

where

$$F^k(ij) \equiv \int_0^\infty \int_0^\infty \frac{2r^k}{2r^{(k+1)}} |P_i(r_1)|^2 |P_j(r_2)|^2 dr_1 dr_2 \tag{1.36}$$

$$G^k(ij) \equiv \int_0^\infty \int_0^\infty \frac{2r^k}{2r^{(k+1)}} P_i^*(r_1) P_j^*(r_2) P_j(r_1) P_i(r_2) dr_1 dr_2 \tag{1.37}$$

The radial integrals F^k and G^k are frequently referred as Slater integrals.

If we substitute into E_{av}(1.32) the expressions of kinetic (1.33), electron-nuclear (1.34) and electron-electron Coulomb (1.35) energies we arrive at a set of equations (one for each value of i) known as the Hartree-Fock equations.

Atomic multiplet theory is able to accurately describe the 4d and 5d XAS spectra of the rare-earths and actinides systems. As will be discussed in the Chapter 2 section 2.1 and section 2.2 4d, 5d XAS is shown a complex multipeaked structure, which makes 4d, 5d XES ideally suitable for resonance study. Therefore, next section begins with a discussion of the resonant X-ray emission spectral shapes.

1.3 Resonant Inelastic X-ray Scattering

Resonant X-ray emission spectroscopy with monochromatic photon excitation for rare-earth systems can be described as an analog of resonant inelastic X-ray scattering (RIXS) process [2]. The RIXS technique study the decay of the core-excited final states, depending on where the electron is filling the core vacancy [3]. Fig. 1.2 illustrates two cases of the RIXS depending on where the electron filling the core vacancy.

The main features associated with resonant X-ray emission spectra can be understood from second order perturbation theory between light and matter, as described by the Kramers-Heisenberg equation.

$$I_{q,q'}(\Omega,\omega) = \sum_f \left| \sum_i \frac{\langle f|D|i\rangle\langle i|D|g\rangle}{E_g + \Omega - E_i - i\Gamma_i/2} \right|^2 \tag{1.38}$$

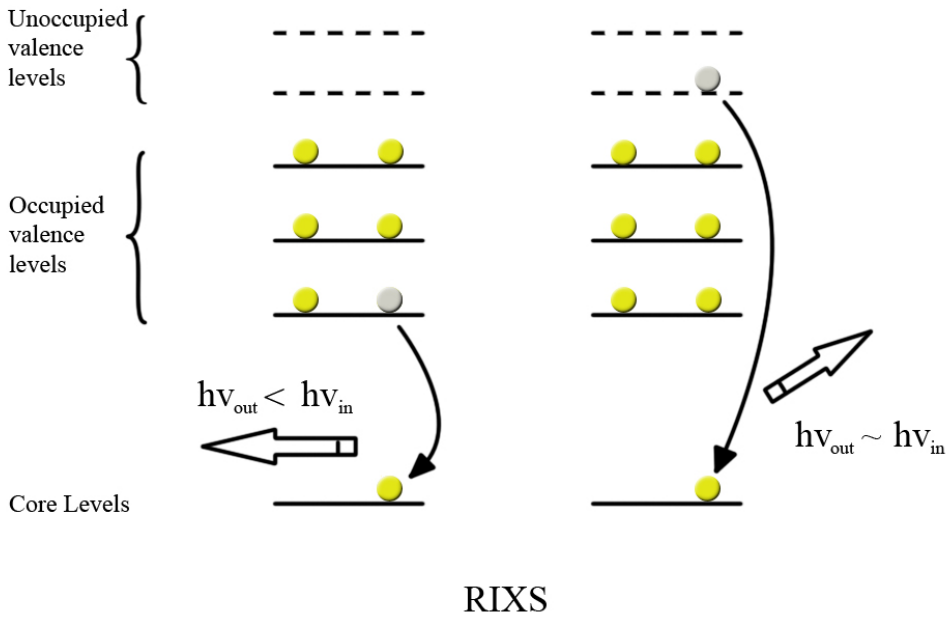

Figure 1.2: Illustration of two types of RIXS depending on where the electron is filling the core vacancy

Here, $|g\rangle, |i\rangle$ and $|f\rangle$ are the ground, intermediate and final state with energies E_g, E_i and E_f, respectively, while Ω and ω represent energies of incident and scattered photons respectively. D is the dipole operator, Γ stands stands for the intermediate state lifetime.

This formulation can be rewritten in form

$$I_{q,q'}(\Omega,\omega) = \sum_i \frac{\langle f|D|i\rangle\langle i|D|g\rangle^2}{E_g+\Omega-E_i-\Gamma_i/4}+ \tag{1.39}$$

$$+2\sum_i\prod_{k=1}^{k\neq i}\frac{\langle f|D|i\rangle\langle i|D|g\rangle\langle f|D|k\rangle\langle k|D|g\rangle[(E_g+\Omega-E_i)(E_g+\Omega-E_k)+\Gamma^2/4]}{(E_g+\Omega-E_i)^2+\Gamma^2/4)((E_g+\Omega-E_k)^2+\Gamma^2/4)}$$

The improvement of the theoretical understanding of the physics underlying X-ray spectroscopy has been accompanied by advances in experimental techniques.

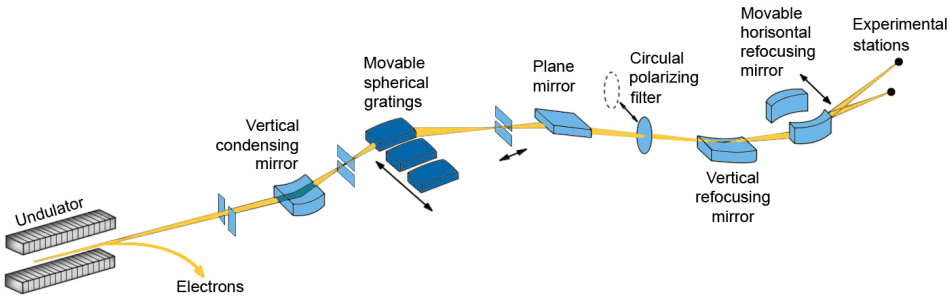

Figure 1.3: Schematic layout of Beamline 7.0.1 at the Advanced Light Source of Lawrence Berkeley National Laboratory.

1.4 Experimental Equipment

A charge particle, usually electron, subject to acceleration such as in a curved trajectory, emits radiation. At a speed close to the speed of light the radiation gets collimated and is called synchrotron radiation. Synchrotron radiation sources have been developed as powerful tools for a broad number of applications in science and technology [4] and can offer light with very high brightness, high spatial and spectral resolution, polarization and high flux for researchers to perform experiments [5].

The experiments reported in all Papers I-IX were carried out at beamline 7.0.1 [6,7] of the Advanced Light Source at Lawrence Berkeley National Laboratory (USA). This undulator beamline covers the photon energy range of 50-1200 eV. In an undulator the distance between the magnets is such that the light emitted when an electron of a particular energy passes one magnet is in phase with the light emitted when it passes all the other magnets. Constructive interference is then obtained for certain wavelengths or harmonics. The intensity distribution of the emitted light has several rather narrow peaks corresponding to these harmonics. The energy of the peaks in the undulator spectrum is determined by the vertical gap between the magnets. The magnets can be moved vertically, to change the energy of the peaks.

Fig. 1.3 shows experimental arrangement of beamline 7.0.1, including prefocusing optics and a spherical grating monochromator (SGM) [8]. Calculated flux (1.9 GeV, 400 mA) for that beamline is 3×10^{12} photons/s/0.01% BW (at 800 eV) and the vertical spot size at the sample is usually 50-100 μm.

The SGM contains three water-cooled spherical gratings with ruling densities of approximately 150, 380, 925 lines/mm. The gratings are interchanged by shuttling them back and forth into the photon beam path and they cover

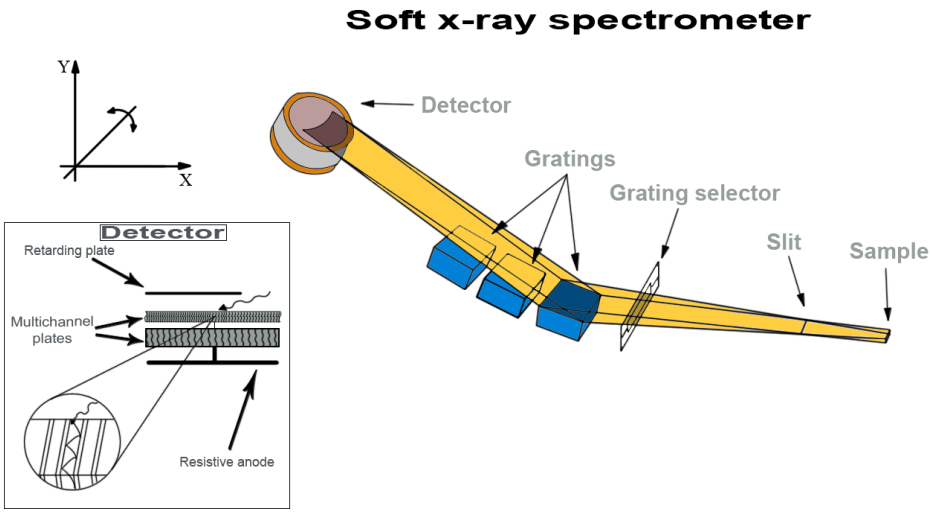

Figure 1.4: Schematic picture of the soft x-ray emission spectrometer

the approximate photon energy range of 50-1200 eV. The gratings are only rotated to select the wavelength of the radiation focused onto the exit slit. The exit slit opening can be adjusted from fully closed to over 0.5 mm to allow the user to select the resolution or flux desired.

X-ray absorption measurements were made using two different setups. The Total Electron Yield (TEY) was recorded by measuring current from the sample while scanning the incident photon energy. The Total Fluorescence Yield (TFY) was recorded using a channeltron or photodiode mounted for photon detection. The X-ray scattering processes are measured using a grazing-incidence spectrometer[7].

1.5 Grazing Incidence Spectrometer

The working principle of the spectrometer is explained in Fig. 1.4. The spectrometer provides a choice of three different spherical gratings. It has an entrance slit with adjustable width and uses a two-dimensional multichannel detector that can be aligned at the focal curve defined by the Rowland circle (a circle that is tangential to the grating but with half its radius and on which the entrance slit and detector are positioned).

The three gratings are optimized for different energy ranges and resolutions. The grating is selected by an aperture that limits the light so that it only falls on one grating. This aperture can also be used to determine how much of the surface area of the grating is illuminated. This affects the resolution, since there is a maximum width that can be used for a certain resolution.

The detector consists of a repelling grid, five multichannel plates and a resistive anode. A photon impinging on the top plate is converted into electrons. The MCPs have channels where electrons going into them are multiplied and exit the channels as bunches of electrons. Ideally each bunch corresponds to one detected photon. A photon impinging at a certain position on the top plates gives rise to a bunch of electrons exiting the fifth plate in the corresponding position further down. This electron bunch then hits the resistive anode and the position is noted. The repelling grid is at a negative voltage with respect to the MCPs to help push electrons created in the areas between the channels go down into the channels. To further increase the efficiency of the MCPs, the top plate is coated with cesium iodide. The position of each count is transferred to a computer using a special collection system and stored in a two dimensional array representing the detector. The data can be exported to another system and analyzed with some data analysis program.

The highest resolution of the spectrometer is determined by next factors: grating radius of curvature, slit width and diffraction order. Other factors can limit the resolution, such as misalignment, grating illumination and detector settings.

1.6 The Liquid Cell

One of the part of this thesis is to study the changes in the electronic structure during interaction between copper and groundwater solutions. Liquid cells with different concentrations of chloride, sulfate and carbonate ions were used for the in-situ studies. A schematic picture of the cell is shown in Fig.1.5. One of the difficulties is that the cell contains liquid and the soft X-ray experiments have to be under vacuum conditions. Thus if a liquid is simply introduced into a high vacuum system it will instantly be vaporized and pumped out from the system before any measurements could be obtained. By keeping the liquid in a small vacuum tight container, soft X-ray spectroscopy on liquids could be pursued.

The cell consists of a plastic container, made from PEEK polymer. Diameter of the cell is 20 mm and thickness is 4 mm. The X-rays penetrate thought a Si_3N_4 membrane window. The size of the used membrane was 1 mm x 1 mm. Membrane was held by 10 mm x 10 mm Si frame of the window, which was attached to the cell. The volume of the cell is sufficient to hold one drop (approximately 4 μL) of the liquid. Because of safety issues, in case the window breaks, the amount of liquid inside the cell has to be minimized. Other precautions are also taken, such as pinholes between the experimental chamber and the beamline, and fast interlock systems for protection of the high-voltage-biased detectors. Once the cell is properly sealed, it can be mounted on any of our standard sample-holders and brought into vacuum system via the loadlock setup. The normal pump-down/transfer time is about 20 minutes.

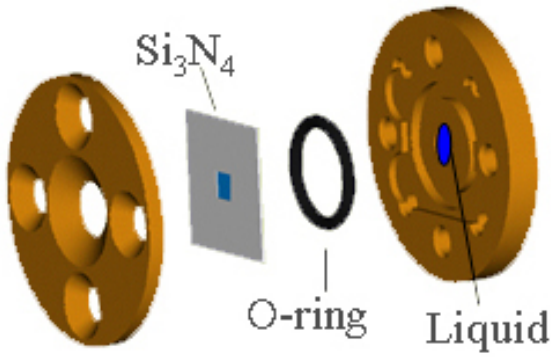

Figure 1.5: Schematic illustration of the cell used for liquid experiments.

In order to study the chemical reactions between copper and different solution, a 100A copper film was deposited on the backside of the 100 nm Si_3N_4 window. Detail information about the studies involving liquid-surface interfaces are given in Chapter 2 section 2.3.

2. Results

The next sections attempt to present a review of the properties of rare-earth systems. The rare earths consist of two series of elements, the lanthanides (Z = 57 to 70) and the actinides (Z = 89 to 102), which roughly involve filling of the 4f [9] and 5f subshells [10], respectively. For simplicity, we will first consider only the lanthanide elements, and postpone the discussion of the actinides. Experimental and theoretical research is more precisely documented in the papers I, II and III.

2.1 Lanthanides

2.1.1 Holmium and Gadolinium Metals

XAS and XES spectroscopic methods provide new possibilities to study the local electronic structure near the exited atom in complex rare-earth systems [11-16]. In order to simply reproduce the experimental results by theoretical calculations the gadolinium and holmium systems were chosen.

In Paper I and Paper II, the electronic structure of gadolinium, holmium metals and their hydrides were reported. Experimental XAS and RIXS spectra across the 4d edge were compared with atomic multiplet calculations of the 4d-4f transitions for Ho^{3+} and Gd^{3+} ions.

The lanthanides in the solid state are generally triply ionized [17-19] and show valence subshells running from $4f^1$ to $4f^{14}$(Ce to Lu). Because of the small radii of the $4f$ orbitals, the $4f$ electrons necessarily lie rather close together. Consequently, in the case of 4d-4f transitions, the Coulomb repulsions are quite large, and the values of the Slater integrals $F^k(4f,4f)$ are also large.

The parameters for the Ho^{3+} and Gd^{3+} configurations were calculated using Cowan's program [1, 20], which includes Hartree-Fock plus statistical exchange methods to evaluate and adjust the Slater integrals and the spin-orbit constants. Those Slater integrals F_k(4f,4f) were reduced to 80% , the F_k (4_d,4_f) and G_k(4d,4f)integrals to 75% and 66%, respectively and the spin-orbit constant ξ to 99%.

Because of the gradual contraction of the $4f$ orbital with increasing Z, the parameter values F^k and ξ increase with Z, so that the $4f$ subshells becomes more and more deeply buried within the atom, and therefore interact less strongly with the outer valence electrons. The spin-orbit parameter ξ increase much faster with Z than do the Coulomb parameters F^k. Although all

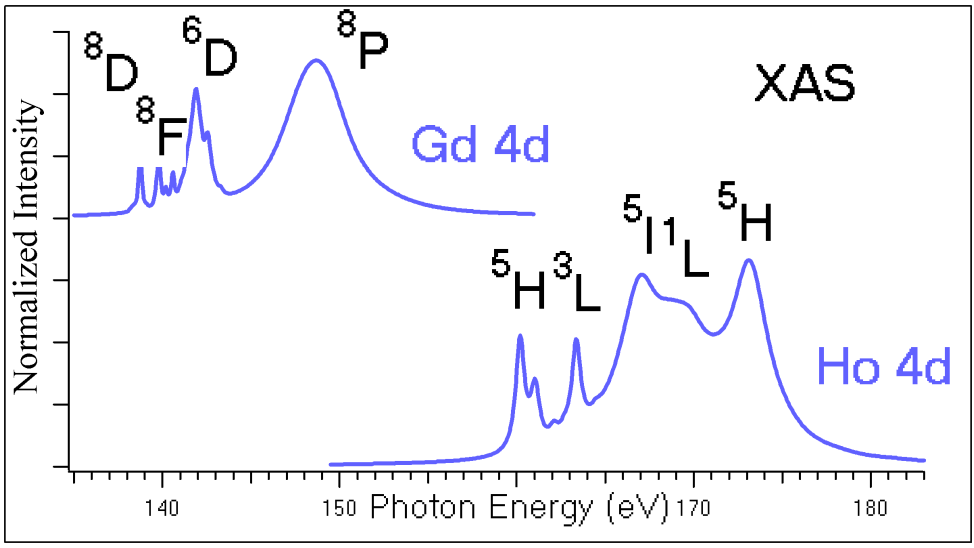

Figure 2.1: Calculated XAS 4d for the Gd^{3+} and Ho^{3+} ions. Arrows on the top of the spectra mark positions for main transitions

lanthanide spectra are exceptionally complex and the absorption spectra show contrasting strong peak and weak lines.

These are shown in Fig. 2.1. There are a few weak pre-threshold peaks and the dipole allowed giant band for both Ho^{3+} and Gd^{3+} ions. Due to strong electron correlations and autoionization these 4d-4f transitions produce a "giant resonance", which extends in the energy range of 10-15 eV for both ions. It is clearly observed that increasing nuclear charge Z shifts all peaks towards to the higher energy [21]. The XA spectrum for the Gd^{3+} ion displays only one strong absorption band preceded by a number of weaker peaks, whereas the spectra of Ho^{3+} are characterized by a very broad and structured maximum. This may be interpreted in terms of the effect of the Slater integral G^1. For a half filled or more the intensities and the multiplet spread are controlled by the exchange parameter G^1 on the energy level $4d^9 4f^{n+1}$.

The XA spectrum for the Gd^{3+} ion (Fig. 2.1) represents transitions from the ground state $^8S_{7/2}$ to the ^8P level. At lower photon energies, weaker features appear as a result of excitations of a core electron to the ^8D and ^6D levels. The calculated energy levels and absorption intensities are in good agreement with experimental data (top panel of Fig. 2.2). In order to reach the best agreement and reproduce the pre-threshold structures and the "giant resonance" as in the experiment, different broadening widths Γ in Lorentzian convolution of the line spectrum were used during the calculations. For the ^8P transitions Γ was set to the 3.0 eV, for the prethreshold transition ^8D and ^6D Γ was much smaller: 0.1 eV and 0.3 eV respectively. The same values were set in the calculations of the 4d RIXS spectra.

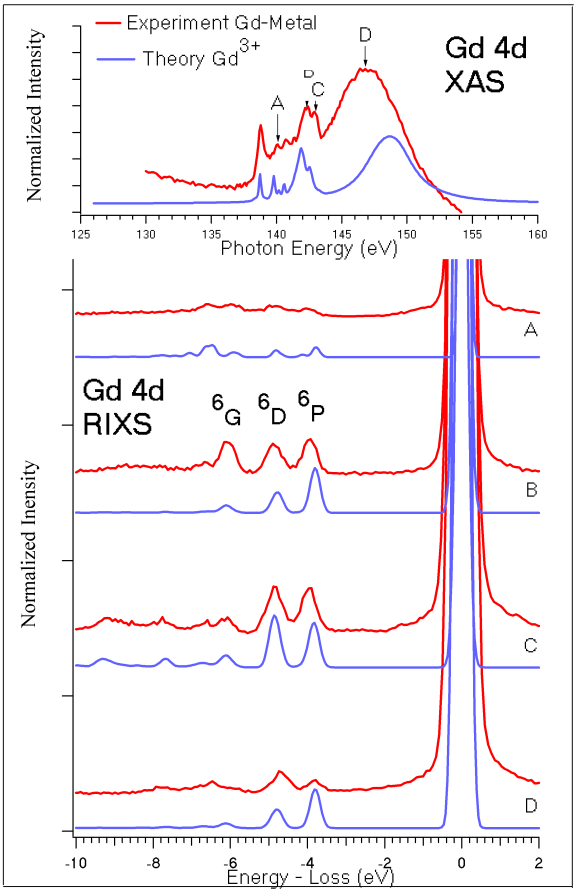

Figure 2.2: Comparison between Gd 4d XAS, RIXS experimental data and calculated results for the Gd^{3+} ion. Excitation energy positions are indicated on the top panel of XAS. RIXS are plotted in the energy-loss scale.

The Gd 4d RIXS spectra were calculated from equation (1.39) using matrix elements to transitions from the ground state to the intermediate and back to the final states. Fig.2.2 shows the results of RIXS calculations carried out for the Gd^{3+} ion together with experimental data for Gd metal taken for the different excitation energies, that are indicated on the top panel of absorption spectra.

Spectral features at about 4-6 eV below the elastic peak represent resonant inelastic x-ray scattering structures as transitions from ground state $^8S_{7/2}$ to final states ^6P, ^6D, and ^6G. These transitions show a constant difference in energy with respect to the elastic peak throughout the varying excitation energies. This inelastic scattering for Gd corresponds to the 4f spin flip transition and bringing Gd to a lower spin in the final state. The separation between the elastic and inelastic scattering features (which is the energy needed to flip a spin) is very handy between theory and experiment.

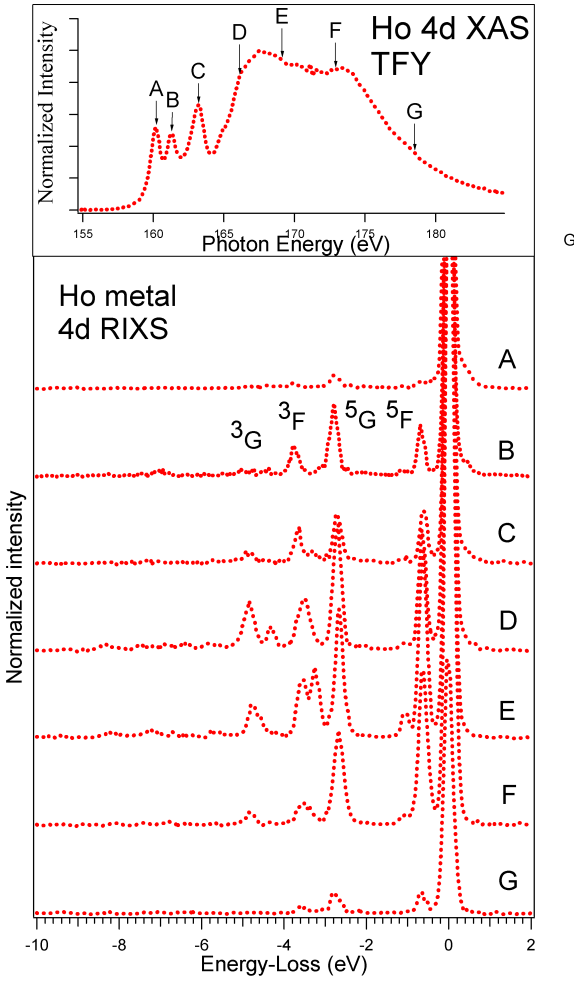

Figure 2.3: RIXS 4d for Holmium metal, excited at different excitation energies, marked on the top of XA spectrum

RIXS spectra for Ho metal also reveal inelastic X-ray scattering structures (Fig. 2.3), but these features are situated $\sim$ 1-4 eV below the elastic peak, which is in contrast with the results for Gd metal. The Ho 4d RIXS spectra show multiple excitations due to the transition from the ground state $^5I_8$ to the final states ^5F, ^5G, ^3F, ^3H. This inelastic scattering structure corresponds to f-f excitations, which are dipole forbidden electronic transitions and give rise to the most pronounced and sharp features in RIXS. In the case of holmium this mechanism consists of excitation of the electron to the empty f state and the injection of another electron for the same f shell. These $f-f$ transitions agree very well with the calculations carried out for the holmium trivalent ion, which was reported in Paper I.

Difference in the electronic structure of holmium and gadolinium metals is not an exclusive case. Gadolinium and holmium hydrides also show substantial difference in RIXS spectra across 4d edge.

2.1.2 Holmium and Gadolinium Hydrides

The interest in the properties of the lanthanide hydrides increased significantly with the discovery that hydrogen can be used to switch the electronic properties of thin metallic La films [22-24]. However, this metal-insulator transition is very unusual and details of the changes in the electronic structure are not fully understood.

The similar systems, gadolinium and holmium di and trihydrides have been studied using RIXS across 4d-4f transitions. In Fig. 2.4 comparison between RIXS spectra of GdH_{2+x}, $GdH_{3-\delta}$ and Gd metal is shown for the excitation energy 140.0 eV, which corresponds to the pre-threshold region in Gd 4d XA spectrum. An additional structure observed for Gd hydrides (in comparison with Gd metal) at about 10 eV below the elastic peak, which follows varying excitation energies on the photon energy scale (Paper I and Paper II). The only difference between GdH_{2+x} and $GdH_{3-\delta}$ is in the intensity of these additional structures, which also depends on the excitation energy. The 10 eV structure below the elastic peak can be attributed to charge-transfer excitations of an electron from hydrogen into unfilled 4f level.

We examined the possibility of using RIXS for probing of charge transfer satellites in the holmium hydride systems. This is reported in Paper I and Paper II. No substantial differences were found between holmium metal and holmium hydrides and no inelastic scattering excitations observed in the region of around 10 ev below the elastic peak for the Ho-H systems. Fig. 2.4 indicate, however, charge transfer satellites in the 4d RIXS spectra for the Gd-H systems. It was suggested that hydrogen in Gd-H systems is an electron acceptor.

This behavior of hydrogen in gadolinium hydrides is similar to that of oxygen in gadolinium oxides. Oxygen is an electron acceptor in the gadolinium oxides systems. It was shown before by Moewes et al. [25] that some inelastic X-ray scattering features appear at 9 to 10 eV below the elastic peak in Gd_2O_3, which can also be assigned to the charge-transfer states as well. For Gd-H systems such satellites are shifted about 1 eV to lower energies and appear at 10 to 11 eV on the energy-loss scale, which can't be due to the oxidation of the gadolinium films. Such changes on a high-energy scale suggest that the electronic structure is best described by a model based on negatively charged hydrogen (H^-). Different behavior of hydrogen in the Gd and Ho hydrides can possibly be connected with the half-filled 4f shell of Gd, thus leading to a difference in chemical bonding.

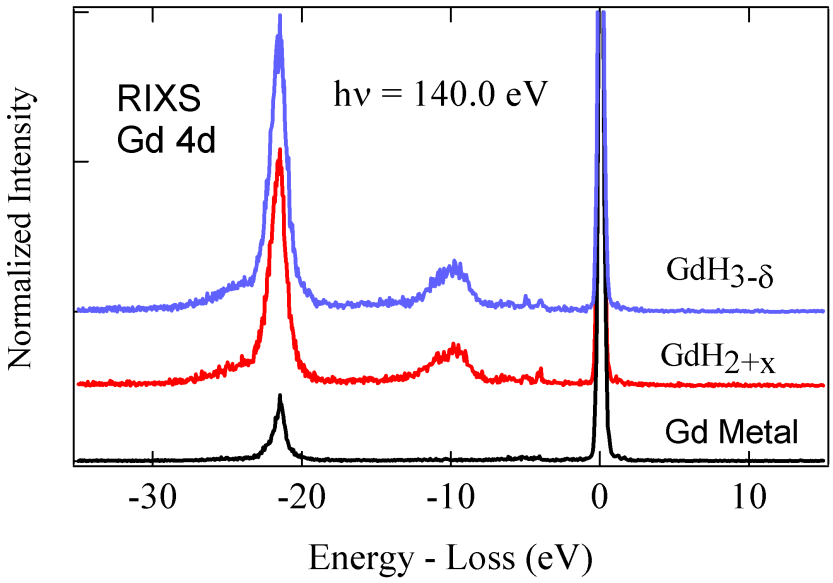

Figure 2.4: Comparison of 4d RIXS between GdH_{2+x} and $GdH_{3-\delta}$ and Gd metal at excitation energy 140.0 eV, which correspond to the excitation of pre-threshold of XA spectrum of Gd

2.2 Actinides

Atomic Multiplet Theory works quite well for describing lanthanide systems across 3d and 4d edge. The 4d, 5d and 5f shells for actinides element have similar general characteristic as the 3d, 4d, 4f shells for rare-earth elements. This suggests that this theoretical approach will be suitable for actinides as well. On the other hand, actinides show less similarity in their chemical properties than do the lanthanides, exhibiting, for instance, a wide range of oxidation states.

The electronic structure of curium as an analogue of gadolinium has been probed by XAS and RIXS across 5d edge. Since the oxidation state of the 248-curium isotope was unknown during the experiment, we calculated the Cm 4d XAS and RIXS spectra for the oxidation states (III) and (IV).

The configuration of the outer electrons in curium is similar to that of gadolinium and has a half filled 5f shell. The calculation of Cm 5d RIXS has been made in a similar way as for gadolinium in the previous section, where the Slater integrals F^k(5f,5f) were reduced to 80%, and the F^k (5d,5f) and G^k(5d,5f) to 75% and 66%, respectively and the spin-orbit constant ξ to 99%.

Calculations of XA spectrum, reported in Paper III, for both Cm^{3+} and Cm^{4+} ions do not provide information about oxidation state of investigated 248-curium isotope. Thus, RIXS data, governed by dipole selection rules and

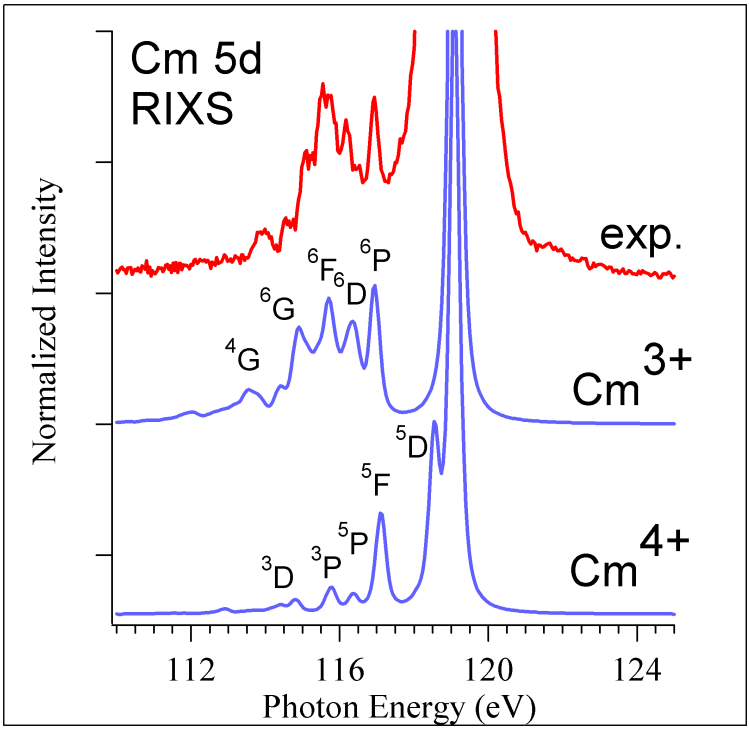

Figure 2.5: Cm 5d RIXS of curium oxide taken at excitation energy of 119.0 eV and compared with calculated spectra for Cm^{4+} and Cm^{3+} ions at the same excitation energy.

along with calculations, provide valuable information on energies of intra-atomic f-f excitations for curium oxide, which found to be extremely sensitive to the oxidation state [11].

Fig. 2.5 shows comparison of experimental data with theoretical calculations for the Cm^{3+} and Cm^{4+} ions at excitation energy 119.0 eV. The observed inelastic scattering features of the Cm^{3+} described by transitions from the $^8S_{7/2}$ ground state to the final states ^6G_J, ^6F_J, ^6D_J, ^6P_J with different J levels, which are situated 2-4 eV below the elastic peak and then weaker transitions due to the final state ^4G_J observed at 5 eV below the elastic peak. The observed inelastic scattering structure of the Cm^{4+} situated 1-4 eV below the elastic peak and caused by transition from the $^7F_0$ ground state to the final states ^5D_J, ^5F_J, ^5P_J. Weaker transition due to the ^3P_J , ^3D_J final state terms are also observed.

The inelastic scattering features for both ions are attributed to the 5f-5f intra-atomic transitions (f-f excitations), which appear 1-2 eV below the elastic peak. The energy separation between elastic and inelastic scattering structures are different for the calculated Cm^{3+} and Cm^{4+} ions. By comparing the energies of the f-f excitations for the calculated and experimental 5d RIXS spectra, it could be concluded that curium-248 isotope in the oxide sample

has oxidation state (III). Detailed comparison between the experimental results and the calculated spectra for $Cm^{3+}$and Cm^{4+} ions at different excitation energies is given in Paper III.

The data from this experiment shows that atomic multiplet theory turns to be very appropriate for actinide systems and demonstrate satisfactory agreement with experiment for curium oxide.

Understanding of the atomic levels in actinides systems has been a particular research challenge for many scientific groups and laboratories. Fundamental studies of actinides are needed for the environmental issues. Actinides such as uranium, neptunium and plutonium are the major contributors to the long-term radioactivity of nuclear waste. Thus, an important aspects of actinides research is studying how these elements behave in the environment, particularly how they migrate dissolved in groundwater.

2.2.1 Spent Fuel and Actinides Studies

Spent nuclear fuel from commercial nuclear power plants is planned to be disposed in deep underground repositories sited in geological formations. A way to predict possible risks during long-term storage is to study the reactions and interface phenomena of the spent nuclear waste after it has been placed in the geological environment.

In the Swedish disposal concept, the waste package consist of a canister with an outer copper shell, as a corrosion resistant barrier and the inner cast of iron, in order to add strength to the canister [26]. The essential part in a safety assessment involves the understanding of the interactions of materials and environment inside the canister if the isolation of the waste is broken due to failure of the canister and water has intruded into the waste package. This section will provide information about interactions between actinide ions and corroded iron surfaces. Thus the next section 2.3 will focus on corrosion problems of copper films in various aqueous solutions.

Scientific understanding of processes that control chemical changes of radioactive species from spent fuel can be achieved by studying interactions of actinide ions (U, Np, Pu) with corroded iron surfaces. The systems were studied with the help of RIXS spectroscopy, which enables us to determine the oxidation states of actinides in different species. In this chapter we present the investigation on uranium and neptunium species. More results are reported in Paper IV, V and VI.

The RIXS technique is sensitive to the oxidation state [11] and the speciation of uranium contrasting to XAS where the 5d core-hole lifetime broadening is large. As a result, the actinide 5d absorption spectra do not exhibit many sharp features [27], thus reducing the utility of XAS. In particular, it is difficult to distinguish between uranium species with different oxidation states, especially in the case when one of the species has a much lower concentration than another. The relative resolution, defined by the response function

of the instrument [7] of the RIXS technique, makes this technique especially powerful.

The uranium in the waste comes as UO_2, which has low solubility in water. However, it is possible that some UO_2 can transform into UO_3 under certain conditions. UO_3 is a more soluble compound that can be leached out by groundwater. The presence of iron in the canister walls is expected to prevent this course of events.

The Fe samples with U were made by exposing iron strip (99.9994%) to anoxic synthetic groundwater solutions of uranyl carbonate for the 17 days and 8.5 months. The neptunium containing samples were also prepared by Fe foil exposure to the neptunyl solutions in groundwater. The starting concentration was 2 x 10^{-6} M for uranium and 4 x 10^{-7} M for neptunium.

Fig. 2.6 shows the RIXS 5d measurements on a set of reference systems UO_2 and NpO_2 and comparison with atomic multiplet calculations, which reproduce all of the RIXS structures very well, which supports the assignment of the inelastic scattering structure to intra-atomic f-f excitations. Such structures uniquely identify the oxidation state of the actinide, because 5d RIXS spectra of UO_3 do not show the inelastic scattering structure below the elastic peak. Therefore, the RIXS profile provides a good fingerprint for the valence state of U, Np in different systems.

According to this, a reduction of the uranium valency from (VI) to (IV) on the iron surface should be indicated by an appearance of the f-f excitations in the resonant spectra. Left panel of Fig. 2.6 clearly indicates the presence of the f-f excitations on the 5d RIXS spectra for the uranium on the iron film, thus allowing us to conclude that U(VI) is reduced by iron to U(IV).

The amount of reduced uranium was derived by comparing the area under the shape of the f-f excitations for the UO_2 and the investigated iron films. The spectra were normalized to the characteristic core-to-core U 6p$\longrightarrow$5d fluorescence lines, which allowed us to deduce the total amount of reduced U (IV) after 17 days of exposure (73%).

Similar results were obtained for the Np sample. The right panel of Fig. 2.6 shows the Np 5d RIXS spectra of Np formed on the iron strips together with spectra of NpO_2, recorded at two excitation energies. The RIXS spectra of Np on Fe reveal f-f excitation patterns similar to those of NpO_2, thus indicating the existence of Np(IV) on the iron strips and that reduction of Np(V) had been taken place.

Our results show that actinide ions with high valences in ground water solutions became reduced by the iron surfaces. This fact became significantly important, since the reduction of actinides inside the canister can prevent their release due to the much lower solubility of reduced Np (IV), U(IV) or Pu (IV) than those species with valency V (Np, Pu) and VI (U, Pu).

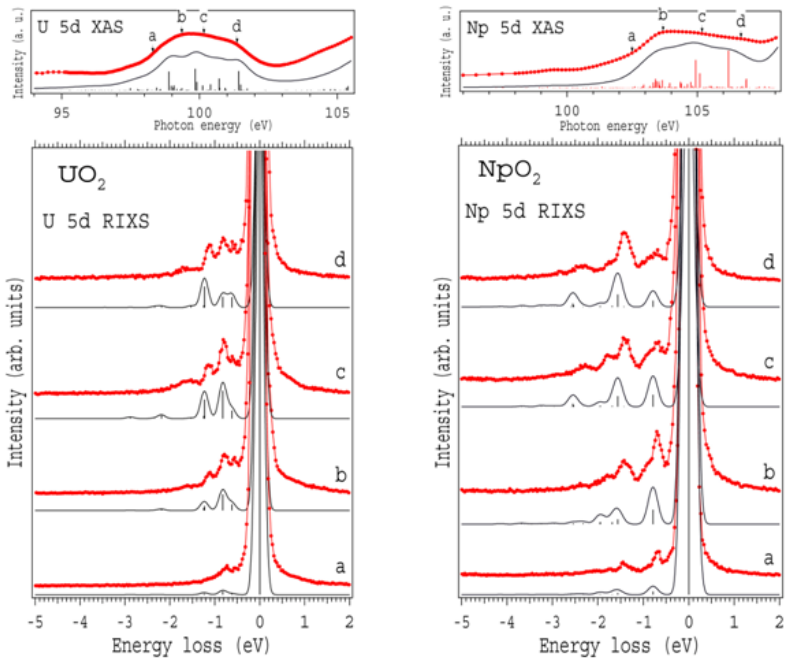

Figure 2.6: RIXS spectra of single-crystal UO_2 and poly-crystalline NpO_2 across 5d edge, recorded at different excitation energies around pre-threshold structure in 5d XAS (the excitation energies are indicated in the top panel of XAS). The figure also shows the results of atomic multiplet calculations for the U(IV) and Np(IV) ions.

Table 2.1: *Groundwater composition*

Na^+	Ca^{2+}	Mg^{2+}	K^+	SO_4^{2-}	Cl^-	HCO_3^-
52.5 mg/L	5.1 mg/L	0.7 mg/L	3.9 mg/L	9.6 mg/L	48.8 mg/L	65.0 mg/L

2.3 Corrosion of Copper Films in Aqueous Solutions

The disposal canister for the spent nuclear fuel has an outer shield made of copper, which is responsible for the corrosion protection of the inner canister. The thickness of the wall of the copper canister is 50 mm and this sets a limit of $0.5 \mu m\, y^{-1}$ for the maximum corrosion allowance of copper for a predefined lifetime of 100 000 years.

General corrosion of copper may occur in deep repository conditions due to the availability of corrosive groundwater components at the surface of copper canister. The composition of deep groundwaters vary considerable from site to site as well as in time [28]. Typical content of different ions in a low salinity groundwater is given in Table 2.1.

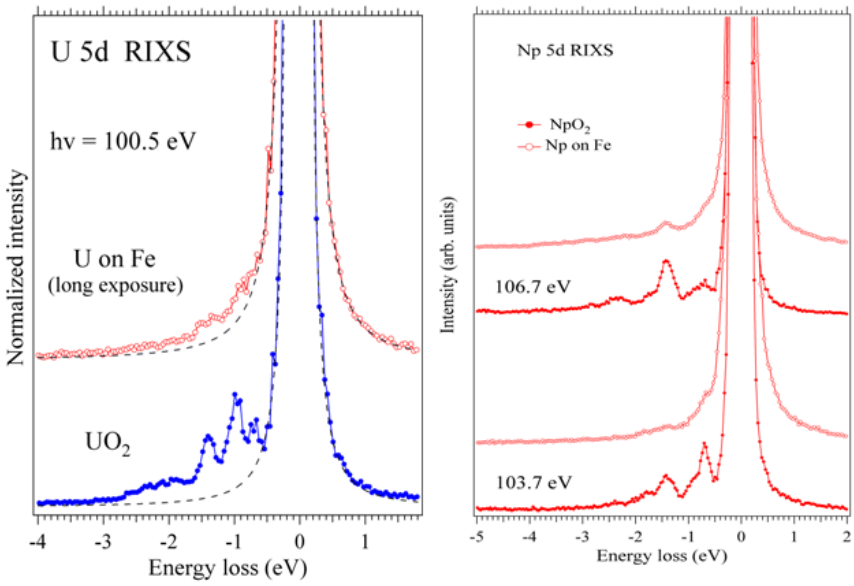

Figure 2.7: Comparison of 5d RIXS spectra of Np, U oxides and Np, U formed on the Fe strip, recorded at the excitation energies, close to that of the pre-threshold structure in the Np 5d and U 5d XA spectra.

The repository environment is oxidizing for some time after closure, but the oxygen will be consumed through reactions with minerals in the rock and also through microbial activity. It is therefore important to investigate the copper behavior in essentially oxygen-free conditions. In our experiments, we used liquid cells for the in-situ studies (Fig. 1.5) with synthetic groundwater (Table 2.1) and with de-ionized water with different concentrations of chloride, sulfate and carbonate ions.

2.3.1 Cu 2p XAS of Copper Films in Various Solutions

The surface modifications induced by chemical reactions on 100A Cu films with Cl^-, SO_4^{2-} and HCO_3^- ions in aqueous solutions were studied by XAS. It has been shown before that XAS can be used to determine the oxidation state of the copper for different types of compounds [29-31]. In the present study, Cu 2p XAS was applied to a number of liquid cells with different water compositions. In order to study the chemical reactions between copper films and various solutions, on the backside of the 100 nm Si_3N_4 windows 100A copper films were deposited. The spectral shape of the Cu 2p edge and the

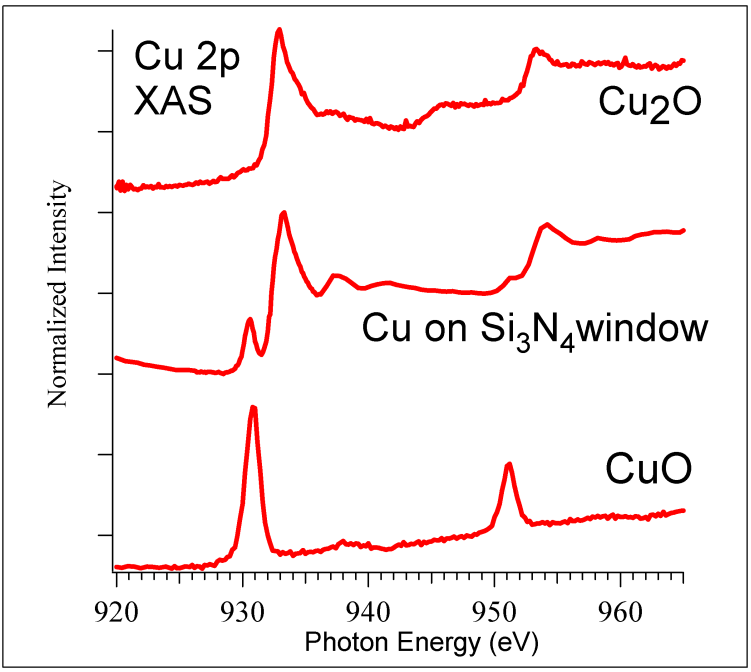

Figure 2.8: Cu 2p XA spectra of CuO, Cu_2O, and copper deposited on the 100 nm Si_3N_4 window, recorded in Total fluorescence yield (TFY) mode by photodiode.

chemical shift of the main Cu 2p absorption line served as a tool in monitoring the changes during the reaction.

First, we examined the 100A copper thin film deposited on the Si_3N_4 window by XAS (Fig. 2.8). For comparison Cu 2p XA spectra of monovalent and divalent copper are plotted. It is evident from Fig. 2.8 that both oxidized and metallic copper is present in the copper film on the window membrane. A discussion of whether copper is monovalent or divalent is relevant for studies of the corrosion processes because it is commonly considered that a corrosion product layer formed on copper consists of an inner layer of Cu_2O and an outer layer of Cu^{2+} oxides and other Cu^{2+} compounds, depending on the composition of the aqueous solution in contact with copper. The extent of the corrosion progress can, therefore, be evaluated by the valence state of the copper i.e. by the presence or absence of the divalent copper signal. Fully corroded copper will give very strong divalent copper signal in the XA spectrum. Relative intensities of Cu^{1+} and Cu^{2+} signals depend very strongly on the nature of the species present in the water solutions.

The main assumption in planning this experiment is that the surface films formed on copper in the repository environment is determine by concentration of Cl^- and HCO_3^- ions and pH values of the solutions. We also performed long-term corrosion experiments for a number of liquid cells with various compositions.

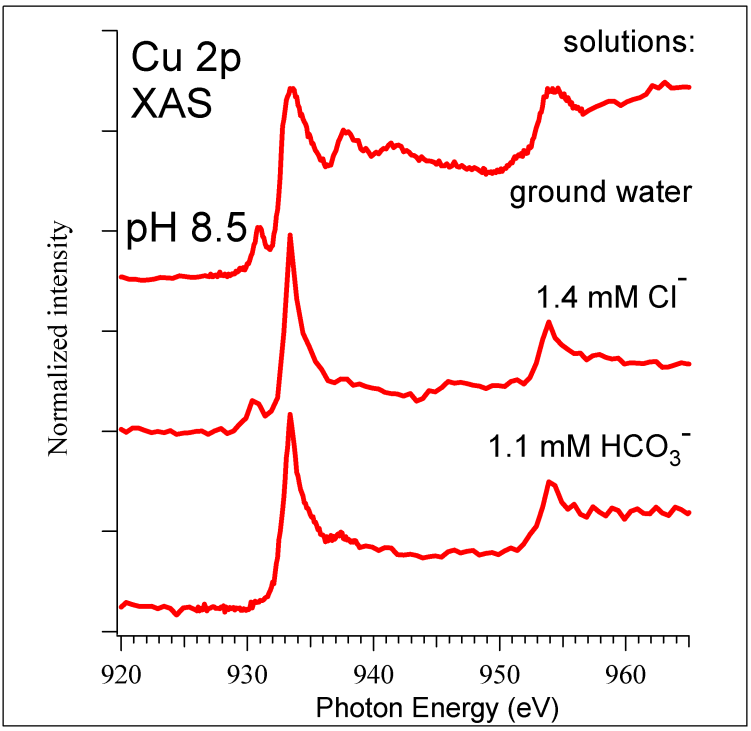

Figure 2.9: Cu 2p XA spectra of 100A thick copper film in liquid cells with: ground water solution and 1.4 mM Cl^- , 1.1 mM HCO_3^- solutions in ultra-pure distil deionized (MQ) water. pH value for all solutions was adjusted to 8.5.

The corrosion behavior of copper in synthetic groundwater solution was investigated. In order to do this, one drop ($\sim 4\mu$L) of groundwater solution was accommodated in the liquid cell. The Cu 2p XA spectrum of the film exposed to the solution for 1 hour (Fig. 2.9) shows mainly contribution of Cu^{1+} with a small admixture from divalent copper at the lower energy.

We believe that the Cu^{2+} formation in the groundwater will be dominated either by carbonate, chlorine or hydroxide complexes. For that reason, we chose HCO_3^- and Cl^- ions out of the other species in the groundwater solution and investigated independently their influence on the copper film using XAS.

Fig. 2.9 shows the Cu 2p XA spectrum taken from the copper film in the liquid cell after being for 1 hour in contact with Cl^- solution. The main line of the spectrum is at $\sim$ 933.3 eV and corresponds to monovalent copper. The presence of the divalent copper species manifests itself in the peak at 930.8 eV. The spectral intensity of the divalent peak was used to evaluate the corrosion rate of copper films exposed in the liquid cells containing different water compositions.

The main line of the Cu 2p XA spectrum from the copper film exposed for 1 hour in carbonate solution (Fig. 2.9), however, indicates presence of only monovalent copper. The Cu^{2+} peak is not observed in this spectrum thus

suggesting that carbonate species present in the solution protect the copper film from further corrosion. This is in accordance with previous observations [32]. Adeloju and Duan [33] suggest that the increased protectiveness is a consequence of pH buffering by HCO_3^-, which stabilises the Cu_2O film rather than the formation of basic cupric carbonate species.

It can be seen from Fig. 2.9 that the intensity of the divalent copper during the XAS measurements depended on the composition of the solution used in the liquid cell. Moreover, the intensity of divalent copper in copper film taken from Si_3N_4 membrane (Fig. 2.8) is a little bit higher than the intensity of the divalent peak in Cu 2p XAS taken from copper film exposed to groundwater solution (Fig. 2.9), thus indicating the reduction of corrosion processes in groundwater environment. This is unexpected since the groundwater contains the aggressive species, such as chorine and sulfate ions.

The concentration of chlorine ions in the groundwater is quite small (1.4 mM) in comparison with a marine environment (1.5M). The Cu 2p XAS investigations of copper film exposed in solutions with different concentration of Cl^- ions are reported in Paper VIII and Paper IX together with investigations on influence of the pH value in aqueous solutions on the corrosion processes. It was shown that copper film in various solutions corroded much faster with pH value higher than 8.5. Even chlorine ions in small concentrations show surprisingly strong sensitivity to the pH value. It was reported in Papers VIII and IX that monovalent copper predominantly formed on the copper film at pH 6.0 and 8.5. and divalent copper appears to be particular strong at pH 10.0 and 12.0. This pH dependent behavior is consistent with the Pourbaix diagram [34], which shows the formation of divalent copper species at pH higher than 8. It also indicates that the oxidation of copper at pH 8.5 in the presence of 1.4 mM Cl^- ion is less favorable than its oxidation to divalent copper at pH 10.0 and 12.0.

The Cu 2p XA spectrum from a copper film exposed to a 1.4 mM Cl^- solution in the liquid cell for 1 hour is shown on Fig. 2.10. The pH value of the solution was adjusted to 10 by adding a small amount of sodium hydroxide NaOH. The data reveal almost fully corroded copper in this case.

It was suggested that the presence of carbonate ions [32] may lead to a decreasing the amount of divalent copper in Cu 2p XAS from copper film in groundwater solution for compare to those peak in Cu 2p XAS from copper film deposited on the back side of Si_3N_4 window.

In order to understand how copper will respond to the carbonate treatment we added to the above described solution (1.4 mM Cl^- with pH 10.0) 1.1 mM HCO_3^- ions. This is the same concentration of carbonate ions as in the groundwater. A good example of a conflict between corrosion and reduction of copper corrosion rates are presented in Fig. 2.10 (bottom). The monovalent copper signal is clearly observed in this spectrum, which indicates that in a solution already containing 1.4mM Cl^- with pH 10.0, the corrosion of copper

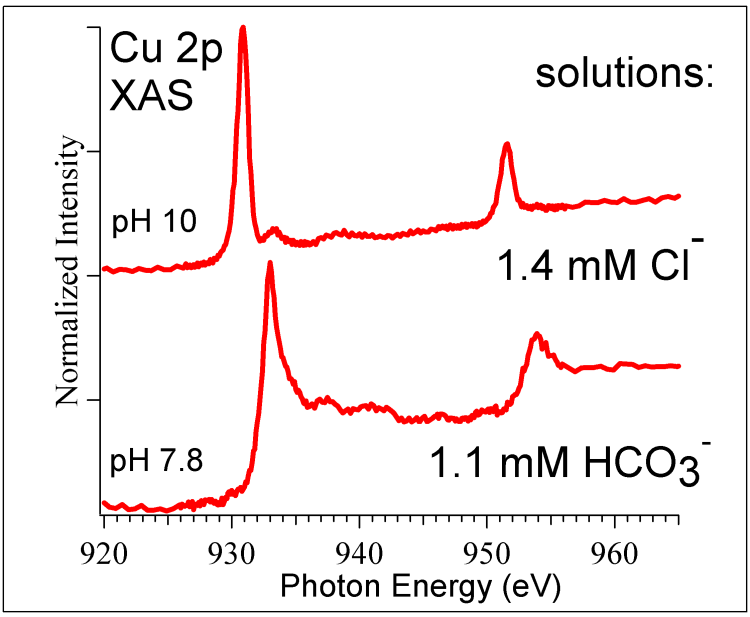

Figure 2.10: Cu 2p X-ray absorption spectrum of the copper film (top) in the liquid cell exposed for 1 hour to the 1.4 mM Cl^- solution in MQ water and increased pH up to 10 by means of NaOH. Cu 2p X-ray absorption spectrum of the copper film (bottom) with the same exposure to the above described solution but with added 1.1 mM HCO_3^- ions.

film had not progressed to form divalent copper in the presence of 1.1 mM HCO_3^- ions.

We, therefore, also investigated the dependence on the exposure time to the groundwater solution. Fig. 2.11 shows how the intensity of the divalent copper signal varies with time for a copper film in a liquid cell containing groundwater solution with pH 8.5. The Cu 2p XA spectrum for the freshly made liquid cell (after 1 hour exposure time) shows the presence of the divalent copper signal but the monovalent copper signal is still dominating. After 5 days exposure time, the intensities of the monovalent and the divalent copper are similar and after 9 days exposure time there is only divalent copper present. However, it is not clear which complexes are formed on copper film after 9 days exposure time in contact with groundwater solution. Copper oxide, hydroxide, carbonate and chlorine ions can be involved in forming the divalent copper species depending on parameters such as pH and carbonate and chlorine concentrations. Fig. 2.12 is summarizing the results from our study of the corrosion of copper films in various aqueous solutions.

It is reported in Paper VIII and Paper IX that the corrosion proceeded to form Cu^{2+} in the several different systems:

- in solution, containing high Cl^- concentration - 1.5M
- in pH solutions higher than 10.0, containing 1.4 mM Cl^- ion

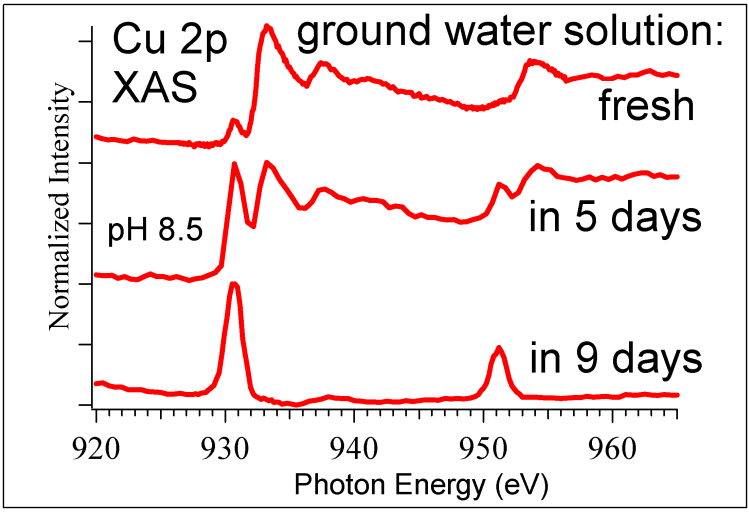

Figure 2.11: Dependence of Cu 2p XA spectra of 100A thick copper film in liquid cells on the exposure time to groundwater solution.

- in groundwater solution after 9 days exposure time of copper film in that solution

A discussion of whether Cu is monovalent or divalent is relevant since copper can form compounds with different valences. In ordinary oxygen containing environments the surface layer is expected to be a duplex Cu_2O/CuO, $Cu(OH)_2$ structure. In that case, XAS is not capable of giving significant difference between the different divalent copper compounds. We examined the possibility of using RIXS to probe the electronic structure of copper films in liquid cells with groundwater solution.

2.3.2 Cu 2p RIXS of Copper Film in Groundwater Solution

The investigations of Cu 2p-3d RIXS for various copper compounds are reported in Paper VII. The Cu 2p-3d RIXS spectra of Cu_2O, CuO, $Cu(OH)_2$, $CuCl_2$, $CuSO_4$, malachite $Cu_2(CO_3)_2(OH)_2$, and atacamite $CuCl_2{\cdot}3Cu(OH)_2$ were measured for different excitations energies. It has been shown that the Cu 2p RIXS spectra are mainly composed of two parts: the 3d intra-atomic excitations and the structures due to charge transfer excitations from the ligand band to the 3d level [35-36]. We found that the RIXS spectra excited at energies in the range of satellite structures in the Cu 2p XA spectrum are different for the different compounds.

It is shown in the Paper VII that using Cu 2p RIXS the characteristic differences in the hybridization between Cu^{2+} and Cl^-, SO_4^{2-}, OH^- and HCO_3^- ions could be found. This can be used as a finger print in interpretation of complex materials.

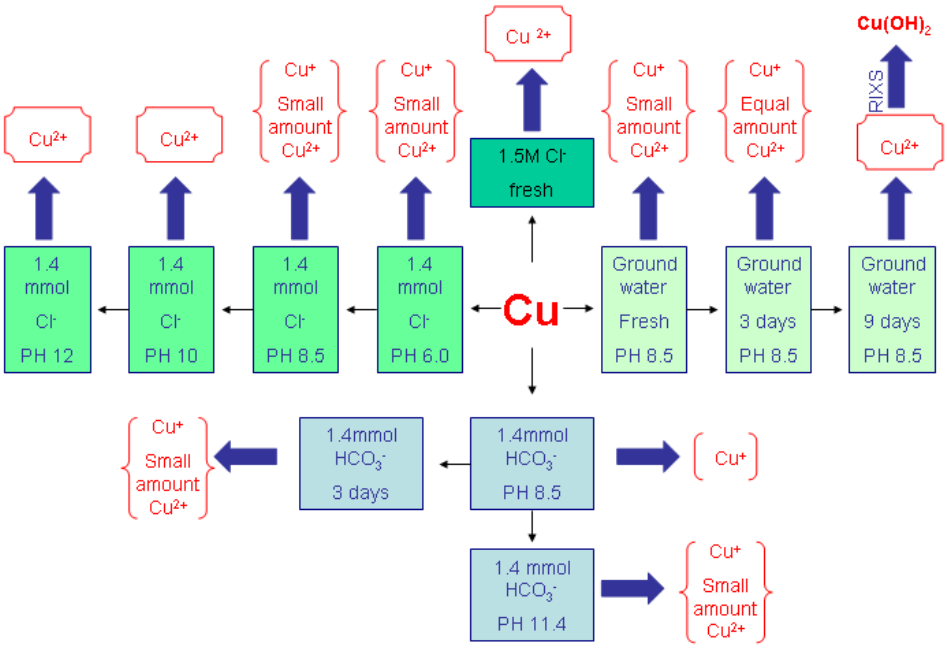

Figure 2.12: Schematic summary of the copper corrosion processes in different solutions.

In the present study, malachite, copper hydroxide and copper chloride were suggested to investigate as predominant phases formed on the surface of the corroded copper in the groundwater solution. Fig. 2.13 show Cu 2p RIXS spectra on $CuCl_2$, $Cu(OH)_2$, and malachite $Cu_2(CO_3)_2(OH)_2$ recorded at the same excitation energy 933.6 eV. This energy corresponds to the satellite structure in the XA spectrum, associated with the $2p^5 3d^9 s$ contribution, which shape is defined by s-density of states in the conduction band. Although, in some publications this satellite structure in the XA spectrum was described being a result of exciting "defect states", i.e. $3d^9\underline{L}$ initial state leading to the $2p^5 3d^{10}\underline{L}$ excitations ($\underline{L}$ stands for a hole in the ligand 2p band) [29]. RIXS spectra clearly show significant differences in the shape which are a result of difference in chemical bonding in these compounds. The spectral difference can be taken as advantage in identification of corrosion products formed on the copper film in the liquid cell with groundwater solution.

Fig. 2.13 also shows the RIXS spectrum of the fully corroded copper film in contact with the groundwater solution. Due to the experimental difficulties, the spectrum was recorded at an excitation energy lower by 0.6 eV than that for the spectra of reference compounds. This energy is still in the range of the satellite structure in the XA spectrum and the energy difference is within total experimental resolution used for RIXS measurements. The shape and the

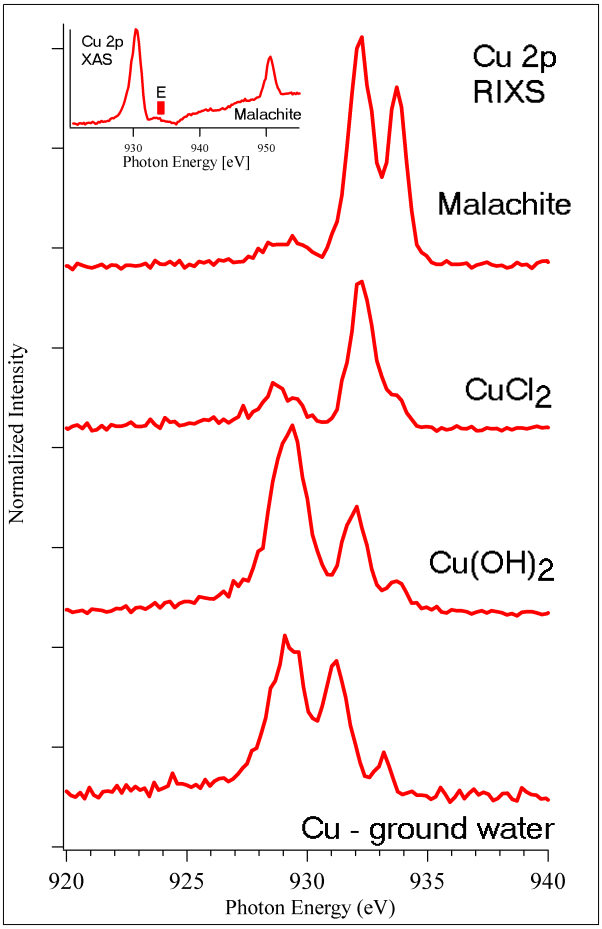

Figure 2.13: RIXS spectra of $CuCl_2$, $Cu(OH)_2$, malachite $Cu_2(CO_3)_2(OH)_2$ and 100A thick copper film in liquid cell with groundwater solution recorded at the excitation energy indicated in the top panel of XA spectrum.

intensities of the RIXS spectrum are similar to that of $Cu(OH)_2$ suggesting the formation of hydroxide species.

The study by Hamilton et al. [37] was performed using Raman spectroscopy, applying 488 nm laser excitations on a copper film in 0.1M NaOH solution. They showed that initially Cu_2O and then $Cu(OH)_2$ were formed by comparison with the oxide spectra. Melenders et al.[38] studied *in-situ* copper oxidation in alkaline media by infrared spectroscopy using synchrotron radiation. The initially formed corrosion product as Cu_2O with later formation of CuO or $Cu(OH)_2$ was identified.

The RIXS spectrum (Fig. 2.13) provides important information on the chemical composition and confirms unambiguously that hydroxide species were formed on the studied copper film in contact with the groundwater solution. The great sensitivity of the RIXS spectra profile to the type of

copper species allows us to better assess the chemical composition of the corroded copper film.

Acknowledgements

I'd like to express my sincere gratitude to people, who guided, encouraged, supported me and work with me every day or occasionally, who have been of great help and kept friendly atmosphere during my education.

Therefore, I would like to start my acknowledgements with Sergei Butorin, my supervisor for his tremendous help, constant support and very interesting discussions about spectroscopy, from which I learned a lot. He shared with me his knowledge about theoretical and practical advises, engineering aspects of the beamlines and all experimental tricks. As a result, I got a great experience and learned how the scientific problems should be solved out in a proper way!

I also would like to thank Prof. Joseph Nordgren for the great opportunity to work in his group, for providing a very pleasant working environment and for excellent support as a head of research group.

This work would not be done without a creative support from Prof. Lars Werme, who became my second supervisor. It was so interesting to be involved in "actinide" project and got the knowledge about nuclear spent fuel studies. Many thanks for all simulating discussions and answering my questions 24 hours in day! Special thanks for all help in writing the papers and this thesis!

My warmest thanks to Jinghua Guo for guidance, hospitality and for sharing extraordinary knowledge in the field of synchrotron radiation and beamline operation. I really appreciate your patience in all problems which I created with vacuum, ion pump and other equipments :))) It was always a pleasant time at ALS! Here I also would like to acknowledge David Shuh together with Brian, Aran, Tim, Per-Anders and Jau-Wern for the all help at ALS during my experiments. My special thanks to Stepan Kashtanov, who never hesitated when help was need and for being a good friend. It was a very nice time in Berkeley, San Francisco, Monterey and in all other places where we were together!

Big thanks to all my collaborators for the input, knowledge and patient teaching, which they have provided: Elke Arenholz, Inna Soroka, Moreno Marcellini, Sergei Arapan, Rajeev Ahuja, Hans Nilsson, Alexandr Talyzin, Mikael Ottosson and Rolf Berger. It was a pleasure to work with all of you!

A lot of thanks to Susanne Mribt, Anne Kronquist and Gunnel Ingelog for the great administrative help.

I would also like to thank all present and former members of the USX-group: Ruben (Prof. Jan-Erik Rubensson), Kevin (Prof. Smith), Calle (Carl-

Johan Englund), Andreas A., Anders O., Conny S., Egil A., Florentina T., Johan S., Johan F., Joakim A., Hakan H., Laurent D., Limin Q., Lia D., Magnus S., Marcus A., Martin M., Misha Y., Natalie S., Thorsten S. and Tanel K. And one more thanks to Anders Modin, who spend with me days and nights at ALS and Maxlab and for all fun which we had together during the last year!

I'd like to thank once more all the people I had pleasure to work, collaborate and all my friends in Uppsala, Stockholm and around the world for their support, help and nice company during these years. Especially, my sincerely thanks go to Boriss Mahrov for unlimited support, patience during the course "Physical Chemistry" and for everything what you did and still doing for us - Spasibo!

Finally, I'd like to thank my parents and all my family, who let me do what I wished to do and everything else that I got during my life, which brought me to this day. Special thanks to my brother, who provided hand made pictures for this thesis. And one more thanks to my grand mother in Ukraine for her constant support in all these years and for being always ready to go to Sweden within next 12 hours.

And last, but most of all, to Jan and Slava for their love, help, belief and love again!

3. Summary in Swedish

Resonant inelastisk röntgenspridning av jordartsmetall- och kopparsystem

Sällsynta jordartsmetall- och kopparsystem studerades med hjälp av röntgenabsorptionsspektroskopi, ”X-ray Absorption Spectroscopy” (XAS), och resonant inelastisk röntgenspridning ”Resonant Inelastic X-ray Scattering” (RIXS). Användandet av monokromatisk synkrotronstrålning tillsammans med den höga energiupplösningen med RIXS gjorde det möjligt att erhålla viktig information om den elektronstrukturen i 4f, 5f och 3d-system. Experimentella resultat för sällsynta jordartsmetaller vidimerades av modellberäkningar baserade på atomär multipletteori. 4d - 4f-övergångar för holmium och gadolinium, uppmätta med XAS och RIXS, jämfördes med beräkningar gjorda för Ho^{3+} respektive Gd^{3+}-joner, vilka approximerar jordartsmetaller väl. RIXS användes också för att bestämma rollen av laddningsöverföringsprocesser i Gd- och Ho-hydridsystem. Det kunde fastställas att RIXS-satelliterna som beror på en elektronexcitation från en H-atom till Gd 4f-nivån endast uppstår i Gd - H-system. Denna observation påvisar att den elektroniska strukturen i Gd-hydrid beskrivs bäst av en modell baserad på negativt laddade vätejoner (H^-).

Atomär multipletteori beskriver ganska väl spektra för lantanidsystem över 4d-kanten. 5d- och 5f-skalen för aktinider har liknande generell karakteristik som 4d- och 4f-skal för lantanider. Detta tyder på att denna teoretiska modell även passar aktinider bra. Elektronstruturen för curium, som motsvarar den hos gadolinium ur valenssynpunkt, har undersökts med XAS och RIXS över 5d-kanten. Aktiniders 5d-absorptionspektra uppvisar inte många skarpa egenskaper, och detta minskar användbarheten för XAS. Inelastiskt spridda strukturer i RIXS spektra över 5d-kanten visade sig dock vara känsliga för oxidationstillståndet i de studerade aktinidsystemen. Jämförelse mellan experimentella och beräknade curium 5d-RIXS- spektra gav direkt information om valensen för 248-Cm-isotopen i syre.

Studier av aktinider är också viktiga ur miljöhänseende. Aktinider, såsom uran, neptunium och plutonium ger stora bidrag till den långsiktiga radioaktiviteten i kärnavfall. Genom att undersöka växelverkan mellan U-, Np- och Pu-joner med korroderade järnytor ökas den vetenskapliga förståelsen för de processer som styr de kemiska förändringarna i radioaktiva ämnen från utbränt kärnbränsle. RIXS-profiler, motsvarande f – f-övergångar ger en god

bild av valenstillstånden för U, Np och Pu i olika system. Det visade sig att järnytor reducerade U(VI), Np(V) och Pu(VI) till U(IV), Np(IV) och Pu(IV), vilket indikerar att förekomsten av järn markant påverkar mobiliteten för aktinider och skapar reducerande förhållanden. Detta resultat är viktigt då reduceringen av aktinider inuti en kärnbränslekapsel med järninsats kan förhindra spridning av aktinider via grundvattnet, på grund av den mycket lägre lösligheten hos de reducerade ämnena U(IV), Np(IV) och Pu(IV) i jämförelse med U(VI), Np(V) och Pu(VI).

Korrosionen av kopparkapseln i slutförvaret styrs av tillgången på korrosiva ämnen i det grundvatten som är i kontakt med kapseln. Det är därför viktig med *in-situ*-studier av korrosionsprocesserna med hjälp av olika metoder. För 3d-system såsom kopparföreningar är XAS en ämnesspecifik teknik och ger detaljerad information om blandade valenssystem. En diskussion huruvida koppar är monovalent eller divalent är relevant för studier av korrosionsprocesser eftersom det är allmänt vedertaget att det korrosionsproduktskikt som bildas på koppar består av ett inre skikt av Cu_2O och ett yttre lager Cu^{2+}-oxider och andra Cu^{2+}-föreningar, beroende på sammansättningen av vattenlösningen i kontakt med kopparn. Omfattningen av korrosionsförloppet kan därför bedömas av valenstillståndet för koppar, genom förekomsten eller avsaknaden av den divalenta kopparsignalen. Fullständigt korroderad koppar ger en mycket stark divalent kopparsignal i XAS-spektrat. De relativa intensiteterna för Cu^{1+}- och Cu^{2+}-signalerna är starkt beroende av vilka ämnen som ingår i vattenlösningen.

Ytförändringar framkallade av kemiska reaktioner mellan 100 Å oxiderade Cu-filmer och olika koncentrationer av Cl^-, SO_4^{2-} och HCO_3^- joner i vattenlösningar studerades in-situ med hjälp av vätskeceller. Kopparkorrosionsprocesser i syntetiskt grundvatten studerades ända upp till nio dagar. Det visade sig att pH-värdet, Cl^- -jonkoncentrationen och förekomsten av HCO_3^--joner i lösningarna påverkar hastigheten av korrosionsreaktionen kraftigt. RIXS användes för att bestämma den kemiska sammansättningen hos kopparkorrosionsprodukten i en vätskecell bestående av en tunn kopparfilm i kontakt med en grundvattenlösning. Röntgenabsorptionsspektrat visade i detta fall förekomst av divalent koppar och RIXS uppvisade en kemisk bindning för Cu-atomerna liknande den i kopparhydroxid.

Bibliography

1 Cowan R.D., The theory of Atomic Structure and spectra (University of California Press, Berkeley, 1981)
2 Ma Y., Wassdahl N., Skytt P., Guo J.-H., Nordgren J.,Johnson P.J.,Rubensson J.-E., Boske T., Eberhardt W. and Kevan S.D., Physical Review Letters, Vol.69, No.17. 1992
3 Rubensson J.-E., Journal of Electron Spectroscopy and Related Phenomena 110-111 (2000)135-151
4 Butorin S. J. of Elect. Spectr. and Relat. Phenom. 110-111 (2000) 235-273
5 Nordgren J., Guo J.-H., Journal of Electron Spectroscopy and Related Phenomena 110-111 (2000)1-13
6 Warwick T., Heimann P., Mossessian D., McKinney W., Padmore H., Rev. Sci. Instrum. 66 (1995) 2037.
7 Nordgren J., Bray G., Cramm S., Nyholm S., Rubensson J.-E. and Wassdahl N., Rev. Sci. Instrum. 60 1690 (1989)
8 Padmore H.A. and Warwick T., J.Synchrotron Radiation, 1, 27 (1994).
9 Lynch D.W., Cowan R.D., Phyical Review B, Vol.36, No.17, 1987
10 Ogasawara H., Kotani A., Thole B.T., Phyical Review B, Vol.44, No.5, 1991
11 Butorin, S. M. Journal of Electron Spectroscopy and Related Phenomena, vol.110-111, no.1-3 (2000), 213-233
12 Butorin, S. M.; Guo, J.-H.; Wassdahl, N.; Nordgren, J., J. Phys., Condens. Matter, vol.12, no.28 (2000)
13 Guo, J.-H.; Butorin, S. M.; Wassdahl, N.; Nordgren, J.; Berastegut, P.; Johansson, L.-G., Physical Review B, V.61, 9140 (2000)
14 Butorin, S. M.; Magnuson, M.; Ivanov, K.; Shuh, D. K.; Takahashi, T.; Kunii, S.; Guo, J.-H.; Nordgren, J., Journal of Electron Spectroscopy and Related Phenomena, V.101-103 (1999)
15 Butorin, S.M.; Duda, L.-C.; Guo, J.-H.; Wassdahl, N.; Nordgren, J.; Nakazawa, M.; Kotani, A. Journal of Physics: Condensed Matter, V.9, 8155 (1997)
16 Butorin S.M., Sathe. C, Agui A., Saalem F., Alonso J.A., Nordgren J. Solid State Communications 135 (2005) 716-720
17 Tanaka S., Okada K. and Kotani A., J. Phys. Soc. Jpn. 63, 2780 (1994)
18 Ogasawara H., Kotani A., Thole B.T., Phys.Rev.B 50, 12332 (1994)
19 Imada S. and Jo T., J. of Phys. Soc. of Japan vol.59, N9,1990, pp.3358-3373

20 Frank de Groot, Chemicals Review V.101 N6 (2000)
21 Richter M., Meyeer M., Pahler M., Prescher T., Raven E.V., Sonntag B., Wetzel H.-E., Phys. Rev A 40, 12 (1989)
22 Huiberts, J.N. et al. Nature 380, 231-234 (1996)
23 Ng, K.K., Zhang, F.C., Anisimov, V.I., Rice, T.M., Phys. Rev. B59, 5398-5413 (1999)
24 Eder, R., Pen, H. A., Sawatzky, G. A., Phys. Rev. B 56, 10115-10120 (1997).
25 Moewes A., Eskildsen T., Ederer D.L., Wang J., McGuire J., Callcot T.A., Phys. Rev. B 57, 20 (1998)
26 Werme L., Technical Report TR 98-08, Design premises for canister for pnt nuckear fuel, SKB, 1998; Wendy Barnaby, Nature vol 274, 6, (1978)
27 Kalkowski G., Kaindl G., Brewer W.D., Krone W., Phys. Rev. B35, 2667-2677 (1987)
28 King F., Ahonen L., Taxn C., Vuorinen U., Werme L., Copper corrosion under expected conditions in a deep geologic repository, Svensk Krnbrnslahantering AB (SKB) Report TR-01-23
29 G. van der Laan, Pattrick R. A. D., Henderson C.M.B. and Vaughan D.J., J. Phys.Solids 53, 9, 1185-1190 (1992)
30 Koster A. S., Molecular Physics, 26, N3, 625-632 (1973)
31 Grioni M., Goedkoop J.B., Schoorl R., de Groot F.M., and Fuggle J.C., Schfers F. Koch E. E., Rossi G., Esteva J.M., and Karnatak C., Phys. Rev. B 39, 1541-1545 (1989)
32 Ribotta S.B., Folquer M.E., Vilche J.R., Corrosion 51 (1995) p. 682.
33 Adeloju S.B. and Duan Y.Y., Br. Corros. J., 29 (1994) p.315.
34 Pourbaix M., PhD Thesis, Unversite Libredes Bruxelles (1945), Pourbaix M., 1966. Atlas of Electrochemical Equilibria in Aqueous Solutions. Pergamon Press, New York
35 Magnusson M., Wassdahl N. and Nordgren J., Phys. Rev B 56, 19 (1997)
36 Ghiringhelli, G; Brookes, N.B.; Annese, E.; Berger, H.; Dallera, C.; Grioni, M.; Perfetti, L.; Tagliaferri, A.; Braicovich, L. Phys. Rev. Let. v 92, n 11, (2004) p 117406
37 Hamilton J. C., Farmer J.C., Anderson R.J., J. Electrochem. Soc. 133, 739 (1986)
38 Melendres C.A., Bowmaker G.A., Leger J.M., Beden B.J.,Electroanal. Chem. 449, 215 (1998)

Acta Universitatis Upsaliensis

Digital Comprehensive Summaries of Uppsala Dissertations from the Faculty of Science and Technology 205

Editor: The Dean of the Faculty of Science and Technology

A doctoral dissertation from the Faculty of Science and Technology, Uppsala University, is usually a summary of a number of papers. A few copies of the complete dissertation are kept at major Swedish research libraries, while the summary alone is distributed internationally through the series Digital Comprehensive Summaries of Uppsala Dissertations from the Faculty of Science and Technology. (Prior to January, 2005, the series was published under the title "Comprehensive Summaries of Uppsala Dissertations from the Faculty of Science and Technology".)

Distribution: publications.uu.se
urn:nbn:se:uu:diva-7094

ACTA
UNIVERSITATIS
UPSALIENSIS
UPPSALA
2006

Paper I

Influence of hydrogen on properties of rare-earth hydrides studied by resonant inelastic x-ray scattering spectroscopy

K.O. Kvashnina[1], S. M. Butorin[1], B.Hjörvarsson[1], J.-H. Guo[2] and J. Nordgren[1]

[1] *Department of Physics, Uppsala University,*

Box 530, S-751 21 Uppsala, Sweden and

[2] *Advanced Light Source, Lawrence Berkeley National Laboratory, Berkeley, CA 94720, USA*

Abstract

In present study, the electronic structure di and trihydrides of gadolinium and holmium were examined by x-ray absorption spectroscopy (XAS) and resonant inelastic x-ray scattering (RIXS) at the Gd and Ho 4d thresholds. Experimental spectra were compared with atomic multiplet calculations of the 4d-4f transitions for Ho^{3+} and Gd^{3+} ions, which indicate that most of RIXS structures correspond to intra-atomic f-f excitations. RIXS was also used to determine the role of charge transfer processes in Gd and Ho hydrides. It was found that RIXS satellites, due to an electron excitation from H atom to the Gd 4f level occur only in Gd-H systems. In the region of around 10 ev bellow the elastic peak no similar charge-transfer structures can be observed for Ho-H systems. These satellite observations suggest the view that negatively charged hydrogen in Gd hydrides is an electron acceptor, which is somewhat unusual for the hydrogen behavior in metals.

I. INTRODUCTION

In the past several decades much interest has been focused on understanding of scattering processes in soft x-ray region. There are two primary reasons for this interest. First of all several third generation synchrotron light sources delivery light with much greater brightness then previous sources. The second one is the increasing complexity of the material systems that are of interest from both industrial and science research. X-ray absorption (XAS) and emission (XES) spectroscopic methods provide new possibilities to study the local electronic structure near the exited atom in complex rare-earth systems.

The pioneering XAS and XES measurements near 4d threshold was done by Zimkina and co-workers using electron-beam bombardment for twelve rare-earths metals[1]. According to their results, 3 types of transition were occurred for all twelve metals: $4d^9 5p^{n+1} 4f^n$ - $4d^{10} 5p^n 4f^n$, $4d^9 4f^{n+1}$ - $4d^{10} 4f^n$ and $4d^9 4f^n$ - $4d^{10} 4f^{n+1}$. Recently Gallet et al.[2] reported inelastic scattering features (RIXS) in Gadolinium metal with an energy loss of 25-27 eV, which was interpreted as 5p-4d transitions. Also weak structure was observed close to the elastic peak and was identified as the result of the spin-flip excitations. Later, gadolinium oxide was studied by Moewes et al. around 4d threshold using the same methods[3]. The excitation energies were chosen near the "giant"[4] resonance (from 133 eV to 168 eV) and discussion was focused on both elastic and inelastic scattering. In all papers experimental results were reinterpreted by the commonly used theory based on the Hartree-Fock calculations. Jack Sugar first presented the details of these types of calculations[5]. Later it was repeated by Tanaka et al.[6] and Ogasawara, Kotani and Thole[7] where they took into account the Beutler-Fano profiles through the 4d-4f Coster-Kronig transition.

L_3[Ref.9] and $M_{[4,5]}$ [Ref. 10,11] edges of gadolinium metal and their compounds, such as chlorides[12], fluorides[13] and hydrides[14] were also studied extensively by resonant inelastic scattering and other spectroscopies. Recently hydrogen-metal systems have been in focus of extended discussions since Huibert et al. reported that hydrogen induced optical switching and metallic lanthanum and yttrium films becoming transparent under hydrogen loading[14]. The underlying principle is a transition between the reflective metallic state and insulating state[16]. Such a switchable mirror can be put to good use in displays and lightning systems, especially when the light source is difficult to reach and adjust. Also Gd-H systems have been studied intesively using broad range of spectroscopic techniques[15].

Special attention paid to the magnetic properties of lanthanides. Magnetic circular dichroism (XMCD) was mostly used to study magnetic behavior of Gd[17−22], Tb[20−22], Dy[22]. Krisch et al.[9] used circular polarized x-rays to study RIXS at Gd 2p threshold and weak $2p^5 4f^{n+1}$ quadrupolar excitation separated from the intense $2p^5 5d^1$ white line at the absorption edge. Magnetic behavior of holmium metal and compounds was investigated in [Ref.23-27] since holmium was recognized as interesting case in development of Ho-Y garnets[28], which have microwave applications. But nobody has before examined holmium metal in terms of RIXS transitions at the 4d edge using synchrotron radiation. In this paper we report on RIXS of holmium and gadolinium metals and their hydrides. Gadolinium and holmium are very similar from a chemical point of view and each of them has its own very specific physical properties including color, luminescent behavior and magnetic properties. This unique chemical similarity is due to shielding of 4f valence electrons by the completely filled $6s^2$ orbitals.

XA spectra for Ho and Gd were first observed by Zimkina et al.[1] but holmium and gadolinium RIXS features near the elastic peak for the different excitation energies will be presented in the first time as well as RIXS data for the Ho dihydrides and trihydrides.

RIXS was used to determine the role of charge transfer processes in gadolinium and holmium hydrides. Our experimental data for the metals compared with theoretical calculations based on the atomic multiplet theory[29]. Theoretical simulations have been made in the similar way as by Imada and Jo [8] for 3+ valences as a good approximation for the metal, using Cowan code [29,30]. Gadolinium and holmium were chosen as interesting systems due to the simplicity in reproducing experimental results by the theoretical calculations. The Gd and Ho metal samples have the advantage that they were grown using molecular - beam epitaxial (MBE) technique[31]. MBE is the most commonly used technique for growth of rare earths films on sapphire substrates and was first exploited by Kwo et al.[32] and Dublin et al.[33]. Niobium was deposited on top of the lanthanide films to prevent an oxidation reaction of metals. Typical thicknesses of the Nb and Ho/Gd layers were 5 and 200 nm respectively. High quality of the metal samples together with high flux x-ray synchrotron radiation allowed us to measure the absorption and scattering spectra with high resolution and make a comparison with theoretical calculations.

II. THEORETICAL CALCULATIONS

The calculations were carried out for free 3+ ions of gadolinium and holmium using atomic multiplet theory described previously [6−8,29]. This theory is a technique used to approximately solve the Schrödinger equation. It was found that the approximate solutions to the Schrödinger equation can be written in the form

$$\Psi(r,\theta,\varphi) \; = \; r^{-1} \cdot R_{nl}(r) \cdot Y_{lms}(\theta,\phi) \tag{1}$$

where the radial and angular matrix elements can be calculated separately. At this stage, the energy levels are characterized by the quantum numbers (nl). The radial wave functions are calculated with standard Hartree-Fock codes which give values of Slater integrals.

The Hamiltonian is given by

$$H \; = \; H_{ee}(F^2(f), F^4(f), F^6(f), F^2(fd), F^4(fd),$$

$$G^1(fd), G^3(fd), G^5(fd)) + H_d(\xi d) + H_f(\xi f) \tag{2}$$

where H_{ee} is the electrostatic interaction between the 4f electrons and between the 4f and the 4d electrons that gives rise to atomic multiplets. H_f (H_d) is the spin-orbit interaction of 4f-4d electrons with the coupling constant ξ_d,ξ_f.

The parameters for the rare-earth configurations were calculated using Cowan's program [29]. This uses the Hartree-Fock plus statistical exchange methods to evaluate and adjust the Slater integrals and spin-orbit constants. Those Slater integrals F_k(4f,4f) were reduced to 80% , the F_k (4_d,4_f) and G_k(4d,4f)integrals to 75%, 66% respectively. This should account for the effect of configuration interactions. This effect was first discussed by Lynch [31] and found that the reduction in Slater integrals should not be the same for all lanthanides. Slater integrals should get smaller with increasing the lanthanide atomic number and will affect broadening of the spectra.

The calculations of Gd and Ho 4d XAS metals were made in a similar way as by Imada and Jo [8] where they took free 3+ ions as a good approximation for metals. The configuration of the outer electrons in Gd^{3+} is $4d^{10}5s^25p^64f^7$ and has the half filled 4f shell. The ground

TABLE I: Parameter values used in the calculations for the ground and excited states. Reduced Slater integrals F and G and spin-orbit constant ξ are given in eV

Z	Ho^{3+}	Gd^{3+}
F^2(4f,4f)	12.7	11.7
F^4(4f,4f)	8.0	7.4
F^6(4f,4f)	5.7	5.3
ξ_{4f}	0.28	0.20
ξ_{4d}	2.8	2.2
F^2(4d,4f)	13.2	12.3
F^4(4d,4f)	8.5	7.9
G^1(4d,4f)	13.7	13.0
G^3(4d,4f)	8.6	8.15
G^5(4d,4f)	6.1	5.7

state $^8S_{7/2}$ has spherical symmetry which is very stable and less affected by the crystal filed. Similar effect is observed for Ho metal. We show in Table I the adopted values of the Slater integrals and spin -orbit constants.

The ground state have J value decided by Hund's rule. The final states have only three possibilities J-1, J, J+1. These dipole selection rules reduce the number of states which can be reached from ground state configuration, but it is still very large. Ho^{3+} has 61 dipole-allowed transitions and gadolinium is more complex case. There are 1077 dipole-allowed transitions for Gd^{3+} and most of them are weak. These are shown in Fig.1, where it is easy to see a few weak prethreshold peaks and the dipole allowed giant band for both lanthanides but. It was clearly observed before by Richter et al.[36] that increasing nuclear charged Z shifts all peaks towards to higher energy. 4d-4f resonance for gadolinium (Z=64) is situated in the energy range between 137-160 eV and for holmium (Z=67) between 158-185 eV. Due to strong electron correlations and autoionization these 4d-4f transitions produce "giant resonance" which extends in the energy range of 10-15 eV for holmium and gadolinium. This may be interpreted in terms of the effect of Slater integral G^1. For the half filled 4f shell or more the intensities and a multiplet spread are controlled to large extent by the exchange parameter G^1 on the energy level $4d^9 4f^{n+1}$. Gadolinium spectra

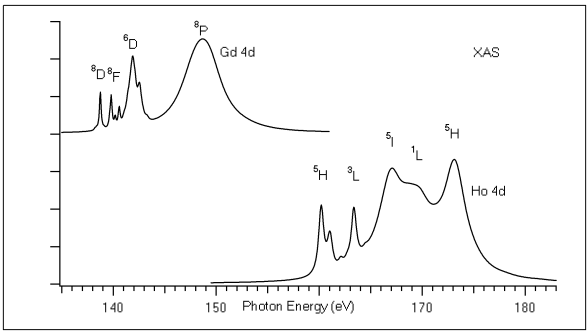

FIG. 1: Calculated absorption spectra for gadolinium and holmium in the photon range of 4d-4f transitions. Arrows mark positions fo main transitions which are summarized in Table II and III

display only one strong absorption band proceeded by a number of weaker peaks, whereas spectra of Ho^{3+} are characterized by a very broad and structured maximum. Z dependence of the giant resonances for lanthanides was intensively studied before by photoabsorption and photoelectron spectroscopy[36,37].

The gadolinium absorption spectrum (Fig.1) represents transitions from the ground state $^8S_{7/2}$ to the ^8P level. At lower photon energies, weaker features appears as a result of excitations of a core electron to the ^8D and ^6D levels. The calculated energy levels and absorption intensities in relative values (the highest value was normalized to one) are summarized in Table II and III. For Ho^{3+}, main transitions occur from ground state $^5I_8$ to the ^3L, ^5H and ^5I levels.

The inelastic and elastic scattered intensity is described by Kramers-Heisinberg formula:

$$I_{qq'}(\Omega,\omega) = \sum_f \Big| \sum_i \frac{\langle f|D|i\rangle\langle i|D|g\rangle}{E_g+\Omega-E_i-i\Gamma_i/2} \Big|^2 \times\delta(E_g+\Omega-E_f-\omega). \quad (3)$$

Here, $|g\rangle$, $|i\rangle$, and $|f\rangle$ are the ground, intermediate, and final states with energies E_g, E_i, and E_f, respectively, while Ω and ω represent energies of incident and scattered photons, respectively. D is the dipole operator, Γ stands for the intermediate state lifetime.

We have calculated the RIXS spectra from equation (3) using matrix element to transitions from the ground state to the intermediate and back to the final states using the same

TABLE II: Calculated energy levels and relative values (highest value was normalized to one) for Gd^{3+} near 4d edge.

Transition		E(eV)	Rel.value
Gd^{3+} $4d^{10}4f^7$	$^8S_{7/2}$		
$4d^94f^8$	$(^7F)^8D_{9/2}$	138.7	0.0471
	$(^7F)^8D_{7/2}$	139.1	0.0005
	$(^7F)^8D_{5/2}$	139.6	0.0034
	$(^7F)^8H_{9/2}$	139.8	0.0155
	$(^7F)^8H_{7/2}$	140.2	0.0046
	$(^7F)^8F_{9/2}$	140.6	0.0079
	$(^7F)^8F_{7/2}$	141.1	0.0034
	$(^7F)^8F_{5/2}$	141.4	0.0011
	$(^7F)^6D_{9/2}$	141.9	0.0341
	$(^7F)^6D_{7/2}$	143.3	0.0027
	$(^7F)^6P_{7/2}$	147.6	0.3520
	$(^7F)^8P_{5/2}$	148.5	1
	$(^7F)^8P_{9/2}$	149.3	0.8756
	$(^7F)^8P_{7/2}$	149.5	0.1912
	$(^7F)^6P_{5/2}$	149.8	0.0261
	$(^7F)^6F_{7/2}$	152.9	0.0057
	$(^7F)^6F_{9/2}$	153.1	0.0043
	$(^7F)^6F_{7/2}$	154.8	0.0007
	$(^7F)^6F_{9/2}$	155.2	0.0010

scaling for the Slater integrals as in [Ref.8]. For simplicity in calculation we assume that the incident photon is unpolarized. Figure 2 and 3 show the results of RIXS for Gd^{3+} and Ho^{3+} ions calculated for the different excitation energies, which are indicated on absorption spectra in the top panel. This elastic scattering is dominant and clearly seen in all of resonant spectra.

TABLE III: Calculated energy levels and relative values (highest value was normalized to one) for Ho^{3+} near 4d edge.

Transition		E(eV)	Rel.value
$Ho^{3+}4d^{10}4f^{10}$	$^5I_8$		
$4d^94f^{11}$	$(^4F)^5H_7$	160.2	0.1543
	$(^4I)^5L_9$	160.9	0.0074
	$(^4F)^5H_7$	161.0	0.0705
	$(^4G)^5I_8$	162.1	0.0183
	$(^4G)^5I_7$	162.7	0.0073
	$(^4G)^5H_7$	162.8	0.0048
	$(^2K)^3L_8$	163.3	0.1262
	$(^4I)^5I_8$	166.6	0.0722
	$(^4I)^5I_8$	167.0	0.6939
	$(^2L)^1L_8$	168.6	0.2667
	$(^4L)^5H_7$	173.1	1
	$(^2L)^3M_8$	175.0	0.0366
	$(^4I)^3I_7$	178.0	0.0125

Spectral structure at about 4-6 eV bellow elastic peak for Gd and 1-2 eV for Ho represents resonant inelastic x-ray scattering. The x-ray inelastic cross section were calculated using resonant terms of the Kramers-Heisenberg equation (3), where the different value of the lifetime broadening in the intermediate state Γ was used. For holmium ion the broadening width in absorption spectra was set to 0.3 eV for the range from 160.69 eV to 163.86 eV and 2.5 eV for the range from 167.47 eV to 178.55 eV. The Gd^{3+} XA spectrum was divided into the three parts. The broadening width was set to 0.1 eV for the range from 142.75 eV to 145.4 eV, 0.3 eV for the range from 145.90 eV to 149.12 eV and 3.0 eV for the last part. The same Γ values were used in the calculations of scattering spectra.

Two types of photon-in-photon-out features can be observed for all spectra - elastic and inelastic scattering. The inelastic scattering for Gd corresponds to spin flip transition, due

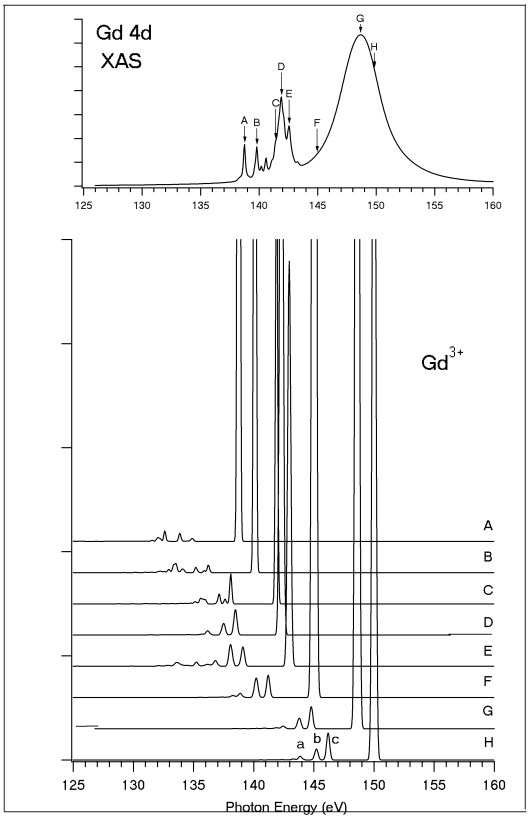

FIG. 2: Theoretical calculations of absorption and resonant scattering spectra for Gd^{3+} ion. Excitation energies (A-H) are indicated in the top panel.

to the fact that final state has lower spin. Spin flip transitions mainly occurs for the higher excitation energy. This can be understood on terms of LS-coupling and was described before by Dallera et al[10]. The inelastic scattering for Ho corresponds to the f-f excitations, which appear at 1-2 eV below elastic peak. The results of calculations are an good qualitative agreement with the experiment presented below.

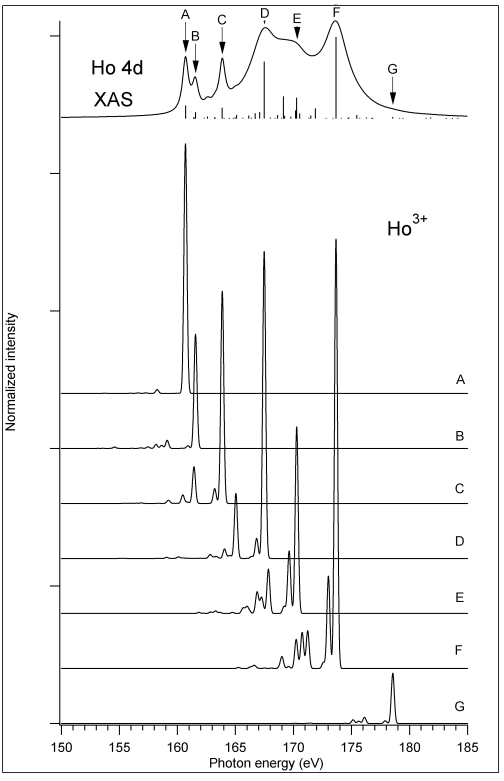

FIG. 3: Theoretical calculations of absorption and resonant scattering spectra for Ho^{3+} ion. Excitation energies (A-G) are indicated in the top panel.

III EXPERIMENTAL RESULTS

The experiment was performed at the undulator beamline 7.0 of the Advanced Light Source at Lawrence Berkeley National Laboratory. The beamline covers the range of 50-1500 eV and equipped with a spherical grating monochromator[34]. Absorption spectra were recorded by measuring the total fluorescence yield (TFY) with 0.2eV monochromator resolution for the metals and 0.25eV for the hydrides. The resonant spectra were detected using a high-resolution grazing-incident grating spectrometer[35] employing a 5m, 400 l/mm grating. The spectrometer has an entrance slit with adjustable width and uses a two-dimensional multichannel detector that can be translated to the focal position defined by

the Rowland circle of the grating in use. During the RIXS measurements , the resolutions of the beamline monochromator and x-ray spectrometer were 0.1 eV and 0.13 eV respectively for the metals and 0.25eV and 0.1 eV for the hydrides. Samples were oriented so that the incident photons were at about 22 degrees to the surface plane.

Normalized XA and RIXS spectra for holmium and gadolinium metals are shown in Fig.4 and Fig.5. The absorption spectra (upper panel) show the pre-edge and "giant resonance" regions. The vertical lines in the figures correspond to the excitation energies, at which high resolution scattering spectra were measured. The scattered intensity is plotted as a function of photon energy. All the spectra are dominated by the elastic peak for both holmium and gadolinium metals.

The observed inelastic profiles for gadolinium (Fig.5) show a triple peak family along with broad structure for all the RIXS spectra, which are shifted together with elastic peak. When the incident photon energy is turned to prethreshold peak A we have weak inelastic structure at about 4 eV below elastic peak. Similar structure is observed for excitation energies B and C. It goes through a resonance upon tuning the incident energy to the D energy and to the energy of the "giant absorption" edge (E, F and G). At the excitation energy higher than the ^8P resonance in absorption curve (G=147.0 eV) the inelastic process become weaker and finally disappears as shown before by Moewes et al.[3]

RIXS spectra of holmium (Fig.4) were also taken at an incident photon energy below, at and above the 4d "giant resonance". The inelastic scattering profile for holmium is more complex. 1 peak is at about 1 ev bellow elastic peak and also multiplet family at about 4-6 eV below the elastic features. The relative intensity of inelastic peaks reaches maximum for D,E and F excitation energies and is weaker before and after the "giant resonance" region. The calculation reproduces this effect fairly well and shows that these f-f transitions strongly depend on the excitation energy .

IV. COMPARISON BETWEEN THEORY AND EXPERIMENT

Calculated absorption spectrum for the Gd^{3+} ion is in agreement with experimental data and reproduces prethreshold structures and "giant resonance" as in experiment. The energy positions for the experimental and theoretical results are the same and indicated on the top panel of Figs. 2 and 5.

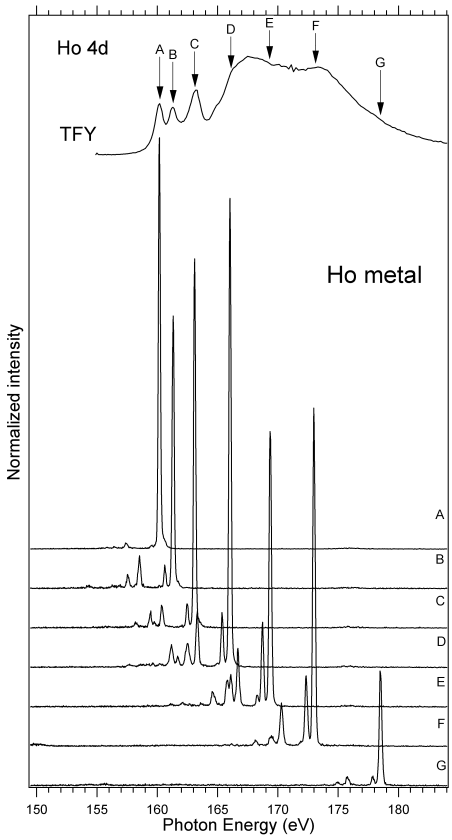

FIG. 4: TFY and resonant soft x-ray scattering spectra of Ho metal across 4d thresholds. Excitation energies (A-G) are indicated in the top panel.

Calculated inelastic structures for Gd can be divided into 3 groups, marked a, b, c (Fig.2). The groups are shown constant difference in energy with respect to the elastic peak through out varying excitation energies. Group c is centered at -3.8 eV bellow the elastic peak in the energy loss scale, group b and a at -4.8 eV and -6.1 eV respectively. The intensity of peaks b and c increases upon going from excitation energy D to G both in experimental and and simulated spectra. For spectra D and E, agreement between theory and measurements is the best and all 3 groups are clearly observed. Theoretical calculations for the F spectrum suggest an intense c peak at -3.8 eV but experimental data show only weak peak in this

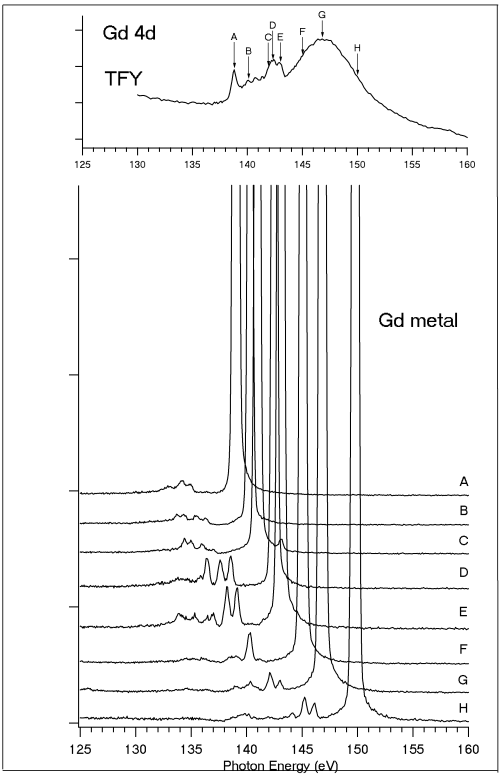

FIG. 5: TFY and resonant soft x-ray scattering spectra of Gd metal across 4d thresholds. Excitation energies (A-H) are indicated in the top panel.

region. This is also weaker at excitation energies F, G and H as compared with simulation. The *a* transitions are much weaker but still well reproduced by theory and can be seen in all spectra. Groups *c*, *b* and *a* can be assigned to transitions from the ground $^8S_{7/2}$ state to the sextet multiplet family for the same electronic configuration $4d^{10}4f^7$.

Intense elastic and inelastic structure were observed for holmium when the icident photon energy is tuned to the 4d-4f resonances. The calculations of the absorption spectrum for Ho^{3+} clearly reproduced prethreshold structures and the "giant resonance". The inelastic scattering consist of one peak at -1 ev bellow the elastic peak and 3 peaks in the energy range of -2-4 eV.

RIXS data for both gadolinium and holmium metals reveal maximum intensities for the

inelastic structures when the incident energy turned to the "giant resonance" band (D, E and F excitation energies). Calculated spectra are in good agreement with experimental results.

V. GADOLINIUM AND HOLMIUM HYDRIDES

One of the interesting phenomena recently found by Huiberts et al.[14] was dramatic changes in the optical properties of lanthanum, and yttrium hydride films with changing hydrogen content. The underlying principle is a transition between a reflective metallic state and a translucent insulating state, induced by converting a thin film of a metal to its ionic hydride. This implies that hydrogen in YH_{3-x} behaves as a negatively charged impurity. The recent discovery of the so called switchable mirror compounds based on YH_{3-x} has renewed the interest in the electronic structure of transition metal and rare-earth hydrides.

Electronic structure investigations for $GdH_{3-\delta}$ and GdH_{2+x} using XAS and RIXS were published before in [Ref.15]. In Fig.6 we made a comparison between RIXS spectra of GdH_{2+x}, $GdH_{3-\delta}$ and Gd metal for the three excitation energies 140.0 eV, 143.6 eV and 144.2 eV, indicated in the top panel. The Gd-H spectra show sharp transitions, corresponding to the f-f excitations and an additional structure at about 10 eV below the elastic peak, which follows varying excitation energies on the photon energy scale. The only substantial difference between GdH_{2+x} and $GdH_{3-\delta}$ is in intensity of these additional structures,which also depends on the excitation energy. The hydride spectra are in contrast with metal spectra, which do not have such transitions. The 10 eV structure below the elastic peak can be attributed to charge-transfer excitations of an electron from hydrogen into unfilled lanthanide 4f level. Such charge transfer effects support the view that hydrogen in Gd-H systems is an electron acceptor, which is in agreement with theoretical results[16].

We examine the possibility of using RIXS for probing of charge transfer satellites in the holmium hydride systems. Figure 7 shows scattering spectra of Ho metal and Ho hydrides recorded at different excitation energies, indicated on the XA spectrum in the upper panel of Fig. 7. The spectra show sharp intra-atomic f-f transitions at about 4-6 eV below the elastic peak in hydrides and metals. No substantial differences were found between holmium metal and holmium hydrides as well as no inelastic scattering excitations were observed in the region of around 10 ev bellow the elastic peak for Ho-H systems. Figs. 6 and 7 show

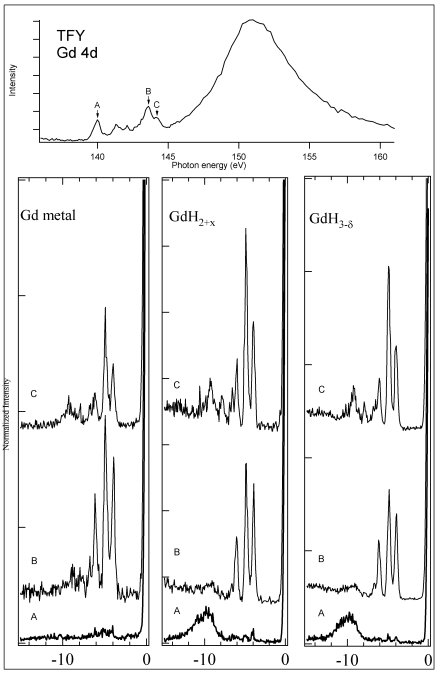

FIG. 6: Comparison between resonant inelastic scattering spectra of GdH_{2+x}, $GdH_{3-\delta}$ and Gd Metal for different excitation energies.

that charge transfer satellites occur only in Gd-H systems. This behavior of hydrogen in gadolinium hydrides similar to that of oxygen in gadolinium oxides. Oxygen is also an electron acceptor in gadolinium oxides systems. It was shown before by Moewes et al.[3] that some inelastic x-ray scattering features appear at -9-10eV bellow the elastic peak in Gd_2O_3 which can be assigned to the charge-transfer states as well. For Gd-H systems such satellites shifted at about 1eV to the lower energies and appear at -10-11 eV on the energy-loss scale. Different behavior of hydrogen in Gd and Ho hydrides can be possibly connected with the half-filled 4f shell of Gd, thus leading to a difference in chemical bonding.

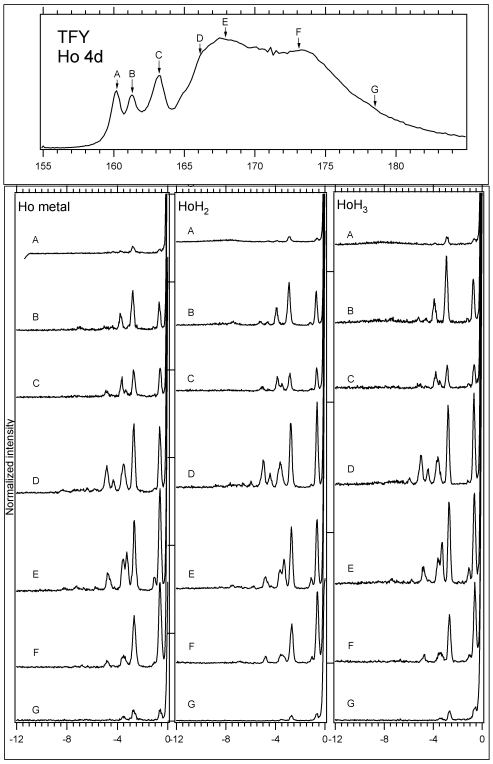

FIG. 7: Comparison between resonant inelastic scattering spectra of HoH_2, HoH_3 and Ho metal for different excitation energies.

VI. SUMMARY

RIXS for holmium and gadolinium systems was shown to be a useful tool in probing transitions between 4d-4f levels and within 4f shell. The atomic multiplet description of the electronic states turns to be very appropriate and demonstrate satisfactory agreement with experiments for holmium and gadolinium systems. Present RIXS data, governed by dipole selection rules and along with calculations provide valuable information on energies of intra-atomic f-f excitations for Ho and Gd metals and their hydrides. RIXS was also used to determine the role of charge transfer processes in gadolinium and holmium hydrides. It was found that charge transfer satellites occur only in Gd-H systems. Such satellite observations

suggest the view that negatively charged hydrogen in gadolinium hydrides is an electron acceptor.

REFERENCES

1. T. M. Zimkina, V.A. Fomichev, S.A. Gribovski, I.I.Zhukova Fiz.Tverd.Tela 9, 1447 (1967) T.M. Zimkina, A.S. Shulakov, A.P. Braiko, A.P. Stepanov and V.A. Fomichev, Sov. Phys. Solid State 25, 1201 (1984)

2. J-J Gallet, J-M Mariot, C.F. Hague, F. Sirotti, M. Nakazawa, H. Ogasawara and A.Kotani Phys. Rev. B 54, 20 (1996)

3. A. Moewes, T. Eskildsen, D.L. Ederer, J. Wang, J. McGuire, T.A. Callcot, Phys. Rev. B 57, 20 (1998)

4. Giant Resonances in Atoms, Molecules and Solids, edited by J.P. Connerade, J.M. Esteva and R.C. Karnatak (Plenum, New York, 1987)

5. Jack Sugar, Phys. Rev. B 5, 5 (1972)

6. S. Tanaka, K.Okada and A. Kotani, J. Phys. Soc. Jpn. 63, 2780 (1994)

7. H. Ogasawara, A.Kotani, B.T. Thole, Phys.Rev.B 50, 12332 (1994)

8. Shin Imada and Takeo Jo, J. of Phys. Soc. of Japan vol.59, N9,1990, pp.3358-3373

9. M.H. Krisch, C.C. Kao, F. Sette, W.A. Caliebe, K. Hamalainen and J.B. Hastings, Phys. Rev. Lett. 74, 24 (1995)

10. C. Dalerra, L. Braicovich, G. Ghiringhelli, M.A. van Veenendaal, J.B. Goedkoop, N.B. Brookes, Phys. Rev. B 56, 3 (1997)

11. B.T. Thole, G. van der Laan, J.C. Fuggle, G.A. Sawatzky, R. C. Karnatak, J.M Esteva, Phys. Rev B. 32, 8 (1985)

12. T.Gregorian, H. D'Amour-Sturm, W.B. Holzapfel, Phys.Rev. B 39, 17 (1989)

13. M.F. Reid, L. van Piterson, R.T. Wegh, A. Mejerink, Phys.Rev. B 62, 22 (2000)

14. Huiberts, J.N. et al. Nature 380, 231-234 (1996)

15. K.O. Kvashnina, S.M. Butorin, J. Nordgren, J.-H. Guo, B. Hjorvarsson, J. of electron spectroscopy 137-140 (2004) 487-489

16. Ng, K.K., Zhang, F.C., Anisimov, V.I., Rice, T.M., Phys. Rev. B59, 5398-5413 (1999)

17. Z. Hu, K. Starke, G. Van der Laan, E.Navas, A.Bauer, E.Weschke, C. Schubler-Langeheine, E. Arenholz, A. Muhig, G. Kaindl, J.B. Goodkoep, N.B. Brooks, Phys.Rev. B 59, 15 (1999)

18. M.H. Krisch, F. Sette, U. Bergmann, C. Masciovecchio, R. Verbeni, J. Goulon, W. Calieble and C. C. Kao, Phys. Rev B 54, 18 (1996)

19. J. W. Cable and R. M. Nicklow, Phys.Rev B 39, 16 (1989)

20. K.Starke, F. Heigi, A. Vollmer, M. Weiss, G. Reichardt, G. Kaindl, Phys.Rev. Lett 86, 17 (2001)

21. G. van der Laan, J.B. Goedkoop, N.B. Brookes, Phys.Rev.B 59, 13 (1999)

22. E.Arenholz, E. Navas, K. Starke, L. Baumgarten, G. Kaindl, Phys.Rev. B 51, 13 (1995)

23. R.A. Cowely, D.A. Jehan, D.F. McMorrow, G. J. McIntyre, Phys. Rev. Lett 66, 11 (1991)

24. T.R. Thurston, G. Helgesen, J.P. Hill, D. Gibbs, B.D. Gaulin, P.J. Simpson, Phys. Rev.B 49, 22 (1994)

25. T. E. Griegereit, J.W. Lynn, Q. Huang, A.Santoro, R.J. Cava, J.J. Krajewski, W.F. Peck, Jr., Phys.Rev Lett. 73, 20 (1994)

26. C.Zhang, J.C.P. Klaasse, E.Bruck, F.R. de Boer, K.H.J. Buschow, J. of alloys and Compounds 267 (1998) 37-40

27. H. Ohsumi, J. of Phys.Soc. of Jpn 71, 7 (2002) pp. 1732-1739

28. C de la Fuente, R.A. Cowley, J. P. Goff, R. C.C. Ward, M.R. Wells, D.F. McMorrow, J. Phys: Condens. Matter 11 (1999)

29. R.D. Cowan, The theory of Atomic Structure and spectra (University of California Press, Berkeley, 1981)

30. Jehan D.A., McMorrow D.F., Cowley R.A., Ward R.C.C., Wells .M.R., Hagmann N. and Clausen K. 1993 Phys.Rev.B 48 5594

31. D.W. Lynch, R.D. Cowan, Phys.Rev. B 36, 17 (1987)

32. J. Kwo, E.M. Gyorgy, D.B. McWhan, F.J. Disalvo, C.Vettier, J.E. Bower, Phys.Rev.Lett. 55 (1985) 1402

33. S.M. Durbin, J.E. Cunningham, J.E. Mochel, C.P. Flynn, J.Phys.F: Met.Phys. 11 (1981) L223

34. 10. H.A. Padmore and T.Warwick, J.Synchrotron Radiation, 1, 27 (1994)and refer-

ences there in.

35. J.Nordgren, G.Bray, S.Cramm, R.Nyholm, J.-E. Rubensson and N. Wassdahl, Rev.Sci. Instrum. 60, 1690 (1989)

36. M.Richter, M.Meyeer, M.Pahler, T.Prescher, E.v.Raven, B.Sonntag, H.-E.Wetzel, Phys. Rev A 40, 12 (1989)

37. M.Richter, M.Meyeer, M.Pahler, T.Prescher, E.v.Raven, B.Sonntag, H.-E.Wetzel, Phys. Rev A 39, 5666 (1989)

Paper II

Available online at www.sciencedirect.com
SCIENCE DIRECT®
Journal of Electron Spectroscopy and Related Phenomena 137–140 (2004) 487–489
JOURNAL OF ELECTRON SPECTROSCOPY and Related Phenomena
www.elsevier.com/locate/elspec

Electronic structure of Gd hydrides studied by resonant Inelastic soft X-ray scattering

K.O. Kvashnina [a], S.M. Butorin [a,*], J. Nordgren [a], J.-H. Guo [b], B. Hjörvarsson [c]

[a] *Department of Physics, Uppsala University, Box 530, S-751 21 Uppsala, Sweden*
[b] *Advanced Light Source, Lawrence Berkeley National Laboratory, Berkeley, CA 94720, USA*
[c] *Department of Materials Physics, Uppsala University, Box 530, S-751 21 Uppsala, Sweden*

Available online 9 April 2004

Abstract

Spectacular changes in the optical and electrical properties were recently discovered in metal–hydride films of yttrium and lanthanum near their metal–insulator transitions: the dihydrides are excellent metals and the trihydrides are insulators and transparent in the visible part of optical spectrum. Such changes are best described by a model based on negatively charged hydrogen (H^-) ions. We have studied the electronic structure of the similar Gd–H system by X-ray Absorption and Resonant Inelastic Soft X-ray Scattering (RIXS) Spectroscopies. During our measurements we found charge transfer excitations, which produce charge-transfer satellite systems. These satellites result support the view that hydrogen is an electron acceptor.

Keywords: Insulator; Satellites; Lanthanum

One of the interesting phenomena recently found by Huiberts et al. [1] was dramatic changes in the optical properties of lanthanum, and yttrium hydride films with changing hydrogen content. The underlying principle is a transition between a reflective metallic state and a translucent insulating state, induced by converting a thin film of a metal to its ionic hydride. This implies that hydrogen in YH_{3-x} behaves as a negatively charged impurity. The recent discovery of the so called switchable mirror compounds based on YH_{3-x} has renewed the interest in the electronic structure of transition metal and rare-earth hydrides. This important result is in agreement with the theoretical views of Ng et al. [2] and Eder et al. [3], who proposed that strong electron correlation effects determine the electronic properties of switchable mirrors.

Stimulated by both fundamental interest and applications, hydrogen in metals and alloys has been studied intensively. This is very attractive since hydrogen can be used to switch the electronic properties of the thin metallic films. Although many metal–insulator transitions are known, this type of switchable optical phenomena is very unusual, and potentially of considerable technological importance since the transition leads to spectacular effects in the visible region. Such switchable mirrors might be put to good use in display devices and interior lighting systems, particularly when the light sources are hard to reach and adjust. Huiberts at al. [1], Ng et al. [2], and Eder et al. [3] have showed that rare-earth metals such as La has a formal valence of 3+. In a dihydride LaH_{2+x}, the 1s orbital of the hydrogen bands are filled, leaving one electron per unit cell in the La conduction bands. This gives the metallic behavior. In a trihydride such as LaH_{3-x}, the H bands can hold all six valence electrons per unit cell, and assumes insulator behavior. The authors also point out that the electronic structure that underlies this behavior is poorly understood.

We have studied a similar system and found similar behavior in $GdH_{3-\delta}$ and GdH_{2+x}. It is obvious that the electronic structure of rare earth hydrides is a key quantity for the understanding of all these properties. We have studied the electronic structure of Gd hydrides by X-ray Absorption (XAS) and RIXS Spectroscopies. RIXS and XAS have been chosen because they are very powerful techniques for electronic structural investigations. Eder et al. [3] proposed an Anderson lattice model, where the hopping integrals depend on electronic occupation number on the H site.

* Corresponding author. Tel.: +46-18-471-3553; fax: +46-18-51-2227.
E-mail address: sergei.butorin@fysik.uu.se (S.M. Butorin).

0368-2048/$ – see front matter © 2004 Elsevier B.V. All rights reserved.
doi:10.1016/j.elspec.2004.02.077

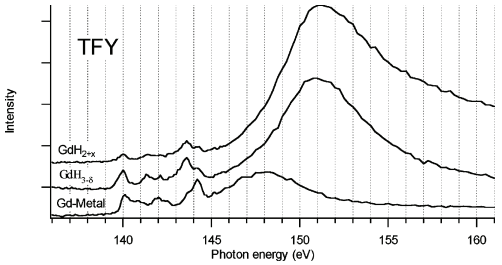

Fig. 1. TFY spectra for $GdH_{3-\delta}$, GdH_{2+x} and Gd–metal.

XAS and RIXS techniques provide information about the valence states, involved in the chemical bonding between the atoms.

Our samples were grown using MBE techniques [4]. The experiments were made at beamline 7.0 of the Advanced Light Source at Lawrence Berkeley National Laboratory. This undulator beamline includes a spherical grating monochromator [5] and is constructed to provide linearly polarized synchrotron radiation of high resolution and high flux with post-focusing mirror capable of focusing the radiation to a narrow beam at the interaction region. The spectrometer [6] provides a choice of three different spherical gratings. It has an entrance slit with adjustable width and uses a 2-D multichannel detector that can be translated to the focal position defined by the Rowland circle of the grating in use.

Absorption spectra were recorded by measuring the total uorescence yield (TFY) with 0.25 eV monochromator resolution. The resonant spectra were recorded using a high-resolution grazing-incident grating spectrometer employing a 5 m, 400 l/mm grating. The X-ray spectrometer had a resolution of 0.1 eV. During the resonant measurements, the resolution of the beamline monochromator was the same as that during absorption measurements. The samples were oriented so that the incident photons were at 45 degrees with respect to the surface plane.

Fig. 1 shows the TFY spectra of the $GdH_{3-\delta}$ and GdH_{2+x} and Gd–metal, respectively as a function of photon energy. One, clearly observes a big difference between metallic states and hydrogen states, and no big difference between $GdH_{3-\delta}$ and GdH_{2+x}. The widths of the transitions are broader in the hydrides than in Gd–metal and shifted towards lower photon energy. It means that the electronic structure of the metal is affected by hydrogen.

The scattering spectra of the metal and Gd hydrides recorded at different excitation energies across the Gd 4d thresholds are displayed in Fig. 2. The upper panel of Fig. 2 shows X-ray resonant scattering spectra of $GdH_{3-\delta}$, while those of GdH_{2+x} are displayed on the bottom panel. The elastic peak is clearly observed in all of the resonant spectra. We also include transitions of 5p character, which can be seen about 22–25 eV below the elastic peak. The comparison between GdH_{2+x}, $GdH_{3-\delta}$ and Gd

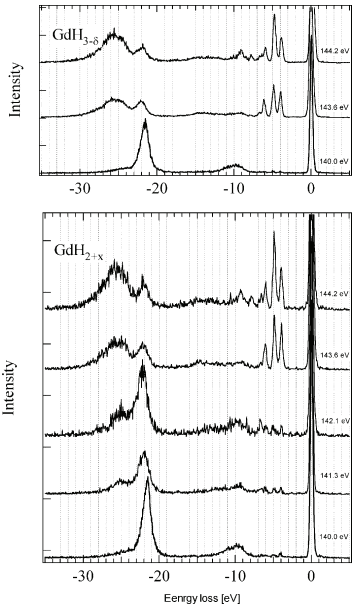

Fig. 2. An enhanced part of resonant inelastic X-ray scattering spectra of $GdH_{3-\delta}$ (upper panel) and GdH_{2+x} recorded at different excitation energies across the 4d thresholds. Excitation energies marked in the right site of the figures.

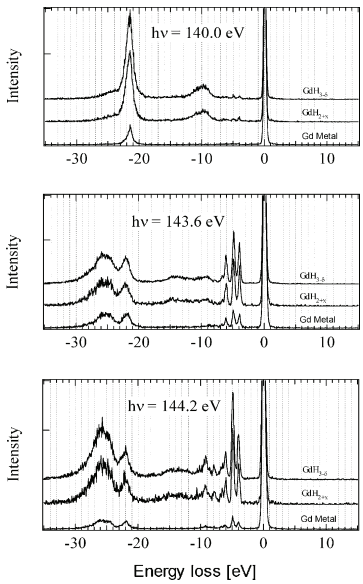

Fig. 3. Comparison between resonant inelastic scattering spectra of GdH_{2+x}, $GdH_{3-\delta}$ and Gd–metal for the same excitation energies ($\hbar\nu$).

Metal for the same excitation energies are also made in Fig. 3.

Different structures resonate in different ways with varying excitation energies. The spectra show sharp transitions, corresponding to the f–f excitations and an additional structure at about 10 eV below the elastic peak in hydrides. The experimental data also show that this additional structure is shifted with excitation energy. The hydrides spectra are in contrast with metal spectra, which do not have such transitions. The only substantial difference between GdH_{2+x} and $GdH_{3-\delta}$ is in intensity of these additional structures. For example, for $GdH_{3-\delta}$ the intensity of additional features is higher compared to that of GdH_{2+x}. They also depend on the excitation energies and shift together. In order to show these transitions for the GdH_{2+x} we recorded a few more spectra with excitation energies in the interval between 140.0 and 143.6 eV, as shown in Fig. 2. The 10 eV structure below the elastic peak can be attributed to charge-transfer excitations. This charge transfer effect produces so-called charge transfer satellites in X-ray absorption and resonant spectra of transition metals compounds. We can interpret Gd–H systems in terms of satellites. These satellites results support the view that hydrogen is an electron acceptor. Such changes on a high-energy scale suggest that the electronic structure is best described by a model based on negatively charged hydrogen (H^-) ions.

Our XAS and RIXS methods allowed as to estimate these charge-transfer satellites directly from the experiments, which gives a big advantage in interpretation of the insulator-metallic behavior for comparison with other techniques. Consequently, hydrogen in GdH_{2+x} and $GdH_{3-\delta}$ behaves as a negative ion, in agreement with recent strong-electron correlation theories [2,3]. These results are quite significant and the present class of compounds is also ideal for basic research in understanding the hydrogen behavior, in general.

References

[1] J.N. Huiberts, et al., Nature 380 (1996) 231–234.
[2] K.K. Ng, F.C. Zhang, V.I. Anisimov, T.M. Rice, Phys. Rev. B59 (1999) 5398–5413.
[3] R. Eder, H.A. Pen, G.A. Sawatzky, Phys. Rev. B 56 (1997) 10115–10120.
[4] D.A. Jehan, D.F. McMorrow, R.A. Cowley, R.C.C. Ward, M.R. Wells, N. Hagmann, K. Clausen, Phys. Rev. B 48 (1993) 5594.
[5] H.A. Padmore, T. Warwick, J. Synchrotron Radiat. 1 (27) (1994), and references therein.
[6] J. Nordgren, G. Bray, S. Cramm, R. Nyholm, J.-E. Rubensson, N. Wassdahl, Rev. Sci. Instrum. 60 (1989) 1690.

Paper III

Resonant Inelastic X-ray Scattering of Curium Oxide

K.O. Kvashnina[1*], S.M. Butorin[1], D.K. Shuh[2], J.-H. Guo[3], L. Werme[1,4] and J. Nordgren[1]

[1] *Department of Physics, Uppsala University, Box 530, 751 21 Uppsala, Sweden*

[2] *Chemical Sciences Division, Lawrence Berkeley National Laboratory, Berkeley, CA 94720, USA*

[3] *Advanced Light Source, Lawrence Berkeley National Laboratory, Berkeley, CA 94720, USA*

[4] *SKB, Stockholm, Sweden*

The measurements on radioactive actinide isotopes (curium-248) were performed using very small sample quantities (micrograms) to minimize the sample activity. Resonant inelastic X-ray scattering (RIXS) spectra of curium oxide at the Cm 5d edge were measured for the first time. RIXS data are compared with theoretical calculations using atomic multiplet theory. The results indicate that isotope curium -248 in the curium oxide sample has oxidation state III due to the best agreement with RIXS calculations for Cm (III) instead of those for Cm (IV).

Introduction

Since the discovery of the transuranium elements there has been a continuing interest in determining the chemical and physical properties of these elements and their compounds. In particular, it was necessary to determine the chemistry of plutonium and

neptunium very accurately because of the requirements for separation and purification of $_{94}Pu^{239}$ from the other materials in uranium piles. As a result of this, it is now stated that the chemistry of plutonium is as well or better understood than that of other actinides in the periodic table. Recently, the electronic structure of actinides has been studied using different experimental and theoretical approaches[1-4].

Uranium has the valence states (III), (IV) and (VI), while neptunium and plutonium have the valencies (III), (IV), (V), and (VI). However, greater oxidizing power is required to oxidize them to their higher states[5]. The stability of the valence state of (III) increases from uranium to plutonium and it is predicted that maximum stability could probably be obtained with curium (element 96), which has seven 5f electrons. The known properties of these transuranium elements make it possible to suggest a subclassification of these elements in terms of a new series similar to the rare earth series. The electronic configuration explains satisfactorily the stable valence state of (III) for gadolinium, which compares with the state of (III) for curium. This prediction is also verified by data, which indicate that spin polarization of the curium 5f electrons stabilizes the curium (III) valency[5].

In the case of curium, there are still numerous open questions ranging from the crystal structure[6] and magnetic properties[7] of curium compounds to the research of the nature of curium ions in various oxidation states. It is, therefore, important to investigate the electronic structure of curium in different oxidation states.

A theoretical study of curium compounds is an additional source for obtaining chemical and structural information, but this entails a mixture of success and difficulties as for other f-elements. The most commonly used are the density function theory (DFT)

and ab initio calculations[2], which have been shown to be sufficient to describe crystal structures with various types of chemical bonding: halides, pnictides, hydrides and oxides of curium[6,8,9]. Recently, relativistic calculations using the Dirac-Slater discrete variational method (DVM) has been carried out in order to obtain the electronic structure of curium fluorides and chlorides[10]. Curium(III) oxide has been studied using Dirac-Hartree-Fock calculations, which provided information about the curium-oxygen distance in the model of hydrated Cm(III)[11]. Using the same theoretical approach, curium fluorides in different valencies from (I) to (IV) were compared to gadolinium fluorides. Since CmF_4 has been successfully prepared[12] whereas GdF_4 has not yet been possible to synthesize, it was concluded that $5f^7$ in CmF_3 is less stable than $4f^7$ in GdF_3[13].

Most of the theoretical investigations of curium have been performed in comparison with gadolinium due to their similar electronic configuration. Optical absorption and selective laser excitation spectroscopy have been used to investigate the electronic structures of the Cm(III) and Gd(III) ions in host crystals of $LuPO_4$, and these two systems were compared[14]. We also would like to mention that not so many experimental investigations have been found in the literature for curium compounds. Mostly these two types of spectroscopy have been used for curium[15-17]. A few more reports on Laser-Induced Fluorescence (LIF) spectroscopy have also been written and this technique was proposed to test curium leaks from waste storage sites into groundwater[18] (REF3Mouchizuki). Later LIF was also applied to evaluate the water hydration number in the first shell around the Cm(III) ion[19]. Some experimental data on aqueous Cm(III) solution are available, but the electronic structure is not clear yet.

The radioactivity of curium makes it difficult to investigate all aspects in detail. Information on electronic properties obtained from theoretical calculations is helpful in analyzing experimental data. We report here Resonant inelastic X-ray scattering (RIXS) of curium oxide near 5d edge. RIXS measurements at the actinide 5d threshold have been performed before[3, 4] and provided high resolution, which makes it easier to study in detail elementary excitations in curium compounds. The technique is sensitive to the oxidation state and the speciation of curium contrasting to X-ray absorption spectroscopy (XAS) where the 5d core-hole lifetime broadening is large. As a result, the actinide 5d absorption spectra do not exhibit many sharp features[3,4], thus reducing the utility of XAS. In particular, it is difficult to distinguish between uranium species with different oxidation states, especially in the case when one of the species has a much lower concentration than another. The superlative resolution (defined by the response function of the instrument) of the RIXS technique and its ability to enhance transitions to low-lying excited states makes this technique especially powerful.

Experimental data was interpreted by the commonly used atomic multiplet theory based on the Hartree-Fock calculations. Sugar first presented the details of these types of calculations[20]. Later it was repeated and used in theoretical studies of most of the rare-earths metals, oxides, and chlorides. The theoretical calculations of curium oxides presented in that paper have been done in the same way as a previous one for gadolinium[21]. Comparison of experimental data with theoretical calculations for Cm(III) and Cm(IV) indicates that isotope curium-248 as curium oxide has oxidation state (III), which is quite similar to the observation of valency stability in the lanthanide series.

Experimental Results

The oxidized curium-248 sample used for the measurements was fabricated by standard techniques used to prepare radionuclide counting plates. The counting plate was prepared from an aqueous solution of about 0.5mM curium-248 in approximately 0.1 M HCl that was localized onto the surface of high purity platinum substrate (25.4 mm diameter, 0.05 mm thickness) by successive, partial micro-pipette aliquots into an area of about 4mm^2. The isotopic composition of the curium solution was determined by alpha spectroscopy to be about 99% curium-248 and 1% curium-246 by mass.

The aqueous solution was allowed to dry and the resulting solid residue was distributed in a ring-shaped manner. This structure was inductively heated to 700°C under atmosphere to oxidize the material and to fix the material onto the substrate to preclude loss in the UHV spectrometer chamber during the measurements. The final amount of Cm-248 on the counting plate was found to be about 2 μg.

The portion of the platinum counting plate containing the curium was cut into a to 3 mm x 3 mm square and mounted with conductive tape on a rectangular aluminum sample holder. This sample holder was then inserted into a slotted aluminum can which served as a catch tray for material that might come loose during handling and the measurements.

The experiments were made at beamline 7.0 of the Advanced Light Source, Lawrence Berkeley National Laboratory, USA[(22)]. This undulator beamline includes a spherical grating monochromator, which gives resolution of 50 meV at ~110 eV. Absorption spectra at the Cm 5d edge were recorded by measuring the total fluorescence yield (TFY) with 0.2 eV monochromator resolution at 110 eV. RIXS spectra were

recorded using a grazing incident grating spectrometer[23-24] with 110 meV resolution at 120 eV. The instrument has three gratings, mounted at fixed angles of incidence and a large two-dimensional multichannel detector. The incident angle of the photon beam was 20 degrees from the surface for solid samples and the spectrometer was placed in the horizontal plane at an angle 90 degrees with respect to the incident beam. The low-activity isotope curium-248 as curium oxide was distributed on a platinum substrate.

RIXS measurements at the actinides 5d threshold provide an opportunity to study in detail elementary excitations in actinide compounds due to the naturally higher resolution of such experiments in comparison with those at the actinide 3d and 4d threshold. Normalized X-ray absorption (XA) and RIXS spectra at the Cm 5d edge measured for the curium-248 isotope is in the oxide sample are shown in Fig.1. The absorption spectra show the pre-edge around 116 eV and the "giant resonance"[25] regions. The lettered arrows in Fig.1 correspond to the excitation energies at which the scattering spectra were measured. RIXS spectra of curium were also taken at an incident photon energy below, at, and above the 5d "giant resonance." The RIXS intensity is plotted on the energy-loss scale. All the RIXS spectra are dominated by the elastic peak and the observed inelastic profiles for Cm (Fig.1) show a multiplet family at about 2–4 eV below the elastic peak.

When the incident photon energy *a* is on the low-energy side of the pre-edge structure, we have extremely weak inelastic features, which show some similarity to RIXS profiles in the spectra recorded at excitation energies *b*-*i*. When the excitation energy is tuned to the peak *b*, the inelastic features appear. The energy difference between the elastic peak and inelastic scattering structures are listed in Table 2. Similar

profiles are observed for excitation energies *c* and *d*. A resonance is encountered upon tuning the incident energy to the energy *d* and to energies of the "giant absorption" edge (*e, f, g, h, and i*). At the excitation energy higher than the *i* resonance in the absorption curve, the relative RIXS contribution becomes weaker. A similar effect was observed for uranium in RIXS spectra across the 5d edge[3,4]. All inelastic features are clearly seen in all spectra but the intensity of the features strongly depended on excitation energy. Thus, the intensity for the feature at about - 2.1 eV below the elastic peak goes up at the excitation energies *b and c,* and reached a maximum at the excitation energy *d*. When the incident photon energy is tuned to the "giant resonance" region in the absorption curve, this inelastic structure became weak (at excitation energies e, f, g, h, and i). The opposite effect is observed for the feature at about -3.9 eV below the elastic peak. At excitation energies below the "giant resonance" (*b, c, d*), this inelastic structure is quite weak and the intensity of this peak increases with the excitation energies *e, f, g, h, and i*. The calculation reproduces this effect fairly well and shows that these structures, corresponding to the f-f transitions strongly depend on the excitation energy and valency of the investigated actinide element.

Theoretical Calculations

The calculations were carried out for free (III) and (IV) ions of curium using atomic multiplet theory [26]. This approximation works quite well for describing rare-earth systems across 3d and 4d edges[3, 21, 27, 28]. The 4d, 5d, and 5f shells for the actinide elements have similar general characteristics as the 3d, 4d, and 4f shells for the rare-earth elements. We expect that for the actinides, this approach will work as well[3]. XA spectra

across 5d edge were already calculated by Ogasawara et al.[29] for most of the actinides, but they only treated trivalent ions, except Th (IV). In this paper we calculated the 5d XA and RIXS for Cm (III) and Cm (IV) ions.

The values for parameters such as Slater integrals and spin orbit coupling constants are obtained using Cowan's program[26]. The effect of crystal field or mixing with ligand bands was not taken into account. However, the effect of configuration interactions should be taken into account and is usually done by reducing the value of the Slater integrals. Lynch et al. [30] proposed that the Slater integrals for lanthanides should get smaller with increasing atomic number and will result in the broadening of the spectra.

The configuration of the outer electrons in curium is similar to that of gadolinium and has a half-filled 5f shell. The calculations of Cm 5d XA spectra were made in a similar way as for gadolinium[21], where the Slater integrals Fk(5f,5f) were reduced to 80%, and the Fk (5d,5f) and Gk (5d,5f) to 75% and 66%, respectively. Values of the Slater integrals and the spin-orbit coupling constants used for calculations of spectra are shown in Table 1 for the initial and final states of Cm (III) and Cm (IV). The configuration of the relevant outer electrons in Cm (III) is $5d^{10}5f^{7}$ and the half-filled 5f shell produces, as a ground state, $^{8}S_{7/2}$. Thus, Cm (IV) has 6 electrons in the 5f shell, producing a $^{7}F_{0}$ ground state. The ground state J value is determined by Hund's rule. The final states have only three possibilities J-1, J, and J+1 and the dipole selection rules reduce the number of states that can be reached from ground state configuration, but it is still very large – Cm (III) has 1076 transitions and Cm (IV) has 212 transitions.

The calculated 5d XA spectra for Cm (III) and Cm (IV) are shown in Fig.2. The plotted curves above the multiplet sticks are their Lorentzian convolutions. Both 5d XA

spectra were divided in two regions: pre-threshold and "giant absorption" region similar to the rare earth systems. The broadening width Γ for the pre-threshold region was 1.0 eV and for the giant resonance region 2.5 eV. It was observed before by Richter et al.[31] for lanthanides that increasing the nuclear charge Z shifts all peaks towards higher energy. The XA spectrum for $_{96}$Cm (IV) should be similar to the $_{95}$Am (III) due to the same number of electrons in the f shell. Fig. 2 clearly indicates the same effect for actinides as for lanthanides: the 5d-5f resonance for Cm (III) (Z=96) is shifted by 3 eV compared to Cm (IV) (as analogue for Am (III) Z=95). In order to achieve the best agreement between theory and experiment, the theoretical spectra for both ions were shifted towards lower energy by 5.8 eV, which is quite similar to situation with Gd 4d XA spectrum where theoretical curve has been shifted by 6 eV[31] for compare with experiment.

The 5d RIXS spectra have been calculated from the Kramers-Heisenberg formula, using the matrix element in transitions from the ground state to the intermediate and back to the final states and using the same scaling for the Slater integrals as for gadolinium[21]. Fig. 2 and 3 show the results for 5d RIXS of Cm (III) and Cm (IV) ions calculated for different excitation energies, which are exactly the same as used during the measurements of 5d RIXS spectra for curium oxide. The spectra are plotted on an energy-loss scale, where the elastic scattering is set to 0 eV and is clearly seen as dominant in all of the resonant spectra. The spectral structures at about 1–6 eV below the elastic peak represents the resonant inelastic X-ray scattering. The X-ray inelastic cross section was calculated using different values for the lifetime broadening in the intermediate state to simulate its significant increase in the "giant resonance" region[32]. The lifetime in the calculations of 5d RIXS spectra at excitation energies *b, c,* and *d* was

set to 0.8 eV and 2.5 eV was used for the rest of the spectra. The plotted curves representing RIXS spectra are Voigt convolutions (combination of a Lorentzian with Γ = 0.2 eV and a Gaussian with Γ = 0.2 eV) of calculated multiplet sticks.

Generally two types of photon-in/photon-out features can be observed in all spectra - elastic and inelastic scattering. The inelastic scattering process of Cm (III) described by transitions from the ground state $^8S_{7/2}$ to the intermediate states of the $5d^95f^8$ configuration and then to the final states of the $5d^{10}5f^7$ configuration. The observed inelastic scattering profile for Cm (III) (Fig. 3) caused by transitions from the $^8S_{7/2}$ ground state to the final states ^6G_J, ^6F_J, ^6D_J, ^6P_J with different J values (according to selection rule), which are situated 2–4 eV below the elastic peak and then weaker transitions due to final state ^4G_J observed at 5 eV below the elastic peak. The observed inelastic scattering features for Cm (IV) (Fig. 4) caused by transitions from the $^7F_0$ ground state to final states ^5D_J, ^5F_J, ^5P_J, and weaker transitions due to the ^3P_J , ^3D_J final state terms. The energy differences between the elastic peak and inelastic scattering structures for Cm (III) and Cm (IV) are listed in Table 2.

The inelastic scattering features for both ions are attributed to 5f-5f intra-atomic transitions (f-f excitations), which usually appear 1–2 eV below the elastic peak. By comparing the energies of the f-f excitations for calculated and experimental 5d RIXS spectra (Table 2), it could be concluded that the energy separation between the elastic peak and the inelastic scattering structure for the Cm (III) ion is similar to that measured for the curium-248 isotope in the oxide sample and quite far from that for Cm (IV). A detailed comparison between the experimental results and the calculated spectra for the Cm (III) ion is given in the next section.

Comparison Between Theory and Experiment

Fig. 5 shows the comparison of experimental data with theoretical calculations for the Cm (IV) and Cm (III) ions at excitation energy 119.0 eV, which is indicated by the lettered arrow *e* on the Cm 5d XA spectrum. The energy separation between the elastic peak and the inelastic scattering features in the calculated spectra for Cm (IV) and Cm (III) (Table 3) allowed us to conclude that the curium-248 isotope had oxidation state (III) in the studied sample. This is supported by the dependence of the whole set of experimental data and calculated spectra for the Cm (III) ion on varying excitation energy (Fig.6).

The calculated inelastic features in Cm (III) 5d RIXS show 5 main peaks due to the final state terms ^6G_J, ^6F_J, ^6D_J, ^6P_J and ^4G_J, which appear at constant energy for varying excitation energies. Exactly the same profile appears in the experimental spectra for the curium oxide.

Generally the same tendency is observed for features ^6P_J and ^6G_J in the simulated and experimental spectra. When the incident photon energy is tuned to the "giant resonance" region of the absorption curve, the intense inelastic structure ^6P_J becomes weak (at excitation energies *e, f, g, h, and i*). The opposite behavior is observed for feature ^6G_J. At excitation energies below the "giant resonance"(*b, c, and d*) the inelastic structure ^6G_J is quite weak and the intensity of this peak increases with increasing excitation energies *e, f, g, h , and i*. This effect confirms the fact that the oxidation state of curium in the studied sample was (III). For the simulated 5d RIXS spectra of Cm (IV), we do not find similar dependence.

The experimental data for excitation energies *b* and *c* show a quite intense ^6F_J peak but the calculated spectra do not reproduce this peak. The peak is also not found pronounced at excitation energy *d* as compared with experiment, but its intensity starts to grow up. The feature ^6G_J is shifted 0.2 eV towards higher energy compared to experimental data as observed for excitation energies *e, f, g, h, and i*. The reason can be in applied uniform scaling of the F^2, F^4 and F^6 integrals, describing f-f interactions in our calculations while configuration interaction and hybridization with O 2p states may reduce these integrals differently.

Similar profile and excitation energy dependence observed for calculated and experimental RIXS spectra demonstrate that atomic multiplet theory is an appropriate tool for description of experimental results obtained for actinides system.

Conclusion

The data from this experiment is the first chemical information from a curium 5d edge obtained with a tunable photon source at a soft X-ray synchrotron radiation facility. The experimental results of the curium-248 isotope are interpreted using the atomic multiplet approach. This theory turns out to be very appropriate for actinide systems and demonstrates satisfactory agreement with experiment. Present RIXS data along with calculations provide valuable information on energies of intra-atomic f-f excitations in curium oxide. Comparison of experimental data with theoretical calculations for Cm(III) and Cm(IV) indicates that investigated curium-248 isotope in the oxide sample has oxidation state (III), which is in agreement with observation of valence stability in actinide series for actinide elements beyond plutonium.

The results of RIXS measurements have major implication for future studies. They show that microgram amounts of radioactive materials, which can be safely handled, is sufficient for detailed chemical and physical characterization of actinide compounds.

Acknowledgements

This work was supported by the Swedish Nuclear Fuel and Waste Management Co. (SKB), by the Swedish Research Council and Goran Gustafsson Foundation for Research in Natural Sciences and Medicine. The ALS work was supported by the Director, Office of Science, Office of Basic Energy Sciences, Division of Chemical Sciences, Geosciences, and Biosciences of the U.S. Department of Energy at Lawrence Berkeley National Laboratory under Contract No. DE-AC02-05CH11231. The curium-248 used in this work was supplied by the U.S. Department of Energy through the transplutonium element production facilities at ORNL.

* - Corresponding author: Kristina Kvashnina, Uppsala University, Department of Physics, Box 530, 75121, Uppsala, Sweden, t. (+46)18-4713540, f. (+46)18-471-3524, Kristina.Kvashnina@fysik.uu.se

References:

1. J.L. Sarrao, L.A. Morales, J.D. Thompson, B.L. Scott, G.R. Stewart, F. Wastin, J. Rebizant, P. Boulet, E. Colineau and G.H. Lander , Nature v. 420, 297–299 (2002)
2. S. Heathman, R.G. Haire, T.Le Bihan, A. Lindbaum, M. Idiri, P. Nomrmile, S. Li, R. Ahuja, B. Johansson, G.H. Lander, Science v. 309, 110–113 (2005)
3. S. Butorin, J. of Elect. Spectr. and Relat. Phenom 110–111 (2000) 213–233
4. S.M. Butorin, D.K. Shuh, K. Kvashnina, K. Ollila, Y. Albinsson, J.-H. Guo, L. Werme, and J. Nordgren (in press)
5. L. Pauling “Nature of Chemical Bonding,” Cornell University Press, p.26, 1939
6. V. Milman, B. Winkler, C.J. Pickard, J. of Nuclear Materials 322, 165–179 (2003)

7. S. Skanthakumar, C. W. Williams and L. Soderholm, Phys. Rev. B 64, 144521, 2001
8. P. Soderlind, R. Ahuja, O.Eriksson, B. Johansson, J.M. Wills, Phys. Rev. B 61 8119 (2000), Phys. Rev.B 50 7291 (1994)
9. C.J. Packard, B. Winkler, R.K. Chen, M.C. Payne, M.H. Lee, J.S. Lin, J.A. White, V. Milamn, D. Vanderbilt, Phys. Lett. 85, 5122 (2000)
10. E. Simoni, M. Louis, S. Hubert, S. Xia, Optical Materials 4, 641–650 (1995)
11. Y. Mochizuki, H. Tatewaki, J. Chem. Phys. 116 N 20, 8838 (2002)
12. K.G. Dyall, I.P. Grant, S. Wilson, J. Phys. B 17, L45 (1984)
13. Y. Mochizuki, H. Tatewaki, J. of Chem. Phys. 118 N 20, 9201 (2003)
14. J. Sytsma, K.M. Murdoch, N.M. Edelstein, L.A. Boatner and M.M. Abraham, Phys. Rev. B 52 N17, 12668 (1995)
15. K.M. Murdoch, N.M. Edelstein, L.A. Boatner and M.M. Abraham, J. Chem. of Phys. 105 N7, 2539 (1996)
16. K.M. Murdoch, A.D. Nguyen, N.M. Edelstein, S. Hubert and J.C. Gacon, Phys. Rev. B 56 N6, 3038 (1997)
17. M. Illemassene, N.M. Edelstein, K.M. Murdoch, M. Karbowiak, R. Cavellec and S. Hubert, J. of Luminescence 86, 45–60 (2000)
18. J.V. Beitz and J.P. Hessler, Nucl. Technol. 51, 169 (1980)
19. T. Kimura and G.R. Choppin, J. Alloys Compd. 213/214, 313 (1994)
20. J. Sugar, Phys. Rev. B 5, 5 (1972)
21. K.O. Kvashnina, S.M. Butorin, B. Hjörvarsson, J.-H. Guo and J. Nordgren, AIP Conf. Proc. 837, 255 (2006)

22. T. Warwick, P.Heimann, D. Mossessian, W. McKinney and H. Padmore, Rev. Sci. Instrum. 66, 2037 (1995)

23. J. Nordgren and R. Nyholm, Nucl. Instrum. Methods Phys.Rs. A 246, 242 (1986)

24. J. Nordgren, G. Bray, S. Cramm, R. Nyholm, J-E Rubensson and N Wassdahl, Rev. Sci. Instrum. 60 1690 (1989)

25. Giant Resonances in Atoms, Molecules and Solids, edited by J.P. Connerade, J.M. Esteva and R.C. Karnatak (Plenum, New York, 1987)

26. R.D. Cowan, The theory of Atomic Structure and Spectra (University of California Press, Berkeley, 1981)

27. S. Butorin, J. of Elect. Spectr. and Relat. Phenom. 110–111, 235–273 (2000)

28. S.M. Butorin, C. Sathe, A. Agui, F. Saalem, J.A. Alonso, J. Nordgren, Solid State Com. 135, 716–720 (2005)

29. H. Ogasawara and A. Kotani, Phys.Rev.B. 44, N5 , 2169 (1991)

30. D.W. Lynch and R.D. Cowan, Phys.Rev. B 36, 17 (1987)

31. M. Richter, M. Meyeer, M. Pahler, T. Prescher, E.V. Raven, B. Sonntag, H.-E. Wetzel, Phys. Rev A 40, 12 (1989)

32. Ogasawara, H. , Kotani, A.; Thole, B.T. Phys. Rev. B v 50, n 17, 1 Nov. 1994, p 12332-41

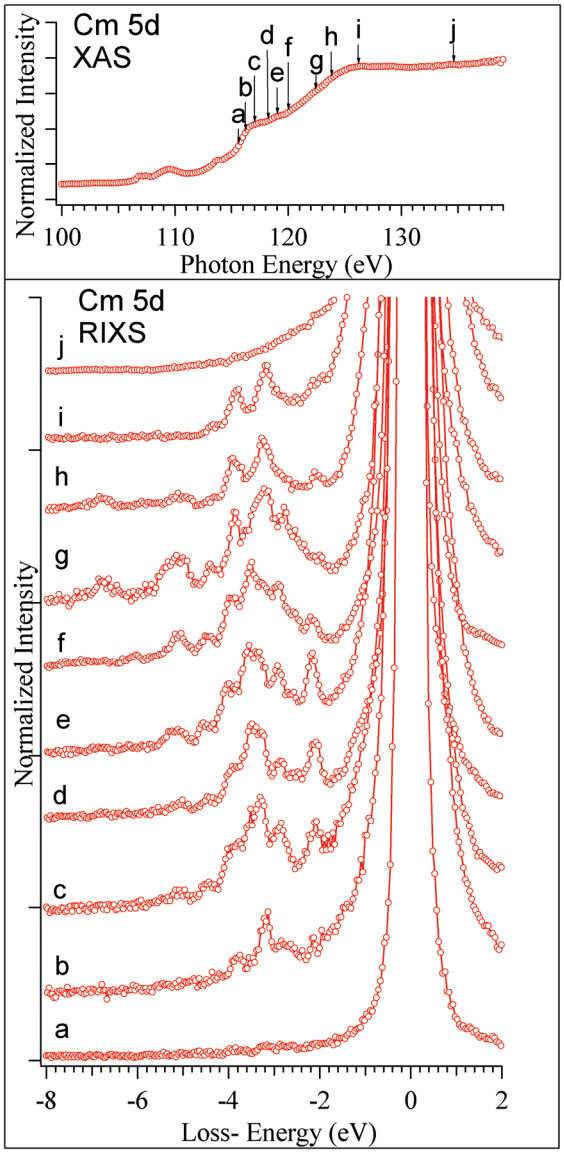

Fig.1. Cm 5d XAS (top panel) and RIXS spectra across the 5d edge plotted on the energy-loss scale. The elastic peak is set to 0 eV. Excitations energies *a-l* are indicated by lettered arrows on the XA spectrum.

Values	Cm (III)	Cm (IV)
$F^2_{(5f,5f)}$	7.97	8.90
$F^4_{(5f,5f)}$	5.21	5.85
$F^6_{(5f,5f)}$	3.82	4.31
$\zeta_{(5f)}$	0.39	0.42
$\zeta_{(5d)}$	4.31	4.34
$F^2_{(5d,5f)}$	8.88	9.12
$F^4_{(5d,5f)}$	5.74	5.99
$G^1_{(5d,5f)}$	9.34	9.74
$G^3_{(5d,5f)}$	5.78	6.05
$G^5_{(5d,5f)}$	4.13	4.32

Table 1. Slater integrals and spin-orbit coupling constants used in model calculations.

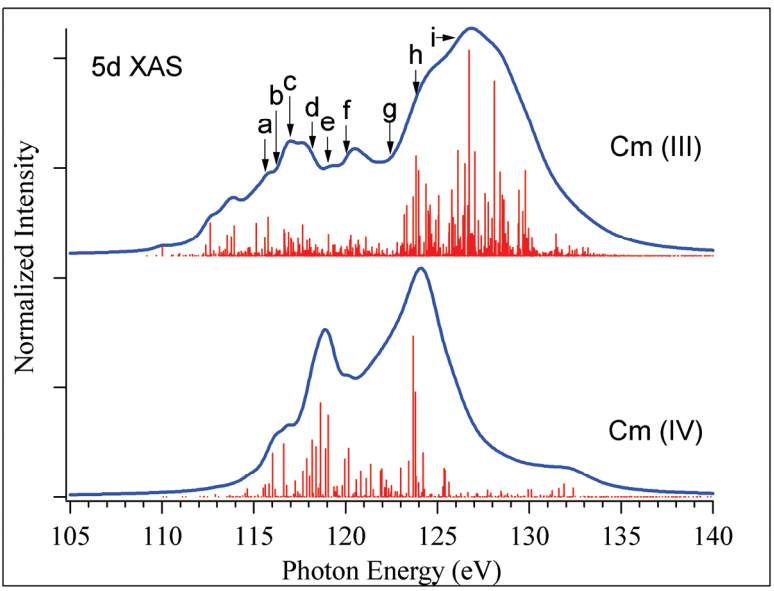

Fig.2. Calculated 5d XA spectra of Cm (III) and Cm (IV) ions using atomic multiplet theory.

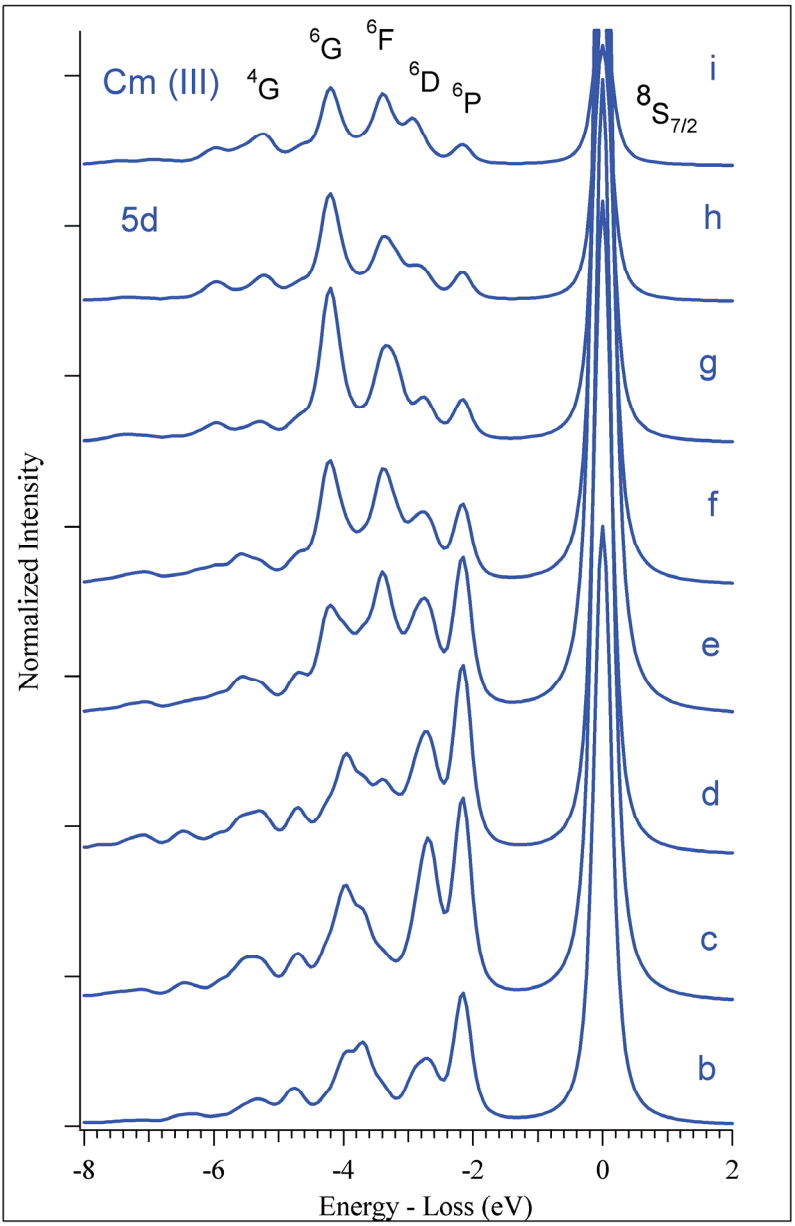

Fig.3. Calculated 5d RIXS spectra of Cm (III) ion. Excitation energies are indicated in Fig.2

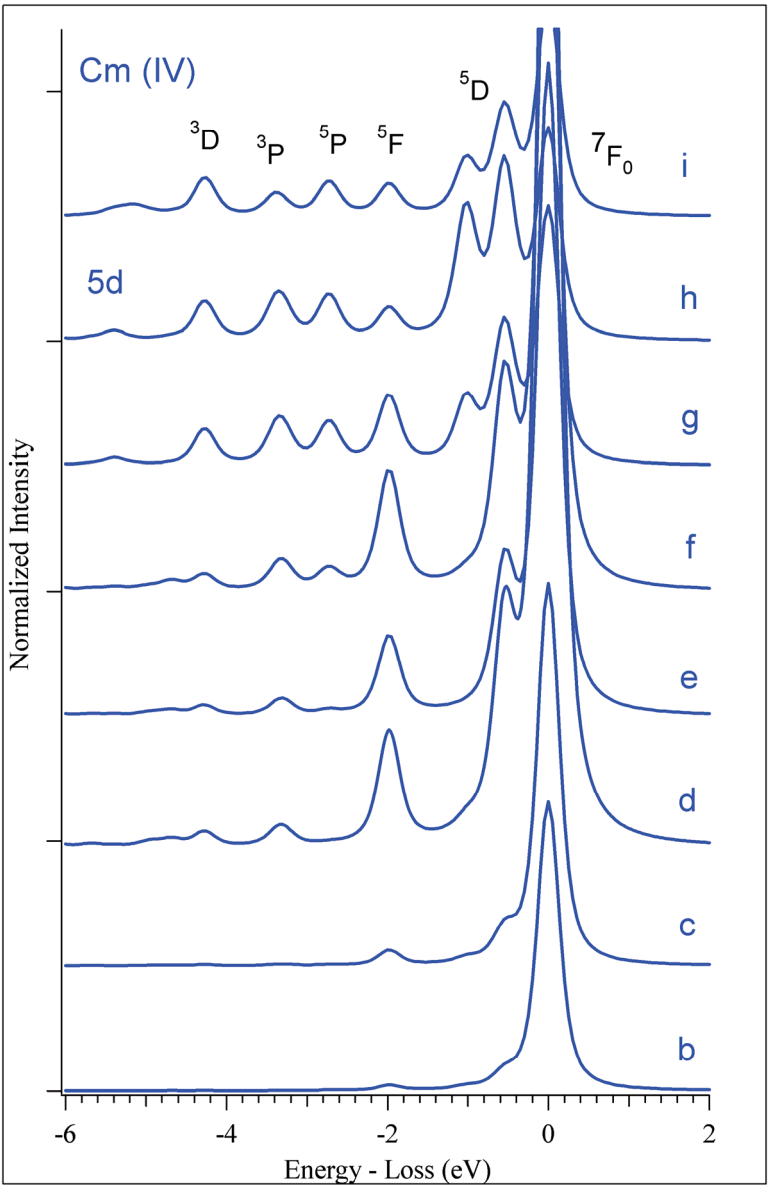

Fig.4. Calculated 5d RIXS spectra of the Cm (IV) ion. Excitation energies are indicated in Fig.2.

5d RIXS experiment	5d RIXS Cm (III)	(eV)	5d RIXS Cm (IV)	(eV)
-2.1	^{6}P	-2.1	^{5}D	-0.5
-2.8	^{6}D	-2.7	^{5}F	-2.0
-3.2	^{6}F	-3.4	^{5}P	-2.7
-3.9	^{6}G	-4.0	^{3}P	-3.3
-4.4	^{4}G	-4.7	^{3}D	-4.2

Table 2. Energy difference between elastic peak and inelastic scattering structure ^{5}D, ^{5}F, ^{5}P, ^{3}P, ^{3}D for Cm (IV) and ^{6}P, ^{6}D, ^{6}F, ^{6}G, ^{4}G for Cm (III) in RIXS spectra across the 5d edge. Table also represents the energy difference between elastic and inelastic features in RIXS 5d experiments for Cm isotope in studied sample.

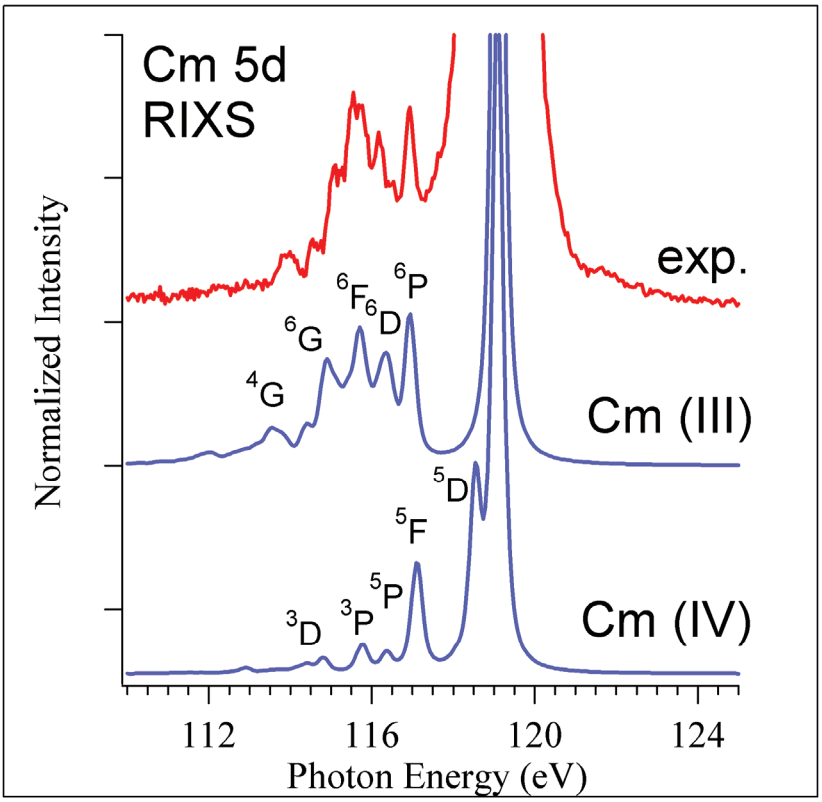

Fig.5. Cm 5d RIXS of curium oxide taken at excitation energy of 119.0 eV and compared with calculated spectra for Cm (IV) and Cm (III) ions at the same excitation energy.

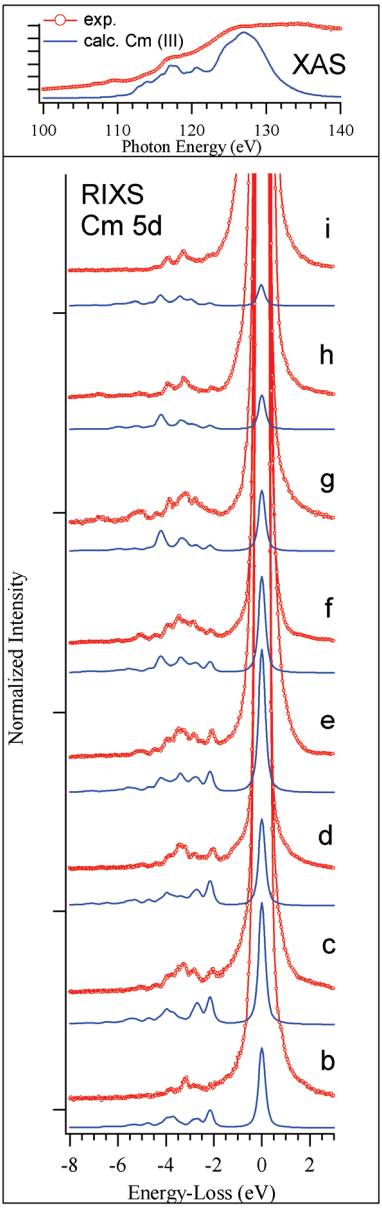

Fig.6. Comparison between Cm 5d XAS and RIXS experimental data and calculated spectra for the Cm (III) ion. Excitation energies are the same as indicated in Fig.1.

Paper IV

Mat. Res. Soc. Symp. Proc. Vol. 807 © 2004 Materials Research Society

Resonant Inelastic Soft X-ray Scattering Studies of U(VI) Reduction on Iron Surfaces

S. M. Butorin[1], D. K. Shuh[2], K. Kvashnina[1], I. L. Soroka[1], K. Ollila[3], K. E. Roberts[4], J.-H. Guo[5], L. Werme[6], and J. Nordgren[1]
[1]Department of Physics, Uppsala University, Box 530, S-751 21 Uppsala, Sweden
[2]Chemical Sciences Division, Lawrence Berkeley National Laboratory, Berkeley, California 94720, USA
[3]VTT Chemical Technology, P. O. Box 1404, FIN-02044 VTT, Finland
[4]Analytical & Nuclear Chemistry Division, Lawrence Livermore National Laboratory, P. O. Box 808, Livermore, California 94550, USA
[5]Advanced Light Source, Lawrence Berkeley National Laboratory, Berkeley, California 94720, USA
[6]SKB, Box 5864, S-102 40 Stockholm, Sweden

ABSTRACT

We report on the spectroscopic analysis of several samples relevant to the processes governing the behavior of oxidized uranium species in groundwater solutions under anoxic conditions. Both Fe samples with different times of exposure to the U(IV) solution and Fe metal-solution inetrfaces in the liquid cell *ex-situ* and *in-situ,* respectively. Resonant inelastic soft x-ray scattering is shown to be sensitive to the chemical state of uranium. The measurements were performed at a number of energies of the primary photon beam across the U 5d absorption edge. The results unambiguously indicate the reduction of U(VI) to U(IV) on the Fe surface.

INTRODUCTION

Disposal of spent fuel from commercial nuclear power reactors in Sweden and Finland will be done using a deep underground repository sited in granitic rocks. The fuel assemblies will be placed in canisters consisting of an outer corrosion-resistant copper shell and an inner cast steel form, which gives mechanical strength and reduces void space in the canister. The canister will be placed in a disposal borehole lined with compacted bentonite blocks. After the borehole is sealed, groundwater seepage will saturate the bentonite. Water will flow between the canister and the host rock via diffusion through the swollen bentonite. Any oxygen trapped in the repository will be consumed by reaction with the host rock and/or pyrite in the bentonite, giving long-term conditions with low redox potential. Under these reducing conditions, uranium dioxide is a stable phase.

Radiolysis of water by the alpha activity in the fuel has been proposed as a means of inducing locally oxidizing conditions at the surface of the fuel and causing the uranium dioxide to dissolve in the more soluble U(VI) oxidation state. Furthermore, the solubility of U(VI) in the presence of bicarbonate/carbonate ions is enhanced. To date, it has been assumed in safety analysis that U(VI) once formed will be released from the canister. The effect of the iron and its corrosion products on the final oxidation state of dissolved U(VI) has not been studied in dilute, near-neutral solutions that are relevant for Scandinavian geological environments.

There is still no realistic picture of which radioactive species might escape from the waste canister and ultimately be transported away from the repository environment. The most serious gap in these understandings concerns the reactivity of components inside the canister and their potential role in reducing oxidized, more soluble, actinide species to lower redox state. U(VI) is important because it is the most abundant soluble actinide and if reduced to U(IV) on the corrosion products inside the canister, this might also coprecipitate other actinides that are present in the solution inside the canister and prevent their release.

The aim of our experiments is to address the issue of possible reduction of oxidized species from solution, i.e. reduction of U(VI) to U(IV), when they encounter the reducing conditions provided by the canister insert corrosion products. The specific spectroscopic technique used in this project is based on resonant inelastic soft x-ray scattering (RIXS) (also called resonant soft x-ray Raman spectroscopy).

RIXS measurements at the U 5d threshold provide an opportunity to study in detail elementary excitations in U compounds due to the higher resolution of such experiments in comparison with those at the U 3d and 4d thresholds [1]. It has turned out that the technique is very sensitive to the valency and the chemical state of uranium in contrast to x-ray absorption spectroscopy (XAS). The 5d core-hole lifetime broadening is quite large, thus reducing the utility of XAS. As a result, the U 5d absorption spectra do not exhibit many sharp features [2]. The substantial smearing of the spectral structures hampers the analysis of the chemical state and the chemical environment of uranium in various compounds. In particular, it is difficult to distinguish between uranium species with different oxidation states, especially in case when one of species has a much lower concentration than another. In this situation, the virtually unlimited resolution (defined by the response function of the instrument) of the RIXS technique and its ability to enhance transitions to low-lying excited states are especially useful. RIXS spectroscopy provides good signatures in terms of new distinct transitions, representing electronic excitations within the 5f shell and having a characteristic profile for U(IV).

EXPERIMENTAL DETAILS

The materials studied were Fe foils polished with diamond spray (1 and 1/4 μm) on one side and exposed to U(VI) solution, reference samples of uranium oxides UO_2 and UO_3, such as powders imbedded into indium, and a single crystal of UO_2. To prepare the Fe samples, an aliquot of U(VI) in the form of uranyl nitrate was added to deaerated Allard groundwater (100 ml) under a N_2 atmosphere in a glove box. Two pieces of polished Fe foil (2×3 cm) were immersed in the solution. The starting concentration of U in solution was 500 ppb. A large decrease in U concentration was observed to occur within 2 to 3 weeks. These two pieces were shipped to Lawrence Berkeley National Laboratory (LBNL) for RIXS analysis after 17 days and 8.5 months immersion, respectively.

A liquid cell was employed for *in-situ* study of uranium reduction in the ground water solution with Fe. The schematic of the cell is shown in Fig. 1. The cell was about 20 mm x 20 mm in size and 4 mm thick with enough volume to accommodate a few drops of liquid, and it was made of tin bronze. X-rays were able to penetrate and be re-emitted through a silicon nitride membrane window. The size and thickness of the membrane used were 0.5 mm x 2 mm and 100 nm, respectively. A 10 mm x 10 mm frame holding the window was attached to the cell with the help of a specially-designed lid. Appropriate sealing was achieved with the use of a standard

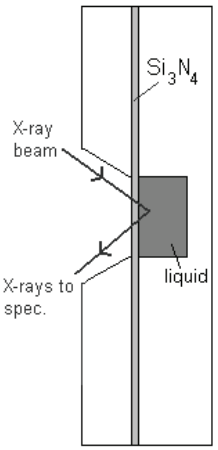

polymer gasket. The internal side of the 100-nm cell window was covered with a thin layer of Fe (50 Å), thus allowing for *in-situ* monitoring of the interaction between the Fe film and U ions in solution. The starting concentration of UO_2^{2+}(IV) in solution was 2 ppm.

The experiments were performed at undulator beamline 7.0 of the Advanced Light Source (ALS), LBNL, employing a spherical grating monochromator [2]. Resonant ultra-soft x-ray scattering spectra from the samples were recorded using a grazing-incidence grating spectrometer [3] with a two-dimensional detector. The incidence angle of the photon beam was approximately 15^o from the sample surface and the spectrometer was placed in the horizontal plane at an angle of 90^o with respect to the incidence beam. The bandwidth of the excitation was about 65 meV. The total energy resolution of the RIXS data was estimated from the full width at half maximum of the elastic peak to be 160 meV.

Figure 1. Schematic drawing of the liquid cell.

RESULTS AND DISCUSSION

Previous measurements on a set of and companion model calculations [2] showed that setting the energy of the incident beam close to the U 5d thresholds enhances the inelastic scattering cross section and ensures that electronic states of 5f symmetry are probed according to dipole selection rules. The spectral contribution of intra-ionic f-f transitions of U is enhanced at excitation energies close to 100 eV while at higher energies of the incident photon beam set to the main 5d absorption edge (e.g. 115 ev) inter-ionic excitations of charge-transfer character, such as ligand 2p – U 5f charge-transfer, dominate the RIXS spectra. The spectral pattern of intra-ionic f-f excitations is mainly determined by the formal valency of U, in turn, the charge-transfer transitions strongly depend on the chemical environment of U ions.

Figure 2 displays a set of scattering data from the Fe sample with 17-day exposure recorded at the incident x-ray energy of 100 eV, which corresponds to the energy of the weak pre-threshold structure in the U 5d x-ray absorption spectrum. A series of spectra were randomly measured from different 1 mm x 150 µm areas on the Fe sample surface. Six of them are shown in the figure along with spectra of reference oxides UO_2 and UO_3 that contain U(IV) and U(VI), respectively. The choice of the excitation energy is defined by the necessity to selectively look at the intra-ionic f-f transitions.

An inspection of Fig. 2 shows the presence of two distinct RIXS structures at energy losses of about –0.8 and -1.15 eV in the UO_2 spectrum. These structures represent f-f transitions as incident x-rays are inelastically scattered on electronic excitations within the 5f shell. The structures are very well reproduced by model calculations of RIXS spectra using atomic multiplet theory for the U(IV) ion. Naturally, these structures are absent in the UO_3 spectrum due to the formal $5f^0$ configuration of the U(VI) ions. In this situation, any reduction of U(VI) on the Fe surface should result in the appearance of characteristic RIXS structures. The present measurements indeed reveal the presence of significant inelastic contribution in spectra recorded

from some areas (spectra #4-6) on the surface of the Fe sample, thus indicating U(VI) reduction in those areas.

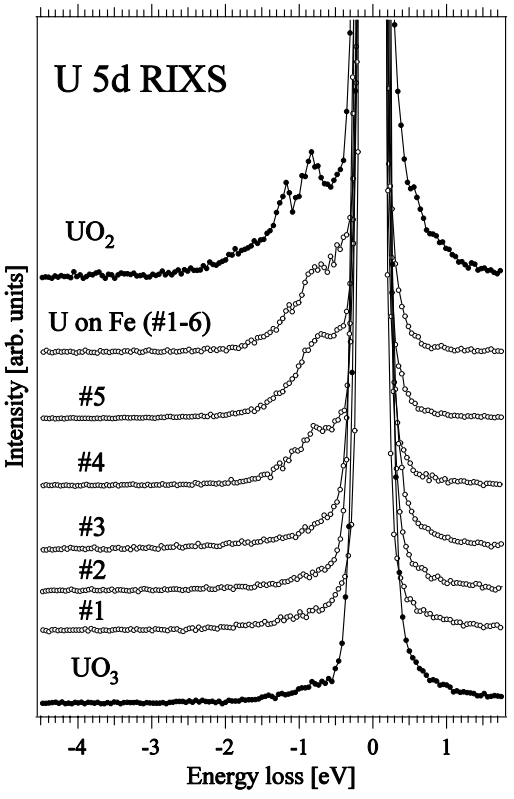

Figure 2. Enhanced inelastic part of soft x-ray scattering spectra of UO_2, UO_3 and U adsorbed on the Fe foil (elastic peaks are at 0 eV). The energy of the incident photons was set to 100 eV. The six spectra of adsorbed U were randomly measured from different 1mm x 150 μm areas on the surface of the Fe sample.

However, a comparison of RIXS spectra of the charge-transfer transitions between the foil and UO_2, made in Fig. 3, suggests that U(IV) species on the Fe foil are not necessarily in the form of uranium dioxide. The RIXS profiles of compared spectra are somewhat different. Similar results were obtained for another Fe foil prepared under the same conditions but with much longer exposure (8.5 month) to the U(VI) solution.

Quantitative estimates of the amount of reduced uranium were made by normalizing the recorded spectra to the characteristic core-to-core fluorescence lines and by comparison to model oxide systems with well-defined oxidation states for uranium.

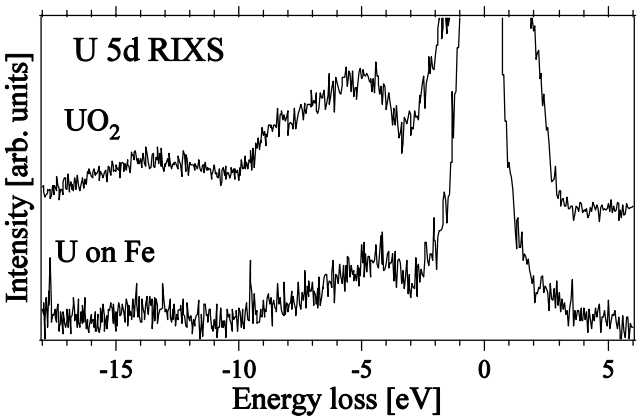

Figure 3. Enhanced inelastic part of the soft x-ray scattering spectra of UO_2 and U adsorbed on the Fe foil recorded at the excitation energy of 115.0 eV.

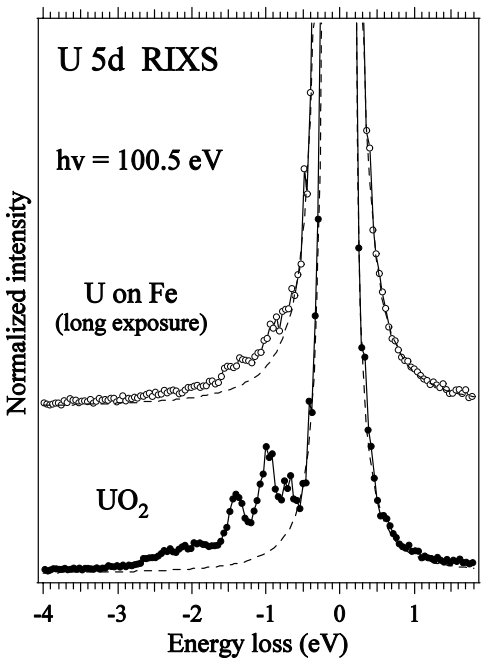

To model oxide systems with well-defined oxidation states for uranium. Using UO_2 single crystal standardss, we were able to compare the recorded spectra from the standards and the samples described above after normalization to the non-resonant U 6p-to-5d fluorescence line recorded with excitation above the 5d edge. An example of such a comparison is shown in Fig. 4. By fitting the elastic peak with the Voigt profile and estimating the area under the spectral curve in the energy-loss range corresponding to the f-f transitions the amount of reduced uranium can be derived. In this manner, we could estimate that 73% of the total uranium on the foil from the 17 days experiment is in fact present as U(IV) and for the 8.5 months experiment 42% was present as U(IV) taking into account the spatial heterogeneity. The reason for this reversed behaviour may be possible peeling off layers of the U(IV) compound.

Figure 4. Enhanced inelastic part representing f-f excitations in the soft x-ray scattering spectra of single-crystal UO_2 and U on the long-exposure Fe sample. Dashed lines represent Voigt fits of the elastic peaks.

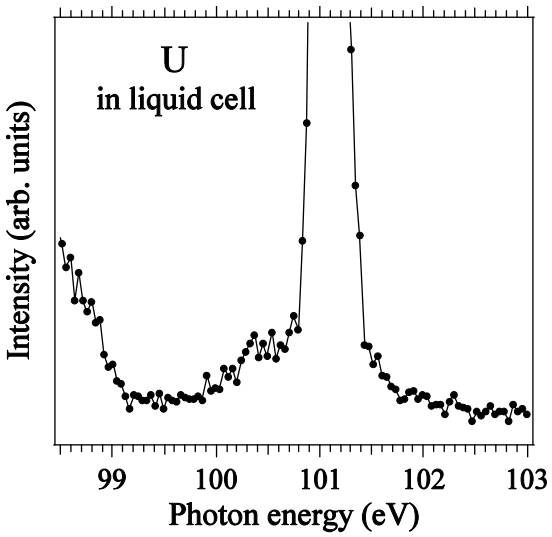

The liquid reaction cell for *in-situ* monitoring of uranium reduction on iron (see Fig. 1) was also tested. The design, used for test purposes, utilized a silicon nitride window and therefore a silicon contribution can be observed on the low energy side of the RIXS spectrum. Despite this, after three days U(IV) formed on the thin layer of iron in the cell (Fig. 5). These results indicate that the reaction cell has potential for being used to determine the kinetics for U(VI) reduction on iron corroding under anoxic conditions.

Figure 5. Enhanced inelastic part representing f-f excitations in the soft x-ray scattering spectrum of uranium in the liquid cell.

CONCLUSION

The results of our studies unambiguously indicate that U(VI) in the ground water solution is getting reduced by the Fe surface to U(IV). This also suggests that U(VI) formed by the radiolysis of water in the disposal canister can be reduced to U(IV) species on the inset corrosion products and prevent release from the canister.

ACKNOWLEDGEMENTS

This work was supported by the European Union via contract FIKW-CT-2000-00019, by the Swedish Research Council, and Göran Gustafsson Foundation for Research in Natural Sciences and Medicine. ALS is operated by the U. S. Department of Energy (DOE), Director, Office of Basic Energy Sciences (BES), Division of Material Sciences under Contract No. DE-AC03-76SF00098 at LBNL. The work was also supported in part by the Chemical Sciences, Geosciences, and Biosciences Division of DOE BES at LBNL under the same Contract.

REFERENCES

1. S. M. Butorin, *J. Electr. Spectros. Rltd. Phenomena* **110-111**, 213 (2000).
2. G. Kalkowski, G. Kaindl, W. D. Brewer, and W. Krone, *Phys. Rev.* **B35**, 2667 (1987).
3. T. Warwick, P. Heimann, D. Mossessian, W. McKinney, and H. Padmore, *Rev. Sci. Instrum.* **66**, 2037 (1995).
4. J. Nordgren, G. Bray, S. Cramm, R. Nyholm, J.-E. Rubensson, and N. Wassdahl, *Rev. Sci. Instrum.* **60**, 1690 (1989).

Paper V

Immobilization of UO_2^{2+} and NpO_2^+ carbonate in groundwater through reduction on corroding iron.

S. M. Butorin[1], D. K. Shuh[2], K.O. Kvashnina[1], K. Ollila[3], Y. Albinsson[4], J.-H. Guo[2], L. Werme[1,5] , and J. Nordgren[1]

[1]*Department of Physics, Uppsala University, Box 530, SE-751 21 Uppsala, Sweden*

[2]*Lawrence Berkeley National Laboratory, Berkeley, CA 94720, USA*

[3]*VTT Processes, P.O. Box 1404, FIN-02044 VTT, Finland*

[4]*Nuclear Chemistry Department, Chalmers University of Technology, SE-412 96 Gothenburg, Sweden*

[5]*SKB, Box 5864, SE-102 40 Stockholm, Sweden*

One-sentence summary: Mobile oxidized uranium(VI) and neptunium(V) aqueous complexes released from high level nuclear waste can be reduced and precipitated as immobile tetravalent species when contacting corroding iron surfaces.

Abstract: Resonant inelastic soft X-ray scattering studies of corroding iron in oxygen-free dilute uranyl and neptunyl solutions show that anionic actinyl complexes can be precipitated and reduced to the insoluble tetra-valent species on the corroding iron surface. This also suggests that the mobile, oxidized actinides U(VI) and Np(V) formed by

the radiolysis of water in the waste package will largely be reduced to immobile U(IV) and Np(IV) species on the anaerobically corroding iron components that are present in the waste package. As a consequence, the U and Np will not be released and transported to the biosphere.

1000 years after removal from the reactor, the radiotoxicity of the spent nuclear fuel is totally dominated by the actinides (see Fig. 1). These actinides are fixed in the UO_2 matrix of the fuel. In countries in which the groundwater level is close to the surface, a deep geologic repository for nuclear waste will have to be constructed under the groundwater level. The deep groundwaters are oxygen-free and reducing and under these conditions the actinides are only sparingly soluble. It has been argued, however, that the reducing conditions near the fuel surface can be upset by radiolysis of the water caused by the radioactivity of the fuel. Strongly oxidizing species, such as H_2O_2, formed during alpha-radiolysis of water have the potential to oxidize the tetravalent form of the the actinides U, Np, and Pu to higher oxidation states. These actinides are much more soluble in groundwater when they are oxidized to V (Np, Pu) and VI (U, Pu). In those oxidation states, the actinyl ions can form strong anionic complexes with components in the groundwater such as carbonate and their solubilities can increase as much as five orders of magnitude in the case of U and Np. These anionic complexes are also known to sorb less effectively than cations on mineral surfaces and have, therefore, a higher potential for transport in the biosphere. Through interaction with solid reducing agents in the immediate

vicinity of the spent fuel, however, these actinide species could be immobilized by reduction and precipitation onto the solids.

The waste will be totally isolated from the environment by encapsulation in a metal container. In most nuclear waste management programs, this container has a mild steel och cast iron component in order to be able to withstand the hydrostatic pressure at the disposal depth (approximately 500 m under the water table) (*1*). Since the groundwaters are oxygen free and reducing, the iron/steel component will corrode anaerobically at a very low rate, typically 0.1 μm per year (*1*). The corroding iron will, therefore, be present in the vicinity of the high level waste for very long times. Anaerobically corroding mild steel or iron could, therefore, act as an actinide scavanger.

There are, however, experimental difficulties associated with demonstrating that such processes occur. Even in the more soluble form, the expected concentrations of actinides in groundwater will be very low, for uranium in the range of a few ppm and for neptunium and plutonium in the ppb to sub-ppb range. An extremely element-sensitive probe will have to be used to determining the valency state of a monolayer-thick precipitate on a corroding iron surface. Soft X-ray spectroscopy has that capacity (*2, 3*).

The objective of our experiments is to address the issue of possible reduction of oxidized species from solution, in this study reduction of U(VI) to U(IV) and reduction of Np(V) to Np(IV), when they encounter the reducing conditions provided by the corrosion of ferrous materials present in the waste package. The specific spectroscopic technique is resonant inelastic soft X-ray scattering (RIXS; also known as resonant soft X-ray Raman spectroscopy). RIXS measurements at the actinide 5d threshold provide high resolution, which makes it easier to study in detail elementary excitations in U compounds (*4*). The

technique is sensitive to the oxidation state and the speciation of uranium in contrast to X-ray absorption spectroscopy (XAS) where the 5d core-hole lifetime broadening is large. As a result, the actinide 5d absorption spectra do not exhibit many sharp features (*5*), thus reducing the utility of XAS. In particular, it is difficult to distinguish between uranium species with different oxidation states, especially in the case when one of the species has a much lower concentration than another. The superlative resolution (defined by the response function of the instrument) of the RIXS technique and its ability to enhance transitions to low-lying excited states makes this technique especially powerful.

The measurements on a set of reference systems and companion model calculations (see also *4*) showed that setting the energy of the incident beam close to the U 5d thresholds enhances the inelastic scattering cross section and ensures that electronic states of 5f symmetry are probed according to dipole selection rules. This is illustrated in Fig. 2, where the first RIXS results from measurements on UO_2 are presented. The atomic multiplet calculations of resonant scattering spectra (details of the calculation formalism are described in *4*) reproduce all of the RIXS structures very well, thus supporting their assignment to the intra-atomic f-f excitations. Such structures uniquely identify the oxidation state of the actinide in RIXS measurements near the U 5d threshold; therefore, they provide good fingerprints for the valence state of U in different systems. The spectral contribution of intra-ionic f-f transitions of U is enhanced at excitation energies close to 100 eV, while at higher incident photon energies towards the main 5d absorption edge (e.g., 115 eV) inter-ionic excitations of charge-transfer character, such as ligand 2p – U 5f charge-transfer, dominate the RIXS spectra (not shown). The spectral pattern of intra-ionic f-f excitations is mainly determined by the formal oxidation state of U. In turn, the charge-

transfer transitions strongly depend on the chemical environment of U ions and provide additional chemical speciation information. Figure 2 shows the same comparison between calculations and the first experimental results for NpO_2.

Samples were prepared in anaerobic synthetic granitic groundwater from uranyl and neptunyl solutions. For uranium, the starting concentration was 2 x 10^{-6} M. For neptunium, the starting concentration was 4 x 10^{-7} M. The species in solution were calculated to be $UO_2(CO_3)_3^{4-}$ (70 %), $UO_2(CO_3)_2^{2-}$ (25 %) and $UO_2(OH)_2$ (5 %) for U and $NpO_2CO_3^-$ (75 %) and NpO_2^+ (25 %) for Np. The U samples were prepared in an inert gas glove box, while the Np samples were prepared in pressure vessels with a 50 bar H_2 overpressure. After the polished iron coupons had been introduced into the vessels, the concentrations of U and Np dropped several orders of magnitude. The iron coupons were removed and investigated by RIXS.

The experiments were performed at undulator beamline 7.0 of the Advanced Light Source (ALS) at Lawrence Berkeley National Laboratory, employing a spherical grating monochromator (*6*). Resonant ultra-soft X-ray scattering spectra from the samples were recorded using a grazing-incidence grating spectrometer (*7*) with a two-dimensional detector. The incidence angle of the photon beam was approximately 15^o from the sample surface and the spectrometer was placed in the horizontal plane at an angle of 90^o with respect to the incidence beam. The bandwidth of the excitation was about 65 meV. From the full-width at half maximum (FWHM) of the elastic peak, the total energy resolution of the RIXS data was estimated to be 160 meV.

Figure 3 displays a set of scattering data from the Fe sample with 17-day exposure recorded at the incident X-ray energy of 100 eV, which corresponds to the energy of the

weak pre-threshold structure in the U 5d X-ray absorption spectrum. A series of spectra were randomly measured from different 1 mm x 150 μm areas on the Fe surface. Six of them are shown in the figure along with spectra of the reference oxides UO_2 and UO_3 that contain U(IV) and U(VI), respectively. The necessity to look selectively at the intra-ionic f-f transitions defined the choice of the excitation energy. In the RIXS spectrum from UO_2, two distinct structures are present at energy losses of −0.8 eV and −1.15 eV. These structures represent f-f transitions as the incident X-rays are inelastically scattered within the 5f shell as was discussed above. Naturally, these structures are absent in the UO_3 spectrum resulting from the formal $5f^0$ configuration of the U(VI) ions. Reduction of U(VI) on the Fe surface should, therefore, result in the appearance of characteristic RIXS structures. The present measurements do, indeed, reveal the presence of a significant inelastic contribution in the spectra recorded from some areas (spectra #4-6) on the surface of the Fe coupon, thus indicating U(VI) reduction in those areas. Similar results were obtained for Np samples. Figure 4 shows the corresponding RIXS spectra of Np species sorbed on the iron coupon together with spectra of NpO_2 recorded at the same excitation energies. The RIXS structures from the Fe coupon and in the NpO_2 reference closely resemble each other. This resemblance unambiguously indicates the existence of Np(IV) on the iron coupon and that reduction of Np(V) had taken place.

Quantitative estimates of the amount of reduced uranium were made by normalizing the spectra to the characteristic core-to-core fluorescence lines and, by comparison, to model oxide systems with well-defined uranium oxidation states. Using UO_2 single-crystal standards, we were able to compare the spectra recorded from the standards and the samples described above after normalization to the non-resonant U 6p-to-5d fluorescence

line recorded with an excitation above the 5d edge. By fitting the elastic peak with a Voigt profile and estimating the area under the spectral curve in the energy-loss range corresponding to the f-f transitions, the amount of reduced uranium can be derived. In this manner, it is estimated that 73% of the total uranium on the foil from the 17-day experiment is, in fact, present as U(IV). For the 8.5-month experiment, 42% was present as U(IV) taking into account the spatial heterogeneity. The reason for this reversed behaviour is believed to be due to expected peeling off of U(IV) compound layers .

The results of our studies unambiguously show that U(VI) and Np(V) in the groundwater solution is reduced by the Fe surface to U(IV) and Np(IV), respectively. This suggests that the mobile, oxidized actinides U(VI) and Np(V) formed by the radiolysis of water in the waste package will be largely reduced to immobile U(IV) and Np(IV) species on the anaerobically corroding iron components in the waste package. Consequently, the U and Np will not be released and transported to the biosphere.

1. N. R. Smart, D. J. Blackwood, L. Werme, *Corrosion* **58**, 627 (2002).
2. T. Wiell, H. Tillborg, A. Nilsson, N. Wassdahl, N. Mårtensson, J. Nordgren, *Surf. Sci. Letters* **304**, L451-L455 (1994).
3. P. O. Nilsson, J. Kanski, J. V. Thordson, T. G. Andersson, J. Nordgren, J., Guo, M. Magnusson, *Phys. Rev. B* **52,** R8643-R8645 (1995).
4. S. M. Butorin, *J. Electr. Spectros. Rltd. Phenomena* **110-111**, 213-233 (2000).
5. G. Kalkowski, G. Kaindl, W. D. Brewer, W. Krone, *Phys. Rev.* **B35**, 2667-2677 (1987).

6. T. Warwick, P. Heimann, D. Mossessian, W. McKinney, H. Padmore, *Rev. Sci. Instrum.* **66**, 2037-2040 (1995).

7. J. Nordgren, G. Bray, S. Cramm, R. Nyholm, J-E. Rubensson, N. Wassdahl, −*Rev. Sci. Instrum.* **60**, 1690-1696 (1989).

8. This work was finacially supported by the European Commission under Contract EU FIKW-CT-2000-00019. The ALS work was supported by the Director, Office of Science, Office of Basic Energy Sciences, and Biosciences of the U.S. Department of Energy at Lawrence Berkeley National Laboratory under contract No. DE-AC03-76SF00098.

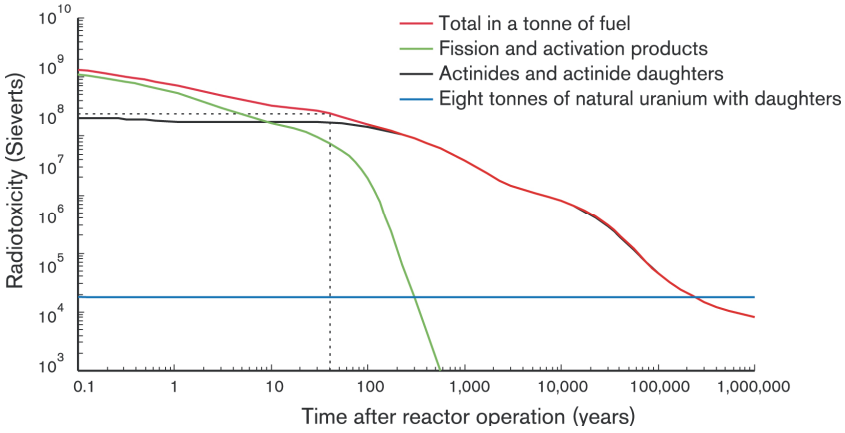

Figure 1. Radiotoxicity of spent fuel as a function of time for Swedish boiling water reactor (BWR) fuel with a burnup of 38 MWd/kg Uranium. The radiotoxicity refers to indigestion through food. The disposal will take place after 30 to 40 years of intermediate storage.

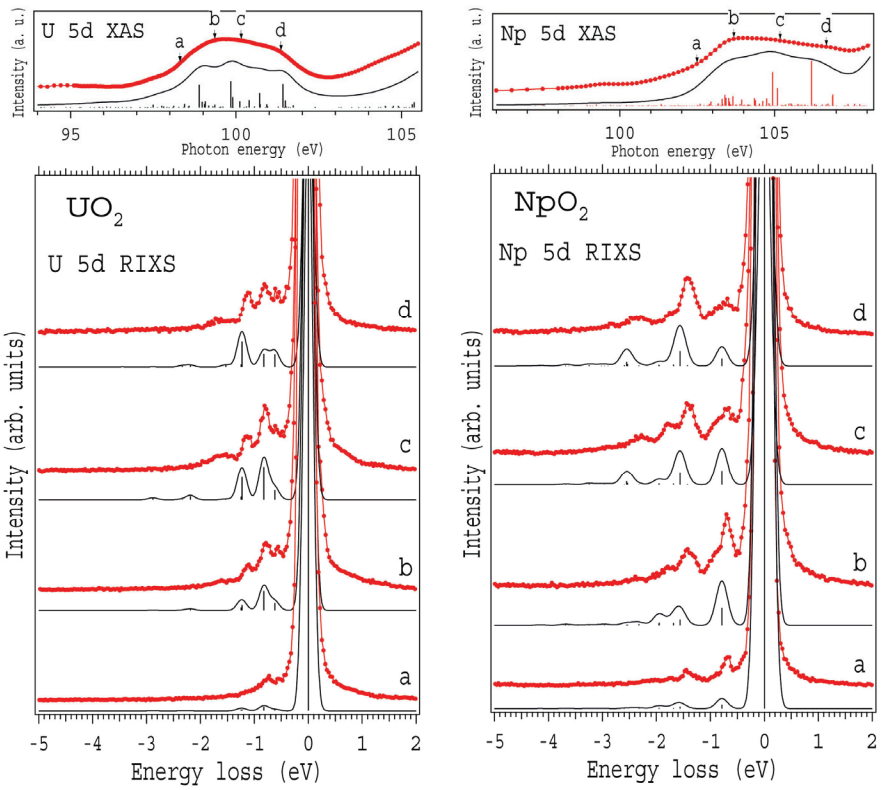

Figure 2. Resonant inelastic X-ray scattering spectra of single-crystal UO_2 and poly-crystalline NpO_2 recorded at different excitation energies of the incident photon beam set to the pre-threshold structure in the actinide 5d X-ray absorption spectrum (elastic peaks are at 0 eV). The excitation energies are indicated with arrows and the corresponding letters. The figure also shows the results of atomic multiplet calculations (bars with thin lines) for the U(IV) and Np(IV) ions, respectively. Excitation energies are indicated by arrows on the total electron yield spectrum at the actinide 5d absorption edge shown in the top panel.

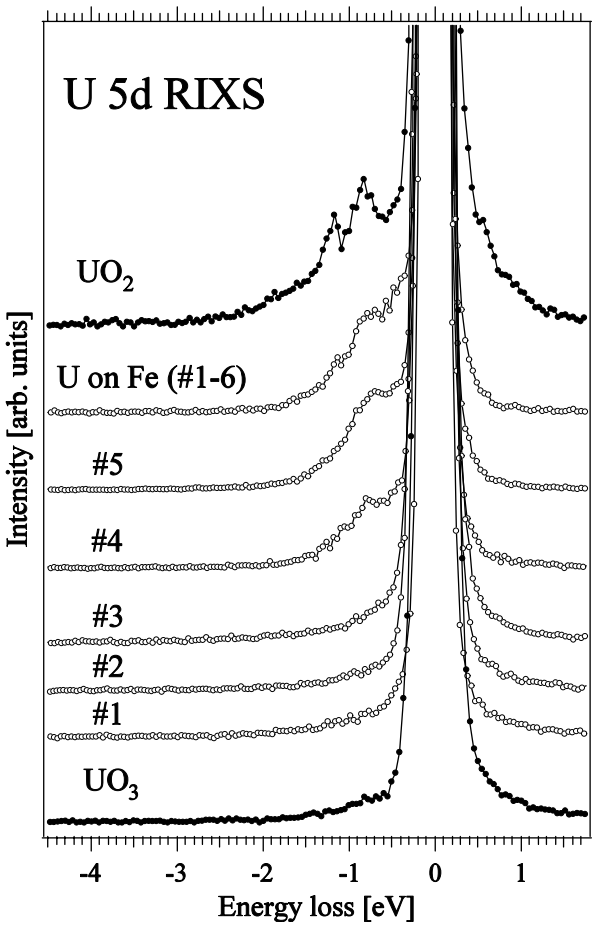

Figure 3. Enhanced inelastic part of soft X-ray scattering spectra of poly-crystalline UO_2, UO_3, and adsorbed U on the Fe foil. The energy of the incident photons was set to 100 eV. Six spectra of adsorbed U were randomly measured from different 1 mm x 150 μm areas on the surface of the Fe sample. The structures typical for U(IV) f-f excitations can be seen in spectra 4-6 indicating reduction of U(VI) in these areas.

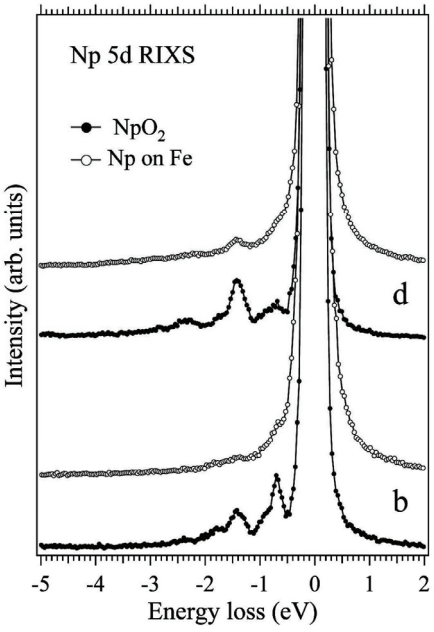

Figure 4. Comparison of resonant inelastic soft X-ray scattering spectra of NpO2 and Np sorbed on the Fe coupon. Letters correspond to the same excitation energies as shown in Fig. 2.

Paper VI

Studies of Actinides Reduction on Iron Surface by means of Resonant Inelastic X-ray Scattering

K.O. Kvashnina[1*], S.M. Butorin[1], D.K. Shuh[2], K. Ollila[3], I. Soroka[1], J.-H. Guo[4], L. Werme[1,5] and J. Nordgren[1]

[1] *Department of Physics, Uppsala University, Box 530, 751 21 Uppsala, Sweden*
[2] *Chemical Sciences Division, Lawrence Berkeley National Laboratory, Berkeley, CA 94720, USA*
[3] *VTT, 90571 Oulu, Finland*
[4] *Advanced Light Source, Lawrence Berkeley National Laboratory, Berkeley, CA 94720, USA*
[5] *SKB, Stockholm, Sweden*

The interaction of actinides with corroded iron surfaces was studied using resonant inelastic x-ray scattering (RIXS) spectroscopy. RIXS profiles, corresponding to the f-f excitations are found to be very sensitive to the chemical states of actinides in different systems. Our results clearly indicate that U(VI) (as soluble uranyl ion) was reduced to U(IV) in the form of relatively insoluble uranium species, indicating that the iron presence significantly affects the mobility of actinides, creating reducing conditions. Also Np(V) and Pu (VI) in the ground water solution were getting reduced by the iron surface to Np(IV) and Pu (IV) respectively. Studying the reduction of actinides compounds will have an important process controlling the environmental behaviour. Using RIXS we have shown that actinides formed by radiolysis of water in the disposal canister is likely to be reduced on the inset corrosion products and prevent release from the canister.

A special issue in constructing the underground repository for used nuclear fuel is questions about safety of the canister in the long-term conditions. A way to predict possible risks during long storage period is to study the reactions and interface phenomena of the spent nuclear waste after it has been placed in geological environment. The canister consists of the outer copper shell, as a corrosion resistant barrier and the inner iron shell, in order to add strength to the canister and reduce space available for water, circulating around after the corrosion barrier will be broken. The essential part in a safety assessment involves a complete understanding of interactions of materials and environment inside the canister.

Scientific understanding of processes that control chemical changes of radioactive species from spent fuel can be achieved by studying interactions of actinide ions (U, Np, Pu) with corroded iron surfaces. We made a study of model systems with different actinides in contact with water and iron. The liquid reaction cell was used in some experiments for the in-situ monitoring of the reaction between iron and uranium. The systems were studied with the help of resonant inelastic x-ray scattering (RIXS) spectroscopy, which enables us to determine the oxidation states of actinides in different species.

Our results indicate that actinide ions with high valences in ground water solutions became reduced by the iron surfaces. This fact became significantly important, since the reduction of actinides inside the canister can prevent their release due to the much lower solubility of reduced Np (IV), U(IV) or Pu (IV) than those spices with valency V (Np, Pu) and VI (U, Pu).

The Fe samples with U were made by exposing iron strip (99.9994%) to the anoxic allard groundwater solutions of uranyl nitride for the 17 days. The neptunium containing samples were also prepared by Fe foil exposure to the neptunyl solutions in groundwater. The starting

concentration was 2 x 10^{-6} M for uranium and 4 x 10^{-7} M for neptunium. The species in solution were calculated to be $UO_2(CO_3)_3^{4-}$ (70%) and $UO_2(CO_3)_2^{2-}$ (25%) for U and $NpO_2CO_3^-$ (75%) and NpO_2^+ (25%) for Np. The U samples were prepared in an inert gas glove box while the Np samples were prepared in pressure vessels with a 50 bar H_2 overpressure.

The liquid reaction cell was utilized for in-situ studies of uranium reduction on Fe from the groundwater solution. The schematics of the cell are shown on Figure1. The liquid cell consists of the 20mm x 20mm frame, which is holding the 10mm x 10mm Si_3N_4 window and O-ring in order to prevent the leaking processes. The height of the liquid cell is 4 mm, which is enough to put one drop of liquid. On the backside of the 100nm thick Si_3N_4 window, the 100Å Fe film was deposited in order to study the chemical reactions between this film and uranium ions in solution. The initial concentration of the UO_2^{2+} (IV) in solution was 2 ppm.

The experiments were made at beamline 7.0 of the Advance Light Source, Lawrence Berkeley Laboratory, USA. These undulator beamlines includes a spherical grating monochromotar, which gives resolution of 50 meV at ~110eV. RIXS spectra were recorded, using grazing incident grating spectrometer [1-2] with 160 meV resolution for U and Np and 110 meV for Pu samples. The instrument is based on three gratings, mounted at fixed angles of incidence and a large two-dimensional multichannel detector. The incident angle of the photon beam was 20º from the surface for solid samples and 35º for the liquid cell.

Figure 2 shows U 5d RIXS spectra of the iron films exposed to the U(VI)solution in ground water for 17 days. Scattering data were recorded at excitation energy of 100.5 eV, which corresponds to the pre-threshold structure U 5d XA spectrum. For simplicity, we plotted RIXS spectra in the energy-loss scale. U 5d scattering spectra for the reference UO_2 sample are also displayed in Fig.2. All the spectra have the elastic peak at 0eV and inelastic scattering structures at -1.0 –2.0 eV on the energy-loss scale. These structures correspond to the f-f excitations and could be very well reproduced by theoretical calculations, using atomic multiplet theory[3]. These excitations are absent in the UO_3 spectrum [4], which could be used as a good "fingerprint" in the investigation of oxidation states of actinides. According to this, a reduction of the uranium valency from (VI) to (IV) on the iron surface should be indicated by an appearance of the f-f excitations in the resonant spectra. Our data clearly indicate the presence of the f-f excitations on the RIXS spectra for the uranium on the iron film, thus allowing us to conclude that U(VI) is reduced by iron to U(IV). We are also able to derive the amount of reduced uranium by comparison the area under the shape of f-f excitations for the UO_2 and investigated iron films. The spectra were normalized to the characteristic core-to-core U 6p→ 5d fluorescence lines, which allowed us to deduce the total amount of reduced U (IV) after 17 days of exposure (73%).

Similar results were obtained for Np and Pu samples. Figure 3 shows the Np 5d and Pu 5d RIXS spectra of Np and Pu species formed on the iron strips together with spectra of NpO_2

and PuO_2 , which were recorded at the excitation energies close to that of the pre-threshold structure in actinide 5d XA spectra. The RIXS spectra of Np and Pu on Fe reveal f-f excitation patterns similar to those of NpO_2 and PuO_2 respectively, thus indicating the existence of Pu(IV), Np(IV) on the iron strips and that reduction of Np(V), Pu (VI) had been taken place.

We also monitored a reaction between U(VI) ions and iron using the liquid cell (Fig.1) for the in-situ studies. We used a silicon nitride window for these measurements and therefore the silicon contribution can be observed below 99 eV (Fig.4). After three days of exposure of Fe film to the solution, the f-f transitions can be observed in RIXS spectrum, thus indicating that U(IV) was formed on the thin iron film in the cell.

The results of our studies unambiguously indicate that RIXS profiles, corresponding to the f-f excitations are very sensitive to the oxidation states of actinides in different systems, which allowed us to suggest that soluble actinides species (U, Pu, Np) in the disposal canister can be reduced by iron to lower solubility form and prevent release from the canister.

Acknowledgements

This work was finacially supported by the European Commission under Contract EU FIKW-CT-2000-00019, by the Swedish Research Councill and Goran Gustafsson Foundation for Research in Natural Sciences and Medicine. The ALS work was supported by the Director, Office of Science, Office of Basic Energy Sciences, and Biosciences of the U.S. Department of Energy at Lawrence Berkeley National Laboratory under contract No. DE-AC03-76SF00098.

* - Corresponding author: Kristina Kvashnina, Uppsala University, Department of Physics, Box 530, 75121, Uppsala, Sweden, t. (+46)18-4713540, f. (+46)18-471-3524, Kristina.Kvashnina@fysik.uu.se

[1] T.Warwick, P.Heimann, D. Mossesian, W. McKinney and H. Padmore, Rev.Sci. Instrum. 66, 2037 (1995)
[2] J. Nordgren, G. Bray, S. Cramm, R. Nyholm, J.-E. Rubensson and N. Wassadahl, Rev. Sci. Instrum. 60, 1690 (1989)
[3] S. M. Butorin, J. of Eletron. Spec. and Rel. Phen. 110-111 (2000) 213-233
[4] S. M. Butorin, D.K. Shuh, K. Kvashnina, I. Soroka, K. Ollila, K.E. Roberts, J.-H. Guo, L.Werme and J. Nordgren, Mat. Res. Soc symp. Proc. Vol 807 (2004) Materials Research Society

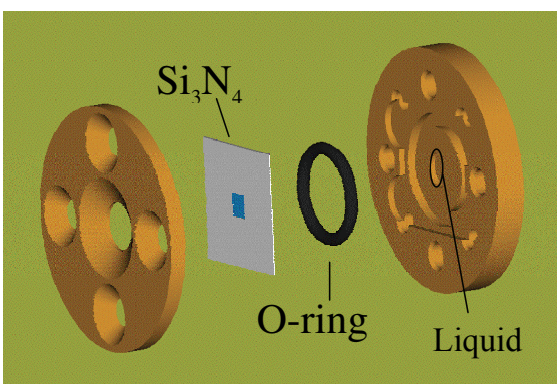

Figure1. Schematic drawing of liquid cell

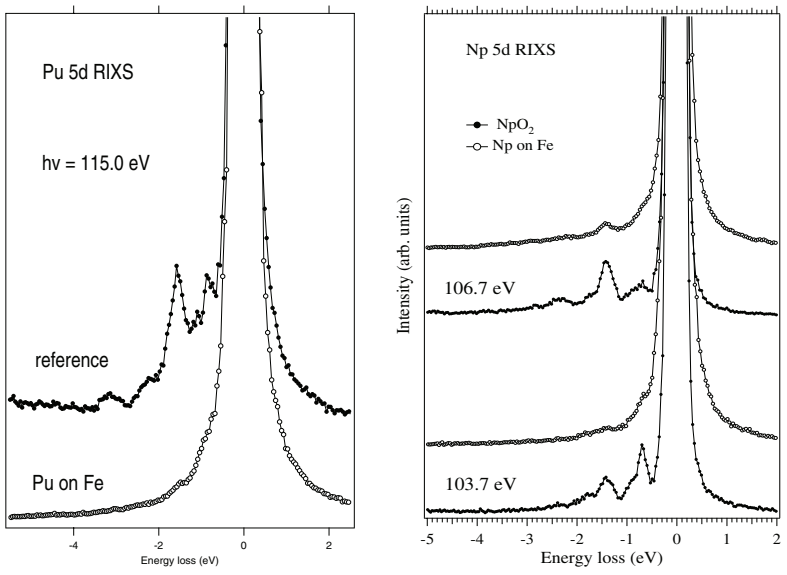

Figure 3. Comparison of RIXS spectra of Np, Pu oxides and Np, Pu formed on the Fe strip, recorded at the excitation energies, close to that of the pre-threshold structure in the Np 5d and Pu 5d XA spectra.

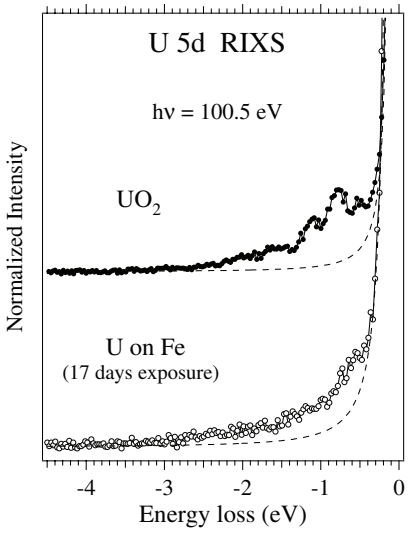

Figure 2. U 5d RIXS spectra reflecting f-f excitations of single crystal UO_2 and U on Fe after 17 days exposure to the U(VI) solution in groundwater.

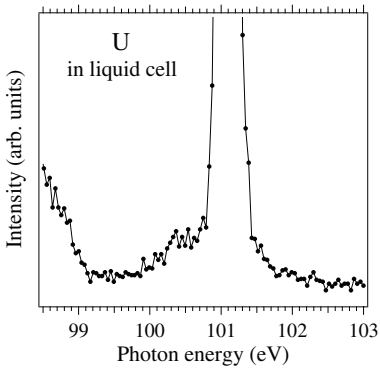

Figure 4. U 5d RIXS spectra of uranium in the liquid reaction cell

Paper VII

Resonant Inelastic X-ray Scattering Study of Copper Compounds and Minerals at Cu L_3 edge

K.O. Kvashnina[1*], S.M. Butorin[1], A. Modin[1], J.-H. Guo[2], R. Berger[3], L. Werme[1,4] and J. Nordgren[1]

[1] *Department of Physics, Uppsala University, Box 530, 751 21 Uppsala, Sweden*
[2] *Advanced Light Source, Lawrence Berkeley National Laboratory, Berkeley, CA 94720, USA*
[3] *Department of Materials Chemistry, Uppsala University, Box 538, 751 21 Uppsala, Sweden*
[4] *SKB, Stockholm, Sweden*

We have used x-ray absorption (XA) and resonant inelastic x-ray scattering (RIXS) spectroscopies to study a series of copper compounds, namely Cu_2O, CuO, $Cu(OH)_2$, $CuCl_2$, Cu_2S, $CuSO_4$, malachite $Cu_2(CO_3)_2(OH)_2$ and atacamite $CuCl_2 \cdot 3Cu(OH)_2$. Cu 2p XA spectra provide information about oxidation states. Divalent copper gives a single narrow line due to excitations into the empty 3d state, whereas monovalent copper gives a broad band at higher energy due to transitions to 4s states. Chemical shifts of the main line in the Cu^{2+} XA spectra of different compounds are observed but in some cases they are too small to make a clear distinction between the species. It is shown here that RIXS at the Cu 2p edge has a great potential to distinguish between the species due to large differences in spectral shapes for the same energy of incident photon beam.

The electronic structure of complex copper compounds is a main topic in the investigation of copper compounds since high temperature superconductors were discovered. Chemical bonding on copper and surrounding atoms in various materials has been studied extensively using known spectroscopic techniques.

It has been shown before that X-ray absorption spectroscopy (XAS) can be used to determine the oxidation state of the copper for different type of compounds: such as copper oxides[1-3], chlorides[3], sulfates[1,2] and other minerals [1,2]. A discussion of whether Cu is monovalent or divalent may be relevant when the elements in a compound have variable valency. But in cases when XAS can not find significant difference between copper compounds with the same oxidation state it makes sense to look for other

techniques that can help to make a distinction between the species when the materials become complex.

In addition to the traditional techniques like XAS, resonant X-ray inelastic scattering (RIXS) has been used to investigate electronic structure of copper systems. RIXS experiments for a number of copper compounds have already been done by several groups at copper K, M, and L edges as well as at the oxygen K edge[4-11]. Until now, most of studies have used incident photon energies around the main X-ray absorption (XA) peak. In this paper we analyze Cu 2p-3d RIXS spectra of Cu_2O, CuO, $Cu(OH)_2$, $CuCl_2$, $CuSO_4$, malachite $Cu_2(CO_3)_2(OH)_2$, and atacamite $CuCl_2{\cdot}3Cu(OH)_2$ recorded at different excitations energies.

In a systematic study of bonding effect in RIXS spectra for the copper compounds we found that Cu 2p spectra show very marked dependence on the chemical composition of investigated samples. This means that a combined study of RIXS and XAS is expected to give more detailed information about the electronic states of copper materials.

We also present Cu 2p XAS studies on a variety of copper compounds, such as Cu_2O, CuO, $Cu(OH)_2$,$CuCl_2$, Cu_2S, $CuSO_4$, malachite $Cu_2(CO_3)_2(OH)_2$, azurite $Cu_3(CO_3)_2(OH)_2$ and atacamite $CuCl_2{\cdot}3Cu(OH)_2$. The chemical shift of the main Cu L_3 line provide information about oxidation state, while the shape of RIXS spectra could be used as a fingerprint in detecting the chemical composition of the copper compounds. The paper is divided into two parts. The first part provides a detailed description of the Cu 2p XA spectra. In the second one we will discuss the behavior of the RIXS spectra for copper compounds at different excitation energies.

Experimental details

The Cu 2p absorption spectra were measured on beam-line 7.0 [12] at the Advance Light Source (ALS) of Lawrence Berkeley National Laboratory. The beamline employs a spherical grating monochromator, which gives resolution of 200 meV at the Cu $2p_{3/2}$ peak of CuO (~931eV). X-ray absorption spectra were recorded in total fluorescence yield mode (TFY) by a chaneltron (Fig. 1a) and by a photodiode (Fig. 1b) under high vacuum conditions. The resonant inelastic x-ray spectra were recorded using a high-resolution grazing incident grating spectrometer[13,14] employing a 5 m radius and 1200 lines/mm grating. RIXS spectra for the $CuSO_4$ and atacamite were recorded with 500 meV resolution and $CuCl_2$, $Cu(OH)_2$ and malachite $Cu_2(CO_3)_2(OH)_2$ with 1.0 eV resolution of the spectrometer. The incident angle of the photon beam was approximately 45 degrees from the sample surface and the spectrometer was placed in the horizontal plane at an angle 90 degrees with respect to the incident beam.

Thin films of CuO and Cu_2O were deposited from CuI as the copper source and O_2 as the oxygen source. Cu_2O was deposited at low O_2 partial pressures (P<0-2 Torr) in a long isothermal hot wall chemical vapour deposition (CVD) [15] reactor (T= 800 °C). The CuO phase was obtained at a certain position in the CVD reactor and a sudden maximum in the deposition rate was then reached. The maximum was attributed to a change in the deposition mechanism upon the formation of CuO. When I_2 was added to the reaction gas mixture, the maximum disappeared and the deposition rate increased[15]. Oxides of monovalent and divalent copper were in form of 200Å thin films on a silica substrate. The samples: $CuCl_2$, Cu_2S, $CuSO_4$, $Cu(OH)_2$ were in powder form. All the studied minerals were in solid form.

XAS

Fig. 1 shows Cu 2p absorption spectra for a number of copper compounds. The ground state of CuO can be described as a mixture of $3d^9$ and $3d^{10}\underline{L}$ character, where $\underline{L}$ is stands for a hole in the O 2p band [1]. The main peak at 930.8 eV in the XA spectrum of CuO corresponds to the $2p^5 3d^{10}$ final state. This state gives a single line without multiplet splittings because the *d* shell is full. At ~20.1 eV above this peak ($2p_{3/2}$) another structure with lower intensity appears ($2p_{1/2}$), which is broader due to shorter core-hole lifetime and the interaction with $2p_{3/2}$ continuum. The XA spectrum of monovalent copper clearly differs from the Cu^{2+} spectra. The main line of the Cu_2O spectrum is at higher energy (~ 933.3 eV) and corresponds to excitations to the empty 4*s* level.

The copper minerals, namely malachite, azurite and atacamite, $Cu(OH)_2$ and $CuCl_2$ (Fig. 1b) show a strong $2p_{3/2}$ peak similar to the CuO spectrum, which is an indication of the presence of $3d^9$ character in the ground state. The peak position differs between the samples up to several hundred meV (values are indicated in Table1). For example, the $2p_{3/2}$ peak for azurite is 0.2 eV higher than that for malachite due to the fact that the crystal field splitting in azurite is larger than in malachite [16]. Satellite structures for the minerals, which are visible at ~7eV above the main peak, are similar to those in CuO and are due to transitions to 4s states. The hydroxide $Cu(OH)_2$ also show an intense $2p_{3/2}$ peak similar to that found in CuO, malachite and azurite spectra. The peak position is close to that of copper oxide and the spectrum also includes the broad satellite structures. But for the atacamite this satellite structure is stronger as those in the spectra of other minerals.

The sulfur-containing compounds (Cu_2S and $CuSO_4$) are displayed in Fig. 1a. The Cu 2p XA spectrum of $CuSO_4$ shows a single $2p_{3/2}$ peak at ~ 930.8 eV and a $2p_{1/2}$ peak at ~ 950.8 eV, which is typical for divalent copper [1]. The Cu_2S absorption structure is more complex. As an analog of the monovalent copper, the ground state of Cu_2S, which is in the form of synthetic chalcocite, has predominantly d^{10} configuration and only the final state $2p^5 3d^{10} 4s^1$ can be reached, which gives rise to the main peak at 934.3 eV. This peak is 1.0 eV higher than in Cu_2O, which corresponds to the difference in electronegativity between oxygen and sulfur[1]. In chalcocite there is also a small peak at ~930.8 eV, thus indicating the presence of Cu^{2+} impurities. The spectrum of chalcocite has been reported earlier[10] with growing intensity of the peak at ~930.8 eV, depending on the sample treatment. Above the main peak in Cu_2S there is a broad structure similar to that in Cu_2O, which is attributed to excitations to the conduction band.

Fig. 1b shows the 2p absorption spectrum for $CuCl_2$. The peaks at 930.4 eV and at 950.3 eV indicate the presence of Cu^{2+} species. For CuO and $CuCl_2$, both square planar coordinated [3], shift of the main XAS peak reflects mainly a change in covalence of chemical bonding. It is higher for CuO than for $CuCl_2$ and we expect Cu L_3 line for CuO at higher energy.

In summary, the whole series of copper compounds could be divided into two classes. The first class consists of spectra in which copper is monovalent: Cu_2O and Cu_2S. The Cu L_3 energy is shifted to a higher value from Cu_2O to Cu_2S, due to the increasing charge on the copper atoms. The other class includes all spectra of the divalent copper compounds. The same effect as discussed above can be found on going from malachite to $CuCl_2$, azurite, atacamite, $CuSO_4$ and $Cu(OH)_2$ respectively, i.e. small shifts

to higher energy. Koster et al.[3] also observed an influence on the width of the spectra for most of the copper compounds. As the compounds are more ionic, the Cu L_3 peak tends to shift to lower energy and becomes sharper.

RIXS

RIXS results for various compounds are presented in Figs. 2-8. Fig.2 and Fig.3 display the Cu 2p-3d x-ray spectra, measured on Cu_2O and CuO. The spectra were recorded at varying excitation energies, indicated on the XA spectra in top panels of each figure. The spectra of Cu_2O appear to be much broader than those of CuO and less dependent on excitation energy. The spectra of CuO show a number of structures. The highest in peak corresponds to elastic peak and its intensity somewhat varies with increasing energy of incident photons. The main structures around –1.5 to –2.0 eV below elastic peak can be assigned to *dd* excitations. The low energy tail, extended down to ~ 6-7 eV is caused by charge-transfer excitations of electrons from O 2p band to the 3d states.

The energy of *dd* excitations has been a main topic in the investigation of the cuprate superconductors and other strongly correlated systems [4,6,7 8-11]. Direct *dd* excitations are dipole forbidden, but Tanaka and Kotani[17] first suggested theoretically that Cu *dd* excitations are potentially accessible with RIXS. The RIXS technique was also used to study the charge-transfer excitations in some correlated systems[18]. It was found before that the electronic structure of cuprates is a result of the hybridization of the Cu *3d* atomic states with the delocalized O *2p* states and could be characterized by the charge-transfer excitations, which appears at ~ 6-7 eV from elastic peak in Cu 2p-3d RIXS

spectra (Fig. 3). These low energy tails, extending down to ~ 6-7 eV have different shape and intensity for different types of copper compounds.

This charge transfer effect in RIXS is well described by the schematic total energy-level diagram shown in Fig. 9. When the incident photon energy is exciting the lower core state, the process is described by the solid line. For an excitation at higher energy, the process is described by the dashed lines. In the case that the inelastic scattering structures have constant energy losses, the elastic peak appears on the emitted–photon energy scale (process is shown as blue lines). On the other hand, inelastic scattering structure presented by *dd* excitations and charge–transfer satellites is shown as red lines.

Tanaka and Kotani[17] compared the energy level structure of the ground and excited states and found that the hybridization of the b_{1g} symmetry [17] are the largest and that the ground state is a strong mixture between d^9 and $d^{10}\underline{L}$ configurations with b_{1g} symmetry. However, significant difference for various copper compounds with a_{1g} symmetry was found [17] and the appearance of the shoulder in RIXS spectra comes from this symmetry.

Fig. 4 - 8 shows Cu L_3 RIXS spectra for atacamite $CuCl_2{\cdot}3Cu(OH)_2$, $CuSO_4$, $CuCl_2$, $Cu(OH)_2$, and malachite $Cu_2(CO_3)_2(OH)_2$ excited at a number of energies marked on XA spectra in top of panel. As mentioned before, RIXS spectra were recorded using different resolutions for different samples.

The basic interpretation for all compounds could easily be seen from the shape of the RIXS spectra, excited at energy A (C for malachite), corresponding to the $2p_{3/2}$ peak in XA spectrum. As described before, the features for all spectra show a characteristic

elastic peak, *dd* excitations and charge transfer satellites. This means that the investigated copper compounds can be assign to nominally divalent copper, which is in agreement with the XA spectra (Fig.1).

The ground state in all compounds is represented by a linear combination of $3d^9$ and $3d^{10}\underline{L}$ configurations. In the intermediate state, a Cu 2p core electron is promoted to the 3d state so that we have the $2p^53d^{10}$ configuration. In the final state, a 3d electron makes a transition to the 2p state by emitting a x-ray photon. The spectra for all copper compounds consist mostly of two parts: one is following the increasing incident photon energy (spectra A- D for atacamite and $CuSO_4$ and spectra A-C for $CuCl_2$, $Cu(OH)_2$ and A-F for malachite), the other part is always appears at a constant emitted photon energy (spectra E - G for atacamite and $CuSO_4$ and spectra D and E for $CuCl_2$, $Cu(OH)_2$ and F-H for malachite) which can be associated with characteristic, non-resonant emission.

It is also interesting to study the origin of the RIXS spectra for the incident photon energies in the region of the satellite structures (around 933.6 eV) in the XA. The existence of such satellite was discussed earlier by Flipse et al. [19] and Van der Laan et al. [1]. Besides its assign went to a structure of the conduction band, defined by the shape of the 4s density of states, it was suggested that the satellite can be due to a final state $2p^53d^{10}\underline{L}$, which indicates presence of a "defect" $3d^{10}\underline{L}$ initial state.

The Cu 2p-3d x-ray scattering spectrum excited at energies C and D for atacamite (Fig.4) shows a significant difference from spectra A-B and E-G, which normally represent the elastic peak, *dd* excitations and satellite structures. The shape and energy position of the structure at ~ 6-7 eV below the elastic peak in spectra C and D are different from those on CuO.

It turns out that development and behavior of this structure in RIXS spectra is different for different compounds. Unique spectral behavior was measured for $CuSO_4$, when excited at C and D energies (Fig.5), for $CuCl_2$, excited at C and D energies (Fig.6), for $Cu(OH)_2$ excited at B and C energies (Fig.7) and for malachite, excited at E energy (Fig.8). This structure in our data does not clearly follow the increasing excitation energy and is observed in the spectra rather at constant photon energy, thus indicating some contribution of characteristic non-resonant emission. It is could be seen quite well from the RIXS spectra for malachite. At excitation energy E some energy difference between characteristic emission line and the satellites structure is observed. The spectrum for the next excitation energy F reveal a complete separation between satellites structure (at ~ 937 eV) and the characteristic normal emission line (~928 eV).

Fig. 10. illustrates differences between RIXS spectra of $CuCl_2$, $Cu(OH)_2$, and malachite $Cu_2(CO_3)_2(OH)_2$ which were recorded at the same excitation energy of 933.6 eV, corresponding to the small satellite structure in XA spectrum. Changes in the spectroscopic profiles are quite significant when going from one compound to another. Observed variations are preliminary due to differences in chemical bonding between Cu and Cl^-, SO_4^{2-} , OH^- and HCO^{3-} ions and can be used as good finger prints in studies of electronic structure of complex systems.

Conclusions

The electronic structure of a number of copper compounds, such as Cu_2O, CuO, $Cu(OH)_2$, $CuCl_2$, Cu_2S, $CuSO_4$, malachite $Cu_2(CO_3)_2(OH)_2$ and atacamite $CuCl_2 \cdot 3Cu(OH)_2$ was studied by a combination of XAS and RIXS. The spectral

properties (shape of the spectra, peak position and chemical shifts for the main Cu L_3 peak) measured, using XAS are in agreement with previously reported results[9,10]. The study of the Cu 2p absorption edge offers an excellent method to determine the presence of monovalent and divalent copper. Based only on the XA spectra, however, it is may be difficult to distinguish a difference between the species that have similar oxidation state.

For that sense we examined the possibility of using RIXS to probe the electronic structure of complex copper compounds. We found that RIXS profiles can be significantly different (at the same excitation energy of incident photons) even between compounds with the same oxidation states for copper. This can be used as a fingerprint in spectroscopic analyses of complex systems and determining of chemical compositions of complex materials.

Acknowledgements

We are gratefully acknowledge Mikael Ottosson for making copper oxides samples available. This work was supported by the Swedish Nuclear Fuel and Waste Management Co. (SKB), by the Swedish Research Councill and Goran Gustafsson Foundation for Research in Natural Sciences and Medicine. The ALS work was supported by the Director, Office of Science, Office of Basic Energy Sciences, and Biosciences of the U.S. Department of Energy at Lawrence Berkeley National Laboratory under contract No. DE-AC02-05CH11231.

* - Corresponding author: Kristina Kvashnina, Uppsala University, Department of Physics, Box 530, 75121, Uppsala, Sweden, t. (+46)18-4713540, f. (+46)18-471-3524, Kristina.Kvashnina@fysik.uu.se

[1]G. van der Laan, R.A.D. Pattrick, C.M.B. Henderson and D.J. Vaughan, J. Phys.Solids 53, 9, 1185-1190 (1992)
[2] M. Grioni, J. B. Goedkoop, R. Schoorl, F. M. F. de Groot, and J. C. Fuggle, F. Schäfers and E. E. Koch, G. Rossi, J.–M. Esteva, and R. C. Karnatak, Phys. Rev. B 39, 1541–1545 (1989)
[3] A.S. Koster, Molecular Physics, 26, N3, 625-632 (1973)
[4] P.Kuiper, J.-H. Guo, Conny Såthe, L.-C. Duda, and J. Nordgren, J. J. M. Pothuizen, F. M. F. de Groot, and G. A. Sawatzky Phys. Rev. Letter 80, 5204 (1998)
[5] G. Ghiringhelli, N.B Brookes, E. Annese, H.erger, C.Dallera, M. Grioni, L. Perfette, A. Tagliaferri and L. Braicovich, Phys.Rev. Lett 92, 117406-1 (2004)
[6] Van Veenendaal, M Phys. Rev. Let. v 96, n 11, 2006, p 117404
[7] M. Z. Hasan . D. Isaacs, Z.-X. Shen, L. L. Miller, K. Tsutsui, T. Tohyama, S. Maekawa Science 288, 1811 (2000)
[8] Y. J. Kim., J. P. Hill, C. A. Burns, S. Wakimoto, R. J. Birgeneau, D. Casa, T. Gog, and C. T. Venkataraman, Phys. Rev. Lett. 89, 177003 (2002).

[9] J.H. Guo, S. M. Butorin, N. Wassdahl, and J. Nordgren, P. Berastegut and L.-G. Johansson, Phys.Rev. B 61, 9140 (2000)
[10] L.C. Duda, J. Downes and C. McGuinness, T. Schmitt and A. Augustsson, K. E. Smith, G. Dhalenne and A. Revcolevschi, Phys.Rev. B 61, 4186 (2000)
[11] M. Magnusson, N. Wassdahl and J. Nordgren, Phys. Rev B 56, 19 (1997)
[12] T. Warwick, P.Heimann, D. Mossessian, W. McKinney, H. Padmore, Rev. Sci. Instrum. 66 (1995) 2037.
[13] J. Nordgren and R. Nyholm, Nucl. Instrum. Methods Phys.Rs. A 246, 242 (1986)
[14] J.Nordgren, G.Bray, S.Cramm, R. Nyholm, J-E Rubensson and N Wassdahl, Rev. Sci. Instrum. 60 1690 (1989)
[15] M. Ottosson and J.-O. Carlsson, Surface and Coatings Technology 78(1996) 273-283
[16] A. N. Platonov, The Nature of the Colors of Minerals, Kiev (1976)
[17] S.Tanaka and A.Kotani, J. Phys. Soc. Jpn. 62, 464 (1993)
[18] S. M. Butorin, D. C. Mancini, J.-H. Guo, N. Wassdahl, J. Nordgren, M. Nakazawa, S. Tanaka, T. Uozumi, A. Kotani, Y. Ma, K. E. Myano, B. A. Karlin, and D. K. Shuh, Phys. Rev. Letter 77, 574 (1996)
[19] Flipse C. F. J., van der Laan G., Johnson A. L. and Kadowaki K., *Phys. Rev. B*. 42, 1997 (1990).

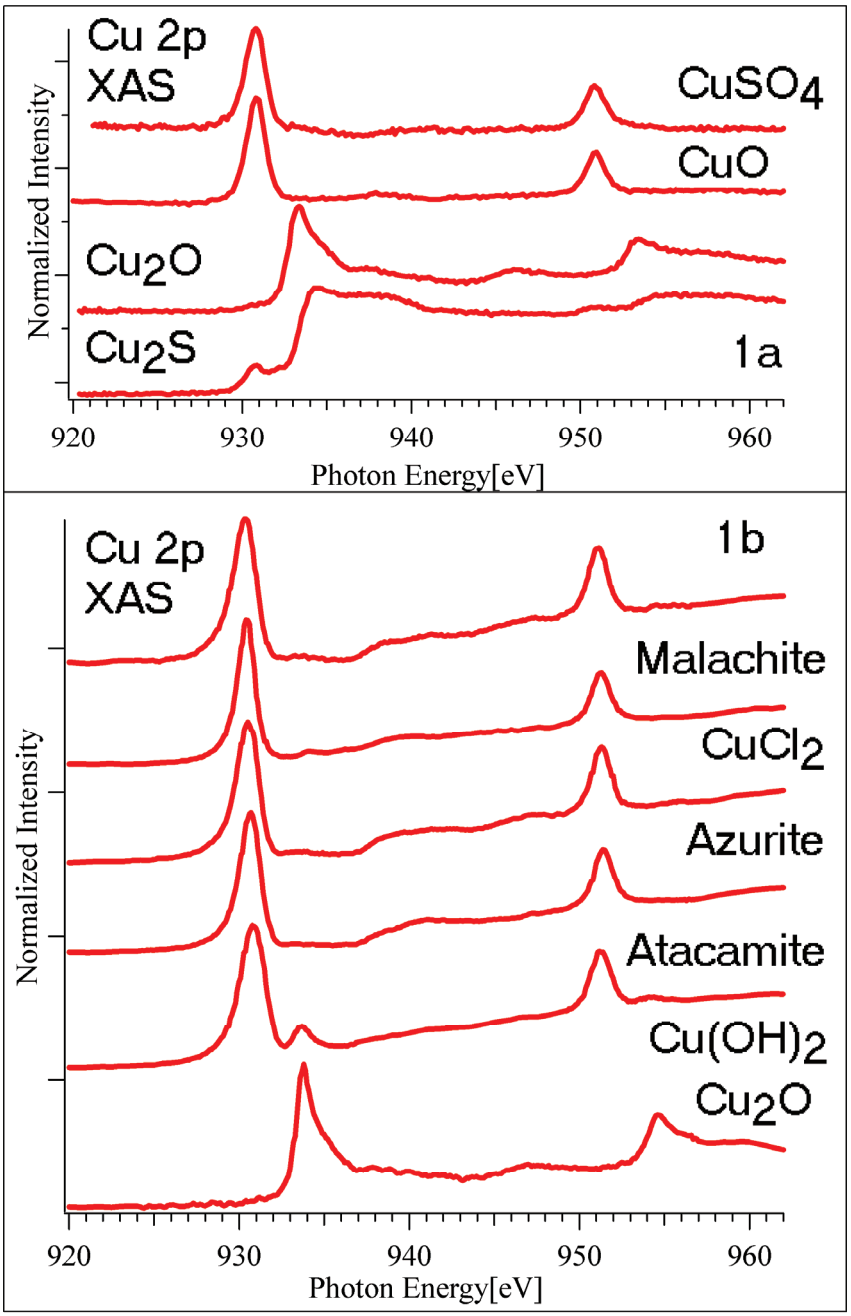
Cu 2p
XAS
CuSO4
CuO
Cu2O
Cu2S
1a
Normalized Intensity
920
930
940
950
960
Photon Energy[eV]
1b
Cu 2p
XAS
Malachite
CuCl2
Azurite
Atacamite
Cu(OH)2
Cu2O
Normalized Intensity
920
930
940
950
960
Photon Energy[eV]

Fig.1. Cu 2p X-ray Absorption (XA) spectra of CuO, Cu_2O, $CuCl_2$, Cu_2S, $Cu(OH)_2$, $CuSO_4$, malachite $Cu_2(CO_3)_2(OH)_2$, azurite $Cu_3(CO_3)_2(OH)_2$, and atacamite $CuCl_2 \cdot 3Cu(OH)_2$ recorded in the total fluorescence (TFY) mode, using chaneltron (1a) and photodiode (1b).

Table1: Energies of the main Cu L_3 absorption line for various copper compounds, in eV.

Compound	**Cu L_3 peak**
CuO	930.8
Cu_2O	933.3
Cu_2S	934.3
$CuSO_4$	930.8
$Cu(OH)_2$	931.0
$CuCl_2$	930.4
Atacamite $CuCl_2 \cdot 3Cu(OH)_2$	930.7
Azurite $Cu_3(CO_3)_2(OH)_2$	930.5
Malachite $Cu_2(CO_3)_2(OH)_2$	930.3

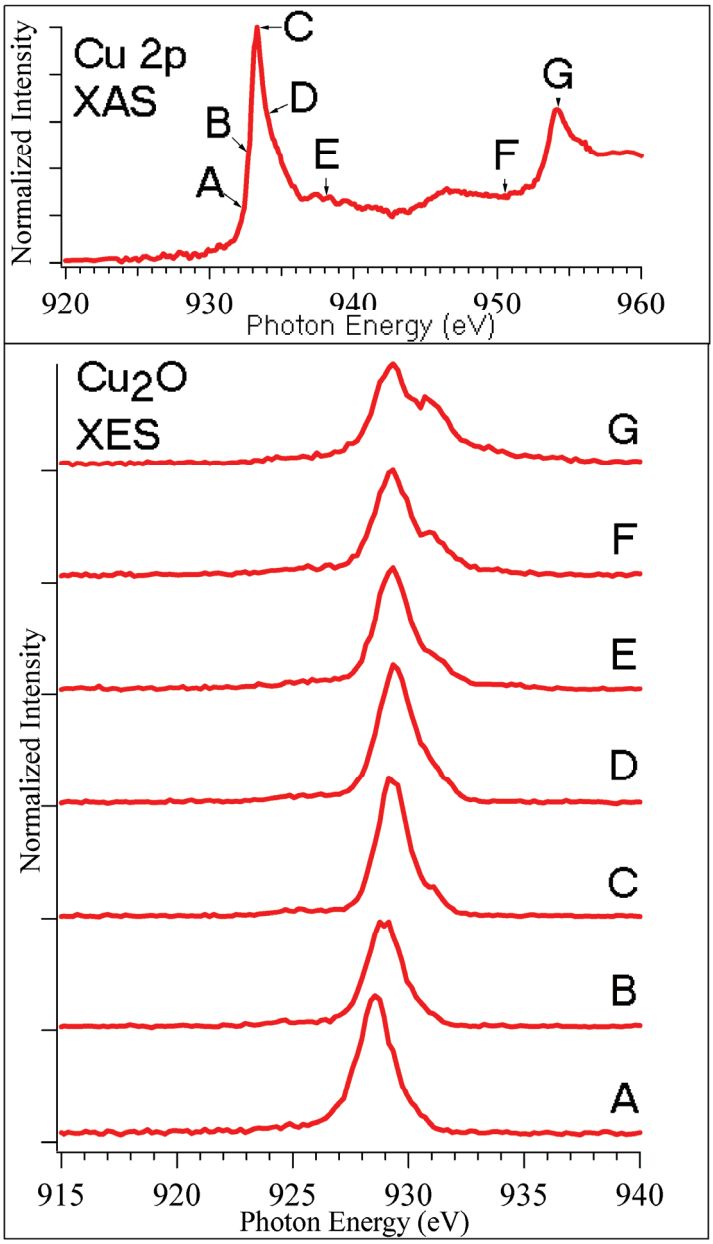

Fig. 2. Cu L_3 RIXS spectra of Cu_2O, recorded at different excitation energies indicated on the XA spectrum in top panel.

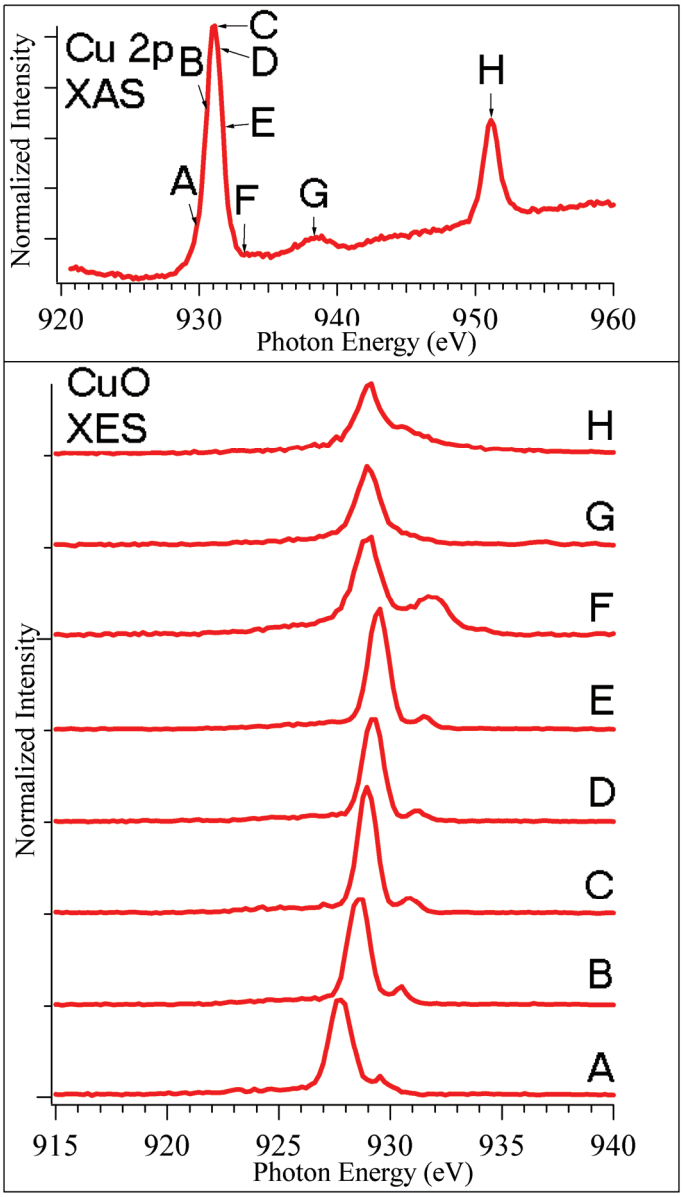

Fig. 3. Cu L_3 RIXS spectra of CuO, recorded at different excitation energies indicated on the XA spectra in top panel.

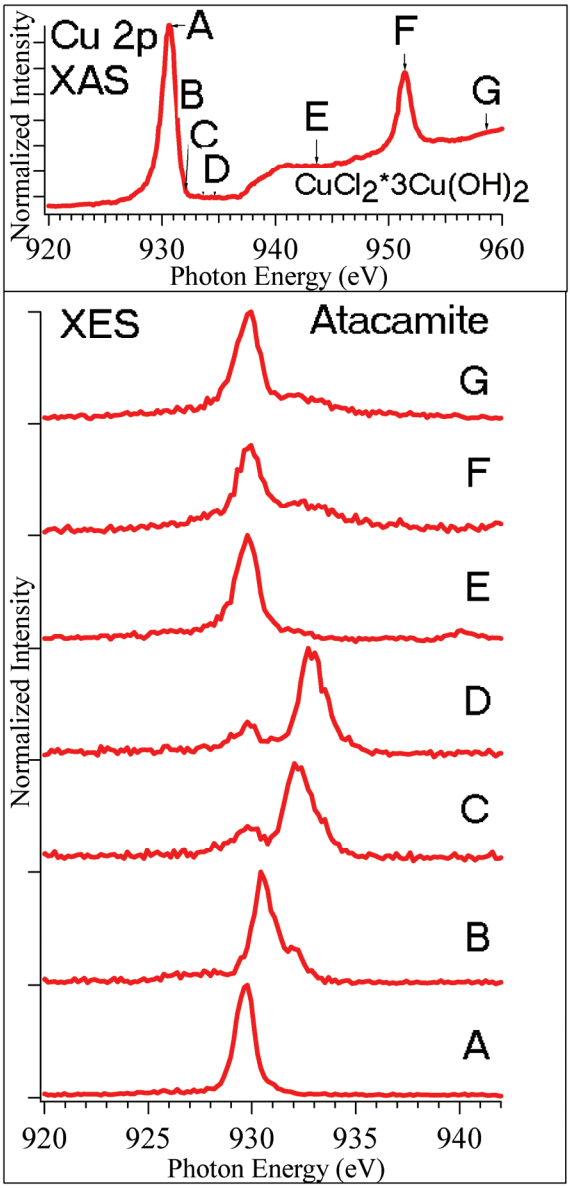

Fig. 4. Cu L_3 RIXS spectra of $CuCl_2 \cdot 3Cu(OH)_2$, recorded at different excitation energies indicated on the XA spectrum in top panel.

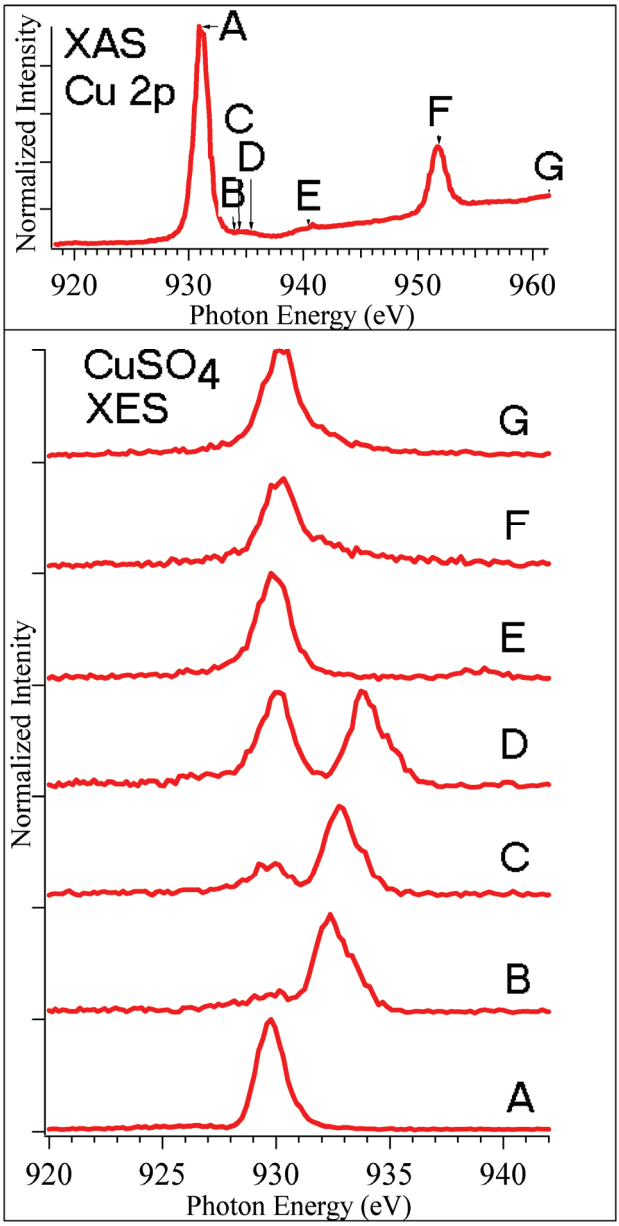

Fig. 5. Cu L_3 RIXS spectra of $CuSO_4$, recorded at different excitation energies indicated on the XA spectrum in top panel.

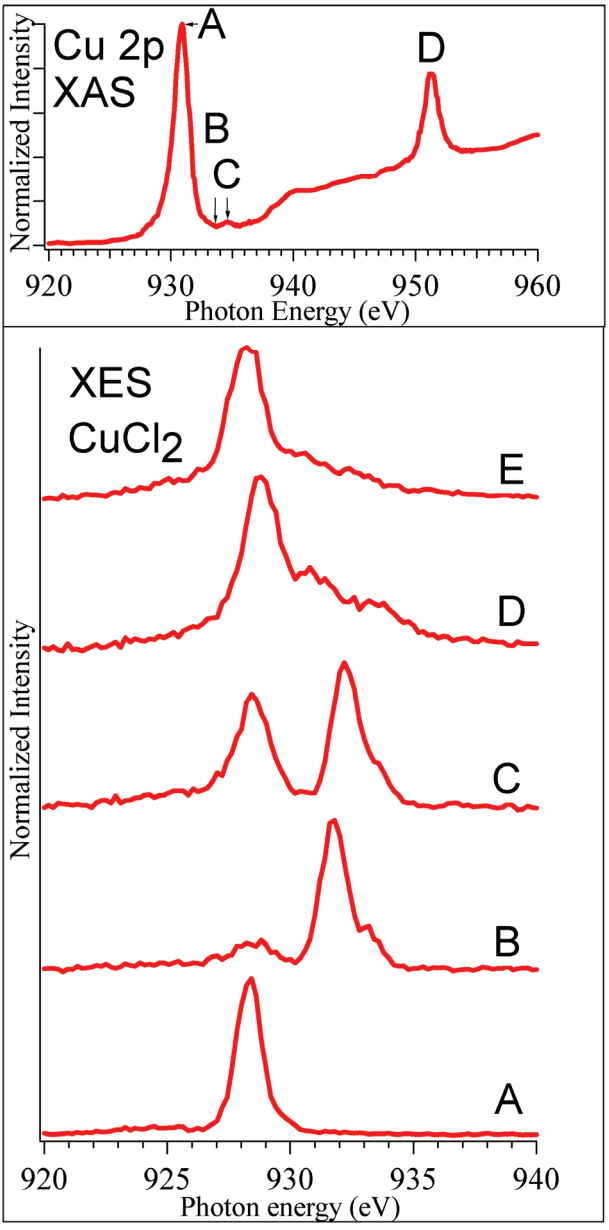

Fig. 6. Cu L_3 RIXS spectra of $CuCl_2$, recorded at different excitation energies indicated on the XA spectrum in top panel.

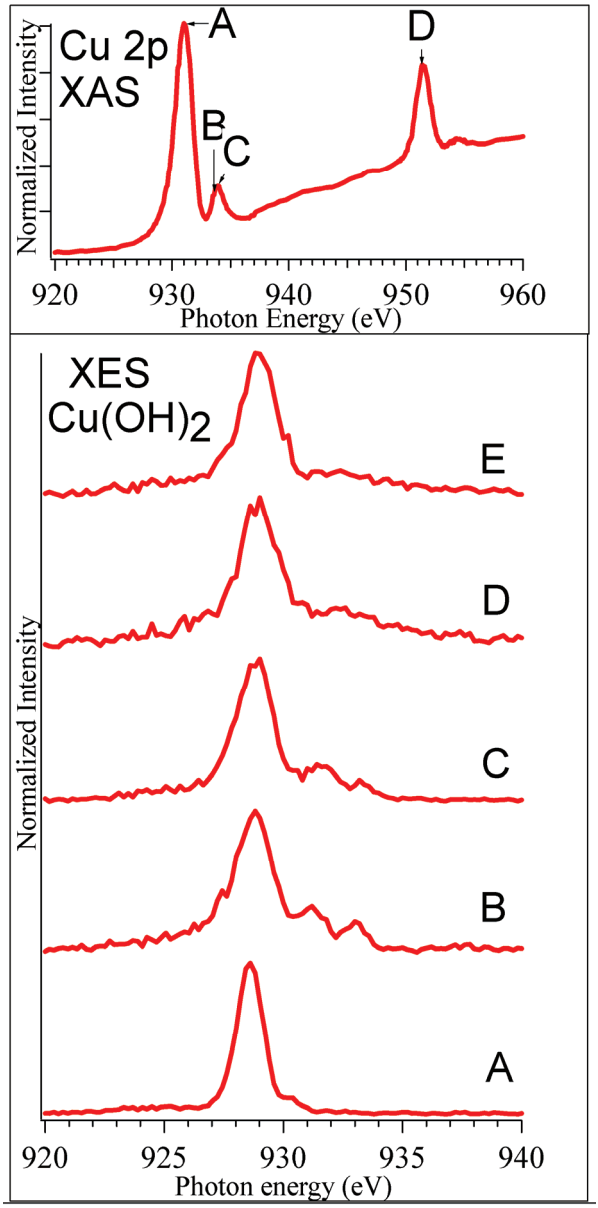

Fig. 7. Cu L_3 RIXS spectra of $Cu(OH)_2$, recorded at different excitation energies indicated on the XA spectrum in top panel.

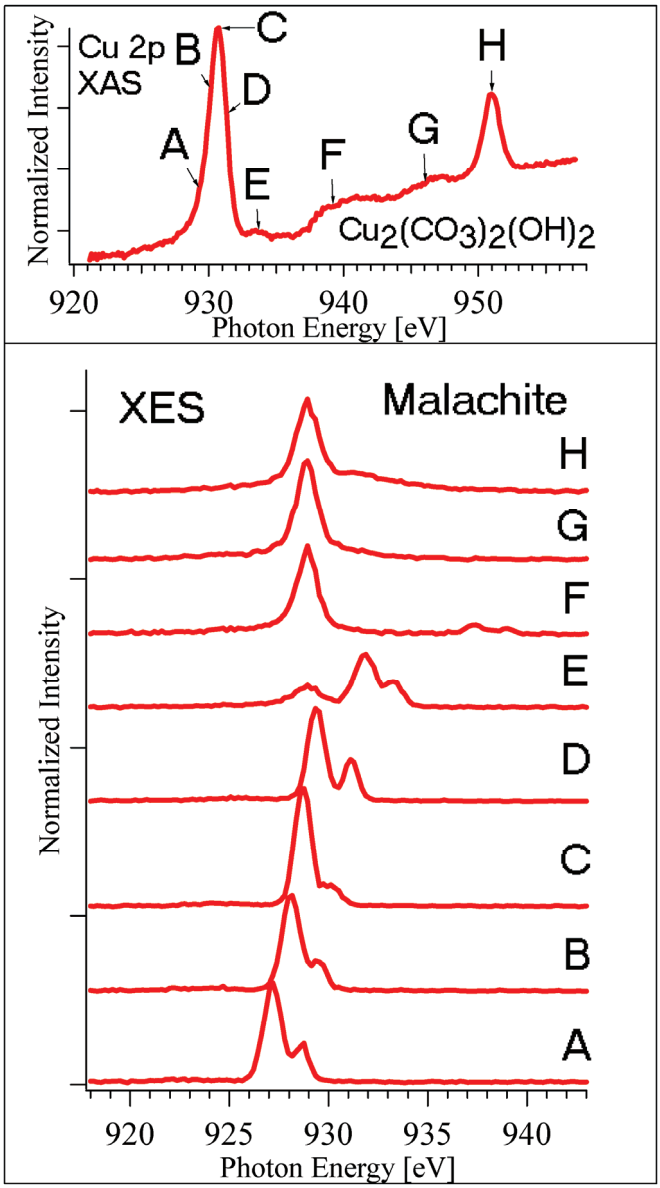

Fig. 8. Cu L_3 RIXS spectra of $Cu_2(CO_3)_2(OH)_2$, recorded at different excitation energies indicated on the XA spectrum in top panel.

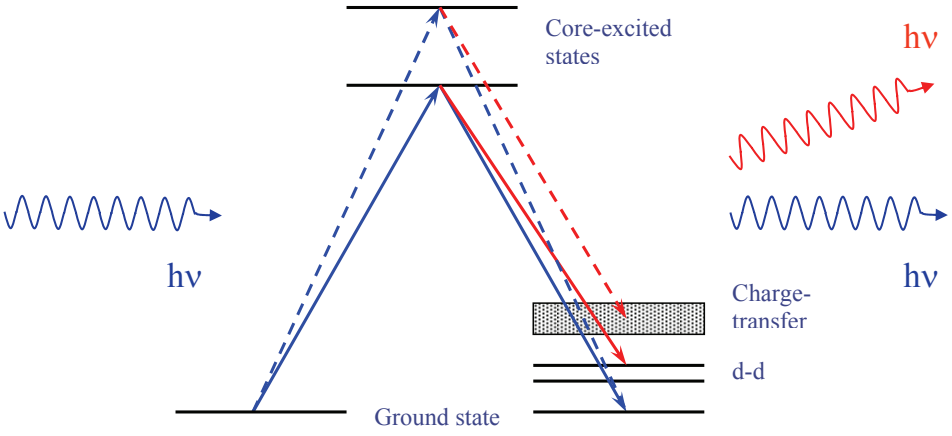

Fig. 9. Schematic representation of the elastic (red lines) and inelastic scattering (blue lines) of insulating 3d compounds.

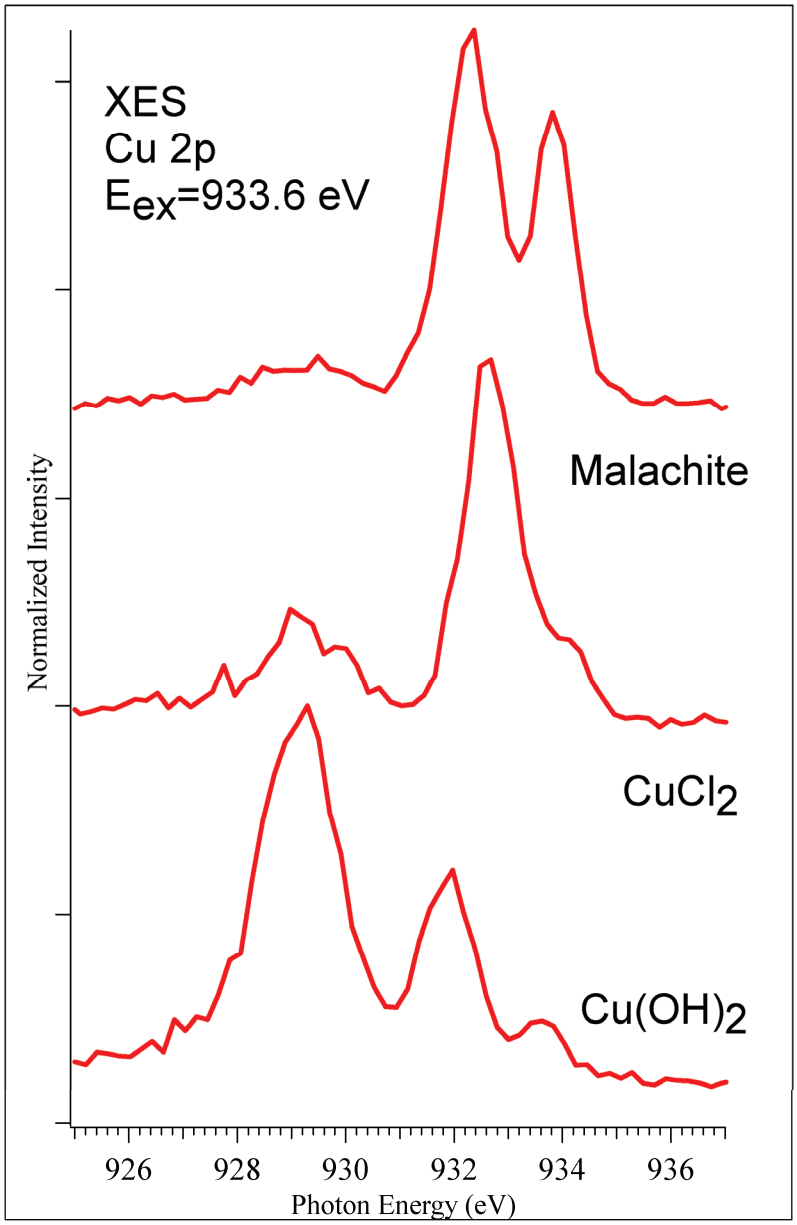

Fig. 10. RIXS spectra on $CuCl_2$, $Cu(OH)_2$, and malachite $Cu_2(CO_3)_2(OH)_2$ excited at the energy of satellites in the XA spectrum (~ 933.6 eV).

Paper VIII

Changes in electronic structure of copper films in aqueous solutions

K.O. Kvashnina[1*], S.M. Butorin[1], A. Modin[1], I. Soroka[1], M. Marsellini[1], J.-H. Guo[2], L. Werme[1,3] and J. Nordgren[1]

[1] *Department of Physics, Uppsala University, Box 530, 751 21 Uppsala, Sweden*
[2] *Advanced Light Source, Lawrence Berkeley National Laboratory, Berkeley, CA 94720, USA*
[3] *SKB, Stockholm, Sweden*

Possibility of using x-ray absorption spectroscopy (XA) and resonant inelastic x-ray scattering (RIXS) to probe the Cu oxidation state and changes in the electronic structure during interaction between copper and groundwater solutions were examined. Surface modifications induced by chemical reactions of oxidized 100Å Cu films with Cl^-, SO_4^{2-} and HCO_3^- ions in aqueous solutions with various concentrations were studied in-situ using liquid cells. Copper corrosion processes in groundwater were monitored up to 9 days. By comparing Cu 2p - 3d, 4s transitions for a number of reference substances previously measured, electronic structure changes of the Cu films were analyzed. The XAS and RIXS spectral shape at the Cu edge, the chemical shift of the main line for Cu^{2+}, and the energy positions of the observed satellites served as a tool for monitoring the changes during the reaction. It was found that the pH value and the Cl^- concentration in solutions strongly affect the speed of the corrosion reaction.

INTRODUCTION

Copper can corrode in both gaseous and aqueous environments. The atmospheric corrosion of copper has been studied intensively since copper is used in many fields, such as contact and wiring materials in electronic parts and devices [1,2]. Corrosion of copper in aqueous solutions has also been studied extensively for more than 100 years. It is the most commonly used material for plumbing because of its high corrosion resistance. One reason for the copper's high corrosion resistance is the fact that it is a noble metal in the sense that it is immune to corrosion in pure oxygen-free water. This property is the background to Sweden's choice to encapsulate spent nuclear fuel in cast iron canisters that have an outer corrosion shield made of copper for disposal at a depth of 400 to 700 m in granitic rock, where the groundwater will be oxygen-free[3].

The deep groundwater is, however, not "pure" water. Oxygen will have intruded into the waste repository area during the construction phase. Later in the service life of the repository, other corrosive substances, mainly sulfides may be present in the groundwater. All forms of corrosion that might affect the canister must, therefore, be considered. The performance assessment in this case includes the understanding of the behavior of copper in the geological environment. Therefore, the monitoring of in-situ corrosion processes becomes an important topic, which is necessary to study by different methods.

The corrosion of copper canister in the repository controlled by the availability of corrosive groundwater components. The composition of deep groundwaters vary considerable from site to site as well as in time[4] . Typical content of different ions in a low salinity groundwater is given in Table 1. The repository environment will be oxidizing for some time after closure, but oxygen will be consumed through reactions with minerals in the rock and also through microbial activity and the original oxygen-free conditions will be re-established. The copper corrosion in early stage when there are still traces of oxygen present is important to study. The development of the original Cu_2O film on the metal surface, formed through oxidation in dry air, after contact with groundwater with low oxygen content is important to establish and understand. It is this surface that later will be contacted by oxygen-free groundwater that may contain trace amounts of sulfide. It's therefore important to investigate the copper behavior in essentially oxygen-free conditions. In our experiments, we used different ions for the in-situ studies liquid cells with synthetic groundwater (see Table 1) and with de-ionized water with different concentrations of chloride, sulfate and carbonate.

Na^+	Ca^{2+}	Mg^{2+}	K^+	SO_4^{2-}	Cl^-	HCO_3^-
52.5mg/L	5.1mg/L	0.7mg/L	3.9mg/L	9.6mg/L	48.8mg/L	65.0mg/L

Table 1. Groundwater composition

The surface modifications induced by chemical reactions on 100Å Cu films with Cl^-, SO_4^{2-} and HCO_3^- ions in aqueous solutions were studied by using soft x-ray absorption spectroscopy (XAS). The simple oxides[5-10], sulfides[8, 9,10], chlorides[7,8,10] and carbonates[5,9,10] have been studied before using x-ray spectroscopic techniques and theoretical approaches due to their diverse electronic structure. It has been shown that XAS can be used to determine the oxidation state of the copper for different types of compounds [5-10]. The advantage of XAS above other techniques is the reduced surface sensitivities of the samples in the total fluorescence yield mode.

In the present study, Cu 2p XAS was applied to a number of liquid cells with different water compositions. Our results show that the corrosion behavior of copper in underground

repository conditions depends very much on the Cl^- concentration and the pH value in the solution contacting the copper surface. It has been shown before that the formation of monovalent or divalent copper depend on the pH value of the solution [11-13]. However, the corrosion of copper over a broad pH range was further investigated to allow us to obtain a better understanding for the processes involved in the chemical interaction between copper and ground water components. We also performed long-term corrosion experiments, using XAS for a number of liquid cells with different compositions.

A discussion of whether Cu is monovalent or divalent is relevant since copper can form compounds with different valences. In ordinary oxygen containing environments the surface layer is expected to be a duplex Cu_2O/CuO, $Cu(OH)_2$ structure[13] . In that case, XAS is not capable of giving a distinct difference between the different divalent copper compounds. Therefore, it makes sense to look for other techniques that can guide even when the materials become complex.

We examined the possibility of using the resonant inelastic x-ray scattering (RIXS) technique to probe the electronic structure of copper in the investigated liquid cell with groundwater solution. In soft x-ray range, this technique has been used to obtained information about the electronic states in copper materials at Cu L and M edges[14-17]. We already studied the Cu 2p-3d RIXS spectra of Cu_2O, CuO, $Cu(OH)_2$, $CuCl_2$, $CuSO_4$, malachite $Cu_2(CO_3)_2(OH)_2$, and atacamite $CuCl_2 \cdot 3Cu(OH)_2$ for different excitations energies[10]. In the present paper, we analyze the electronic structure changes of the Cu film in liquid cells with groundwater solution by comparing copper transitions for a number of reference compounds and determine which species are present in the investigated liquid cells.

EXPERIMENTAL DETAILS

Liquid cells with different concentrations of chlorine, sulfate and carbonate ions were used for the in-situ studies. A schematic picture of the cell is shown in Fig.1. The cell was made from PEEK polymer and has a diameter of about 20 mm and is 4 mm thick. X-rays penetrated though

a silicon nitride membrane window. The size of the used membrane was 1 mm x 1 mm. Membrane was hold by 10 mm x 10 mm Si frame, which was attached to the cell. The volume of the cell is sufficient to hold one drop (approximately 4 μL) of the liquid. On the backside of 100 nm Si_3N_4 windows a 100 Å copper film was deposited in advanced in order to study the chemical reactions between the copper film and various solutions. Copper film was deposited by DC-magnetron sputtering deposition in an UHV chamber. Pressure before sputter deposition was lower than 10^{-9} Torr. In order to achieve the glow discharge, Ar gas with a purity of 99.9999%. at a pressure of 2 mTorr was injected at constant flow directly into the chamber. Fixing the power on the magnetron at 50 W, the resulting growth rate was about 0.85 ± 0.05 Å/s. The samples were rotated during the deposition in order to achieve homogeneous thickness of copper. After deposition, windows were removed from the chamber and brought to synchrotron facilities under atmospheric conditions.

The corrosion behavior of copper in the groundwater solution was investigated under nearly anoxic conditions. The groundwater was deoxygenated by pumping vacuum and backfilling three times with argon. Through this procedure, we expect to have reduced the oxygen level in the groundwater by about three orders of magnitude. An oxygen concentration in the ppb range will, however, be sufficient to oxidize the investigated copper film to Cu^{2+}. The pH value during the investigation was adjusted using sodium hydroxide NaOH, in order to increase the value and hydrochloric acid HCl in order to decrease the pH value.

The XAS and RIXS measurements were performed on beam-line 7.0[18] at the Advance Light Source (ALS) of Lawrence Berkeley National Laboratory using a spherical grating monochromator with energy resolution set to 200 meV at the Cu $2p_{3/2}$ peak of CuO (~931eV). The XAS were recorded in the total fluorescence yield (TFY) mode under high vacuum conditions. The RIXS were recorded using a high-resolution grazing incident grating spectrometer[19], which has an adjustable slit, MCP detector and 3 gratings covering 3 energy intervals (Fig. 1). RIXS spectra was detected with resolution of 500meV, using high energy grating which has 5 m radius and 1200 lines/mm. The incident angle of the photon beam was

approximately 45 degrees from the liquide cell surface and the spectrometer was placed in the horizontal plane at an angle 90 degrees with respect to the incident beam.

OXIDATION REACTION OF COPPER

First we examined by Cu 2p XAS the 100Å copper thin film deposited on the inside of the Si_3N_4 window, see Fig. 2. For comparison, spectra of monovalent and divalent copper oxides are also presented in Fig. 2. The ground state of CuO can be described as a mixture of $3d^9$ and $3d^{10}\underline{L}$ character [8], where $\underline{L}$ stands for a hole in the O 2p band. The main peak at 930.8 eV in the X-ray Absorption (XA) spectrum of CuO corresponds to the $2p^53d^{10}$ final state. This state gives a single line without multiplet splitting because the *d* shell is full. At ~20.1 eV above this peak ($2p_{3/2}$) another structure with lower intensity appears ($2p_{1/2}$). This structure is broader due to shorter core-hole lifetime and interaction with $2p_{3/2}$ continuum. The XA spectrum of monovalent copper (Fig. 2) clearly differs from the Cu^{2+} spectra. The main line of the Cu_2O spectrum is at higher energy (~ 933.3 eV) and corresponds to excitations to the empty *4s* band.

By comparing the Cu 2p XA spectra for divalent and monovalent copper, information on oxidation state can be obtained. We can conclude that main contribution comes from oxidized copper in the form of Cu_2O on the membrane surface of the Si_3N_4 window (Fig. 2). This oxide gives rise to the main peak at 933.3 eV. At lower energies, there is also a small peak at ~930.8 eV , which shows the presence of Cu^{2+} impurities and thus indicates that further oxidation of the copper has taken place.

After the initial analyzes of the Cu film, its corrosion behavior in groundwater solution was investigated. One drop of groundwater solution (~4μL) was accommodated in the liquid cell and 1 hour later the XA spectrum was measured in order to detect the reaction between the copper layer and the groundwater solution. The Cu 2p XA spectrum (Fig. 3) shows mainly monovalent copper with small contribution of divalent copper. It is quite obvious that intensity of the Cu^{2+} signal for spectrum of the liquid cell with a water of the given composition, decreases in comparison with the Cu^{2+} signal for the copper film deposited on the back side of Si_3N_4 membrane.

We believe that the Cu^{2+} formation in the groundwater will be dominated either by carbonate, chlorine or hydroxide complexes. For that reason, we chose HCO_3^- and Cl^- ions out of the other species in the groundwater solution and investigated independently their influence on the copper film using XAS.

Aqueous solutions containing 1.1 mM carbonate and 1.4 mM chlorine were prepared from 9.24 mg of sodium bicarbonate $NaHCO_3$ and 8.18 mg of NaCl, respectively, and 100 ml of ultra-pure distil deionzed (MQ) water. The pH of the solution was adjusted to 8.5 (as in the groundwater) by adding small amount of sodium hydroxide NaOH to the Cl^- solution and hydrochloric acid HCl to the carbonate solution in MQ water.

Fig. 3 shows the Cu 2p XA spectrum taken from the copper film in the liquid cell after being for 1 hour in contact with Cl^- solution. The main line of the spectrum is at ~ 933.3 eV and corresponds to monovalent copper. The presence of the divalent copper species manifests itself in the peak at 930.8 eV. It is, however, unclear what percentage of Cu^{2+} is present in the studied copper film. The spectral intensity of the Cu^{2+} peak was used to evaluate the corrosion rate of copper films in liquid cells containing different water compositions.

Carbonate should form strong complexes with divalent copper [20]. The main line of the Cu 2p spectrum however indicates the presence of monovalent copper on the copper film exposed for 1 hour to the carbonate solution (Fig.3). The Cu^{2+} peak is not observed in this spectrum thus suggesting that carbonate species present in the solution protect the copper film from further corrosion. This is in accordance with previous observations[21]. Adeloju and Duan [22] suggest that an increased protectiveness is a consequence of pH buffering by HCO_3^-, which stabilizes the Cu_2O phase rather than leads to a formation of basic cupric carbonate species.

It can be seen from Fig. 3 that the intensity of the divalent copper signal during XAS measurements depends on the composition of the solution used in the liquid cell. We, therefore, need to investigate the influence of pH value and Cl^- concentration. There is some evidence that the transformation from Cu^{1+} to Cu^{2+} depend on the pH value and Cl^- concentration[23].

INFLUENCE OF THE Cl^- CONCENTRATION

We recorded the Cu 2p XA spectrum from the copper film in the liquid cell with 1 hour exposure to the MQ water solution containing 1.5 M of Cl^- (similar to the Cl^- concentration in the marine environment). This spectrum in Fig. 4 shows the presence of mostly divalent copper in the studied copper film. Our data clearly indicate that in waters with chlorine content approaching that of sea water, copper surface became quickly corroded due to the high chlorine concentration. On the other hand, the divalent copper peak in Cu 2p XA spectrum of the copper film after being in contact with 1.4mM Cl^- solution for 1 hour has relatively low intensity. By comparison of the spectra for different concentration (Fig. 4) we can conclude that strong Cu^{2+} chloride complexes are formed on the copper surface at high Cl^- concentration.

This finding can be understood on the basis of the next reaction:

$$Cu \rightarrow Cu^+ + e^-$$

Cuprous chlorine usually formed on the copper film as a major component of corrosion layer:

$$Cu^+ + Cl^- \rightarrow CuCl$$

On the other hand cuprous chloride CuCl is unstable and continue to corrode chemically to form hydrochloric acid and basic cupric chloride[24]:

$$4CuCl + 4H_2O + O_2 \rightarrow CuCl_2 \cdot 3Cu(OH)_2 + 2HCl$$

This effect was observed previously for copper after 4 days exposure to a 0.5 M Cl^- solution[25] and confirmed once more by XAS using 3 times higher concentration of sodium chloride in solution. In our case 100 Å of copper was almost fully corroded after 1 hour in contact with 1.5 M Cl^- in aqueous solution.

pH of the water solution has quite high influence on the corrosion process. According to Pourbaix diagram for copper at room temperature [26-27], Cl^- in small concentrations can form strong complexes with divalent copper at higher pH.

INFLUENCE OF pH

Fig. 5 displays Cu 2p XA spectra obtained for the copper film exposed to the 1.4mM Cl^- solution with different pH values for 1 hour. It is apparent that monovalent copper species are predominantly formed on the copper film at pH 6.0 and 8.5. A signal from divalent copper appears to be particular strong above pH 8.5. At pH 10.0 and 12.0 (Fig. 5) divalent copper peaks are dominating in the spectra. It indicates that the stability of divalent copper over monovalent increases with increasing pH. Adeloju and Duan[22] reported the growth corrosion films on copper in aerated solution with pH values between 5 and 13.5. Only Cu_2O was observed after 7 days exposure at the lowest pH studied with increasing amounts of CuO reported with increasing pH. The higher concentration of OH^- at higher pH promotes a formation of passivating Cu^{2+} layer, most likely $Cu(OH)_2$. This is in keeping with the known fact that copper is more corrosion resistant at high pH in an oxygenated solution.

This pH dependent behavior is consistent with the Pourbaix diagram, which shows the formation of divalent copper species at pH higher than 8. It also indicates that the oxidation of copper in the 1.4 mM Cl^- solution is less favorable at pH 8.5 than its oxidation to divalent copper at pH 10.0 and 12.0. These results are in agreement with Brusic et al. [28], which show that a stable oxide of copper can be formed in water solution at pH higher than 7.0 .

Our results obtained by XAS show that copper corrosion processes in the presence of Cl^- ions are strongly pH dependent. The pH dependence of such processes was also observed for 1.4 mM HCO_3^- solution. Fig. 6 shows the pH dependence of Cu 2p XA spectra obtained for copper film exposed to the 1.1 mM HCO_3^- solution for 1 hour. As can be seen from the Cu 2p spectra (Fig 6), monovalent copper signal gives the largest contribution at pH 8.5 and 11.4. The divalent copper signal is observed for pH 11.4. It is, however, not as intense as in the case of high pH for

the Cl^- solutions. The results for pH 11.4 seem to be contradictory to the observation by Adeloju and Duan[22] that pH buffering by HCO_3^- stabilizes Cu^{1+}.

TIME DEPENDENCE

Since the Cu 2p XA spectra for the copper films in carbonate solution do not show fast corrosion behavior in high or near neutral pH, it is of interest to examine their dependence on the exposure time to the solution. Fig. 7 shows how the intensity of the divalent copper signal varies with time for the 1.1 mM HCO_3^- solution with pH 8.5. The Cu 2p XA spectrum for the freshly made liquid cell (recorded after 1 hour of the exposure time) does not show any divalent copper signal. After 3 days of exposure a small peak appears at the lower energy, indicating the formation of divalent copper species.

Fig. 8 shows the time dependence of the corrosion process in a liquid cell containing groundwater, which also has pH 8.5. After 5 days exposure time we can clearly see that the intensities of the monovalent and the divalent copper are similar and after 9 days exposure time there is only divalent copper present. The intensity and the shape of the peak after 9 days of exposure time clearly indicate the presence Cu^{2+} species in the copper film.

Fig. 8 indicates that complete oxidation to Cu^{2+} had taken place after 9 days exposure time in the groundwater. It is, however, difficult to determine from XA spectra which kind of Cu^{2+} species are formed. Therefore, the copper film in ground water solution was additionally analyzed by RIXS.

SPECIATION

The species present on a copper surface in contact with aqueous solutions have been investigated before using XPS[13]. It was concluded that mainly a mixture of Cu_2O, CuO or $Cu(OH)_2$ was present on the copper surface after being in contact with a borate buffered solution (pH 7.0). This is in agreement with the current understanding that these three compounds are known to be stable as bulk solids [26, 30]. Using RIXS we can provide information on the composition of the corroded copper film with in the groundwater solution. In order to do that we

first monitored by XAS a liquid cell containing groundwater until the copper was fully corroded and then applied RIXS.

It has been shown that on the Cu 2p - 3d resonance, x-ray scattering spectra are mainly composed of two parts: the *dd* intra-atomic excitations and the structures due to charge transfer excitations from the ligand band to the 3d level [16, 17, 31, 32]. Most of the studies were performed when the incident photon energies were set at the energies around the main XA peak. We already analyzed the Cu 2p-3d RIXS spectra of Cu_2O, CuO, $Cu(OH)_2$, $CuCl_2$, $CuSO_4$, malachite $Cu_2(CO_3)_2(OH)_2$, and atacamite $CuCl_2 \cdot 3Cu(OH)_2$ for different excitations energies and found that the RIXS spectra excited at energies in the range of satellite structures in the Cu 2p XA spectrum are different for the different compounds[10]. It was show that using Cu 2p RIXS the characteristic differences in the chemical bonding between Cu^{2+} and Cl^-, SO_4^{2-}, OH^- and HCO_3^- ions could be found. This can be used as a finger print in interpretation of complex materials.

In the present study, malachite, copper hydroxide and copper chloride were suggested to be used as predominant phases formed on the surface of the corroded copper in the groundwater solution. Fig. 9 shows Cu 2p - 3d RIXS spectra of $CuCl_2$, $Cu(OH)_2$, and malachite $Cu_2(CO_3)_2(OH)_2$ recorded at the same excitation energy of 933.6 eV. This energy corresponds to the satellite structure in the XA spectrum, associated with the $2p^53d^9$s contribution, which shape is defined by s-density of states in the conduction band. Although, in some publications this satellite structure in the XA spectrum was described being a result of exciting "defect states", i.e. $3d^9\underline{L}$ initial state leading to the $2p^53d^{10}\underline{L}$ excitations ($\underline{L}$ stands for a hole in the ligand 2p band) [5]. RIXS spectra clearly show significant differences in the shape which are a result of difference in chemical bonding in these compounds. The spectral difference can be taken as advantage in identification of corrosion products formed on the copper film in the liquid cell with groundwater solution.

Fig. 9 also shows the RIXS spectrum of the fully corroded copper film in contact with the groundwater solution. Due to the experimental difficulties, the spectrum was recorded at an excitation energy lower by 0.6 eV than that for the spectra of reference compounds. This energy

is still in the range of the satellite structure in the XA spectrum and the energy difference is within total experimental resolution used for RIXS measurements. The shape and the intensities of the RIXS spectrum are similar to that of $Cu(OH)_2$ suggesting the formation of hydroxide species. The process can be described by the following equations[11, 30]:

$$2Cu + H_2O \rightarrow Cu_2O + 2H^+ + 2e^-$$

$$Cu_2O + H_2O \rightarrow 2CuO + 2H^+ + 2e^-$$

$$Cu_2O + 3H_2O \rightarrow 2Cu(OH)_2 + 2H^+ + 2e^-$$

It is interesting to compare the RIXS results with reports on copper oxidation states in different solution studies by Raman [29, 35] and infrared [36] spectroscopies. The Raman study by Hamilton et al. [35] was performed using 488 nm laser excitations on copper in the 0.1M NaOH solution. They showed that initially Cu_2O and then $Cu(OH)_2$ were formed by comparison with the oxide spectra. Melenders et al.[36] studied *in-situ* copper oxidation in alkaline media by infrared spectroscopy using synchrotron radiation. The initially formed corrosion product was identified as Cu_2O with later formation of CuO or $Cu(OH)_2$. The RIXS spectrum in present paper provides important information on the chemical composition and confirms unambiguously that hydroxide species were formed on the studied copper film in contact with the groundwater solution.

The great sensitivity of the RIXS spectra profile to the type of copper species allows us to better assess the chemical composition of the corroded copper film. RIXS has proven to be a powerful technique for studying the corrosion processes of copper films. The results from our study of the corrosion of copper films are summarized in Fig. 10.

CONCLUSION

The influence of chlorine and carbonate ions concentrations, pH value of the corrosion processes on oxidized copper films as well as their time- dependence were investigated spectroscopically. The significance of the pH value for the copper corrosion rate in the 1.1 mM HCO_3^- and 1.4 mM Cl^- aqueous solution was shown.

We found that the corrosion causes formation of Cu^{2+} species in the copper film in several cases:

- in solution with high Cl^- concentration (1.5M)
- 1.4 mM Cl^- solution with Ph values higher than 10.0
- in groundwater solution after 9 days exposure

We used Cu 2p-3d RIXS for determining the chemical composition of the copper corrosion product in a liquid cell containing the copper film with groundwater solution. The XA spectrum showed in that case the presence of the divalent copper and RIXS revealed a formation of hydroxide species. It was shown that complimentary information can be obtained using both XAS and RIXS. It has been clearly demonstrate the importance of employing spectroscopic techniques in corrosion studies.

Acknowledgements

We would like to thank Kaja Ollila and Hans Nilsson for making ground water solution. This work was supported by the Swedish Nuclear Fuel and Waste Management Co. (SKB), by the Swedish Research Councill and Göran Gustafsson Foundation for Research in Natural Sciences and Medicine. The ALS work was supported by the Director, Office of Science, Office of Basic Energy Sciences, and Biosciences of the U.S. Department of Energy at Lawrence Berkeley National Laboratory under contract No. DE-AC02-05CH11231.

* - Corresponding author: Kristina Kvashnina, Uppsala University, Department of Physics, Box 530, 75121, Uppsala, Sweden, t. (+46)18-4713540, f. (+46)18-471-3524, Kristina.Kvashnina@fysik.uu.se

[1] C. Leygraf and T. Graedel, "Atmospheric Corrosion", John Wiley & Sons, New York, (2000)
[2] R.B. Commizoli, R.P. Frankenthal, P.C. Milner and J. D. Sincilair, Science, 234, 340 (1986)
[3] L. Werme, Technical Report TR 98-08, Design premises for canister for pnt nuckear fuel, SKB, 1998; Wendy Barnaby, Nature vol 274, 6, (1978)
[4] F. King, L.Ahonen, C. Taxén, U. Vuorinen, L. Werme, Copper corrosion under expected conditions in a deep geologic repository, Svensk Kärnbränslahantering AB (SKB) Report TR-01-23.
[5] G. van der Laan, R.A.D. Pattrick, C.M.B. Henderson and D.J. Vaughan, J. Phys.Solids 53, 9, 1185-1190 (1992)
[6] S.Tanaka, K. Okada and A.Kotani, Physica C 185-189 (1991) 1489-1490
[7] K. Nakajima, J. Kawai and Y. Gohshi, Physica C 185-189 (1991) 983-984
[8] [11] A.S. Koster, Molecular Physics, 26, N3, 625-632 (1973)
[9] M. Grioni, J. B. Goedkoop, R. Schoorl, F. M. F. de Groot, and J. C. Fuggle, F. Schäfers and E. E. Koch, G. Rossi, J.–M. Esteva, and R. C. Karnatak, Phys. Rev. B 39, 1541–1545 (1989)
[10] K.O. Kvashnina, S.M. Butorin, A. Modin, J.-H. Guo, R. Berger, L. Werme and J. Nordgren, in press
[11] V. Mauricc, H.H. Strehblow, P. Marcus, Passivity and its breakdown, The Electrochemical Society Proceedings Seires, Pennington, 1998
[12] U. Collisi, H.H. Strehblow, J. Electroanal. Chem. 284, 385 (1990)
[13] J. Hayon, C. Yarnitzky, J. Yahalom and A. Bettelheim, J. Electrochem. Society, 149 (7) B314-B320 (2002)
[14] L.C. Duda, J. Downes and C. McGuinness, T. Schmitt and A. Augustsson, K. E. Smith, G. Dhalenne and A. Revcolevschi, Phys.Rev. B 61, 4186 (2000)
[15] P.Kuiper, J.-H. Guo, Conny Såthe, L.-C. Duda, and J. Nordgren, J. J. M. Pothuizen, F. M. F. de Groot, and G. A. Sawatzky Phys. Rev. Letter 80, 5204 (1998)

[16] M. Magnuson, N. Wassdahl and J. Nordgren, Phys. Rev B 56, 12238 (1997)
[17] Ghiringhelli, G; Brookes, N.B.; Annese, E.; Berger, H.; Dallera, C.; Grioni, M.; Perfetti, L.; Tagliaferri, A.; Braicovich, L. Phys. Rev. Let. v 92, n 11, (2004) p 117406
[18[T. Warwick, P.Heimann, D. Mossessian, W. McKinney, H. Padmore, Rev. Sci. Instrum. 66 (1995) 2037.
[19] J.Nordgren, G.Bray, S.Cramm, R. Nyholm, J-E Rubensson and N Wassdahl, Rev. Sci. Instrum. 60 1690 (1989)
[20] R. J. Gettens, Mineral Alteration Products on Ancient Metal Objects. In *Recent Advances in Conservation*, pp. 89-92. Butterworths, London, 1963
[21] S.B. Ribotta, M.E. Folquer, J.R. Vilche, Corrosion 51 (1995) p. 682.
[22] S.B. Adeloju and Y.Y. Duan, Br. Corros. J., 29 (1994) p. 315.
[23] M. R. Schock, D.A. Lytle, J. A. Clement, Effect of ppH, DIC, Orthophosphate and sulphate on ridrinkig water cuprosolvency, Cincinnati, Ohio, 1995
[24] Oddy, W. A., and M. J. Hughes. 1970. The Stabilization of Active Bronze and Iron Antiquities by the Use of Sodium Sesquicarbonate. *Studies in Conservation* 15:183-189.
[25] B. Millet, C. Flaud, C. Hinnen, E.M.M. Shutter, Corrosion Science, 37, 1903 (1995)
[26] M. Pourbaix, PhD Thesis, Unversite Libredes Bruxelles (1945), M. Pourbaix, 1966. *Atlas of Electrochemical Equilibria in Aqueous Solutions*. Pergamon Press, New York
[27] B. Beverskog, I. Puigdomenech, J. Electrochem. Soc., Vol 144, N10, 1997
[28] V. Brusic, M.A Frishe, B.N. Eldidge, F.P. Novak, F. B. Kaufman, B.M. Rush, G.S. Frankel, J. Electrochem. Soc. 138, 2253 (1991)
[29] H. Y. H. Chan, C. G. Takoudis, M. Weaver, J. Phys. Chem. B (1999), 103, 357-365
[30] B. Beverskog and I. Puigdomenech, J. Electrochem. Soc. 144, N10, (1997), 3476-3482
[31] S. Butorin J. of Elect. Spectr. and Relat. Phenom. 110-111 (2000) 213-233
[32] S.M. Butorin, J.-H. Guo, M. Magnusson, P.Kuiper and J.Nordgren, Phys. Rev B. 54, 4405 (1996)
[33] A. Jagminas, J. Kuzmarskyte, G. Niaura, Applied Surface Science 201 (2002) 129-137
[34] M. M. Hukovic, R. Babic and A. Marinovic, J. Electrochem. Soc., 145, 4045 (1998)
[35] J. C. Hamilton, J. C. Farmer, R.J. Anderson, J. Electrochem. Soc. 133, 739 (1986)
[36] C.A. Melendres, G. A. Bowmaker, J. M. Leger, B. J. Beden, Electroanal. Chem. 449, 215 (1998)

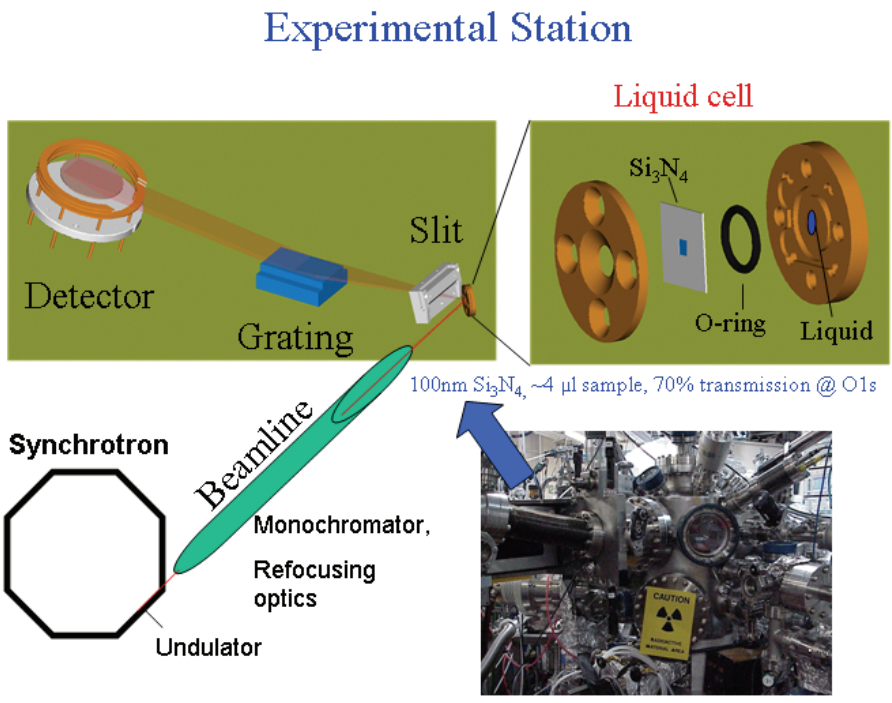

Fig. 1. Experimental station, including layout of spectrometer and liquid cell schematics

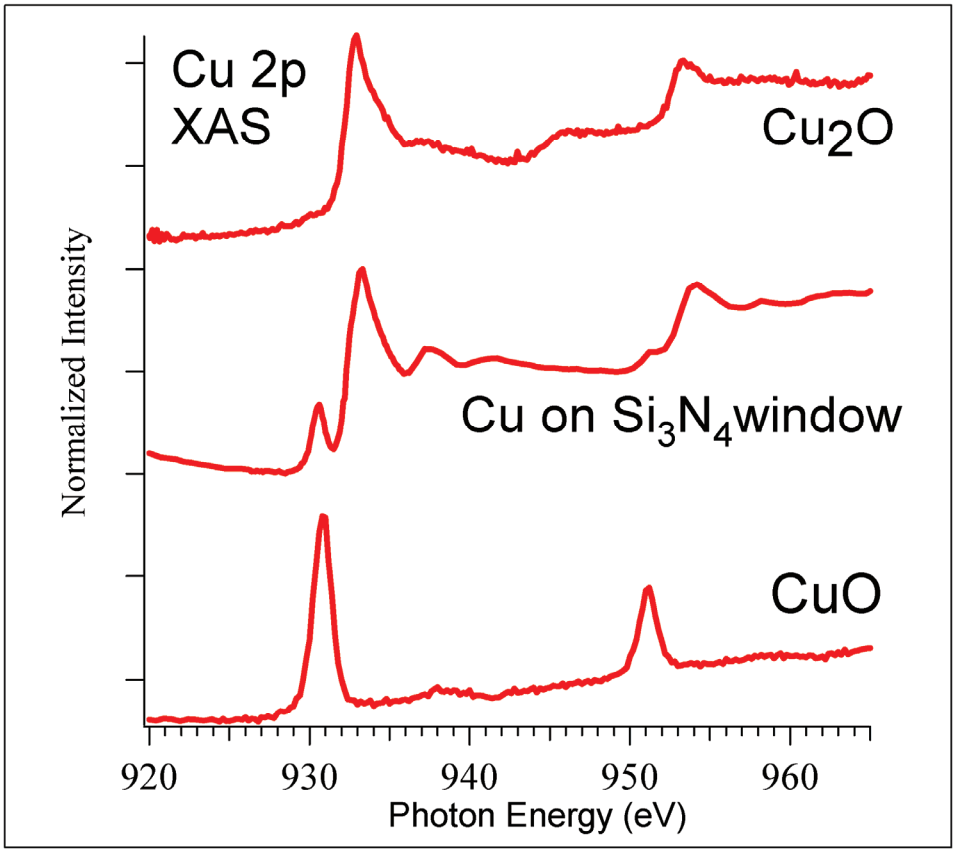

Fig. 2. Cu 2p X-ray absorption (XA) spectra of CuO, Cu_2O, and 100Å thick copper film deposited on the 100 nm Si_3N_4 membrane, recorded in total fluorescence yield (TFY) mode by photodiode.

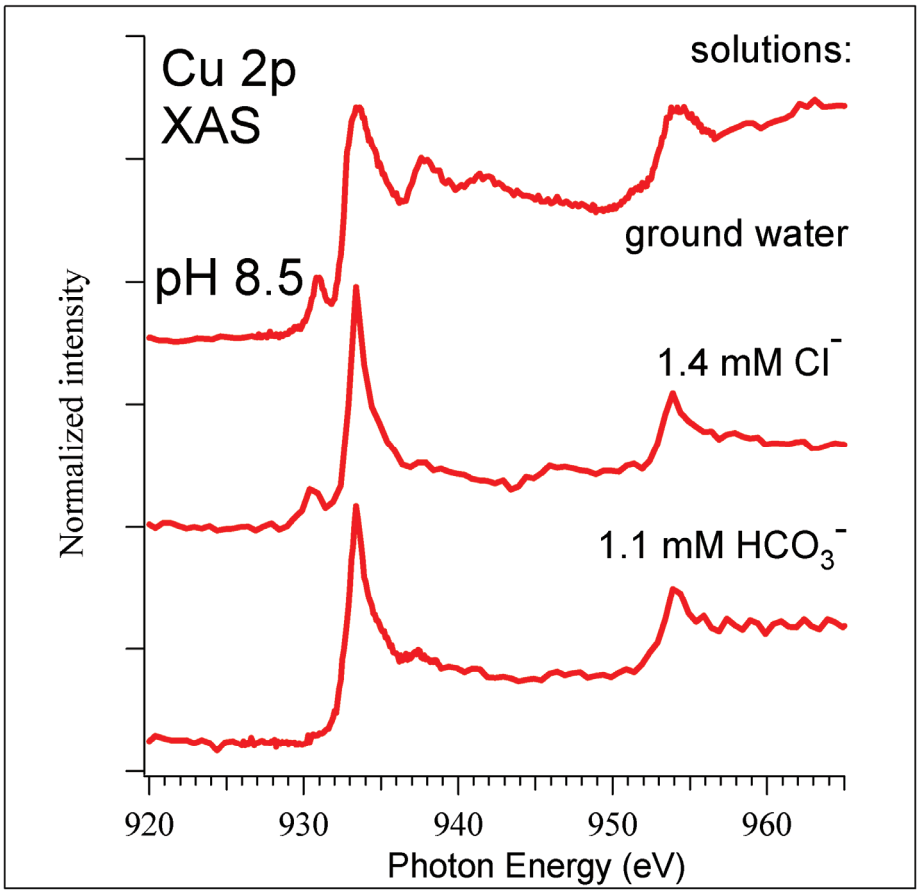

Fig. 3. Cu 2p XA spectra of 100Å thick copper film in liquid cells with: ground water solution and 1.4 mM Cl^- , 1.1 mM HCO_3^- solutions in ultra-pure distil deionzed (MQ) water. pH value for all solutions was adjusted to 8.5.

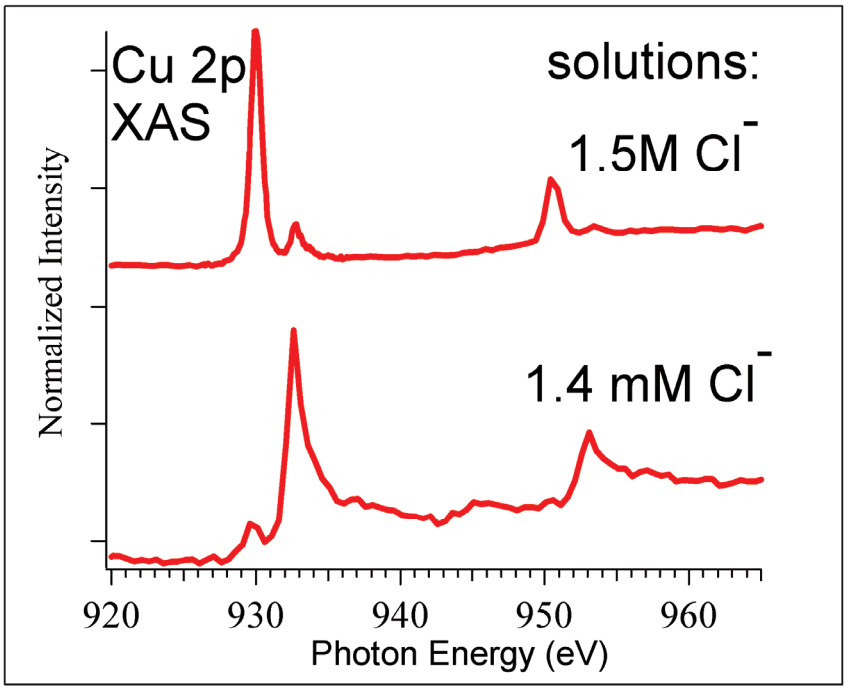

Fig. 4. Cu 2p XA spectra of 100Å thick copper film in liquid cells with 1.5M Cl^- and 1.4 mM Cl^- solutions in MQ water.

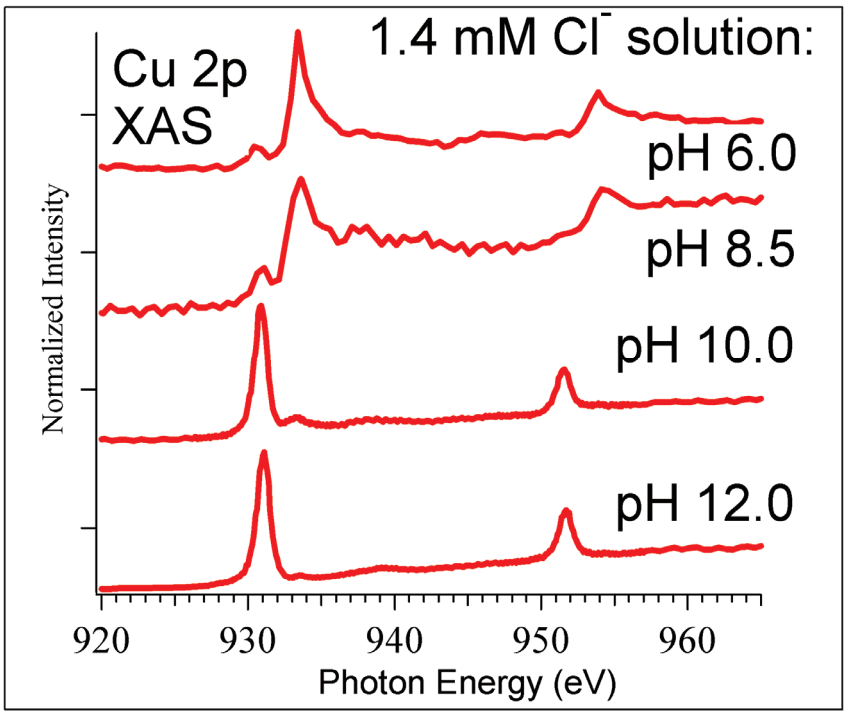

Fig. 5. Cu 2p XA spectra of 100Å thick copper film in liquid cells with 1.4 mM Cl^- solutions in MQ water with different pH.

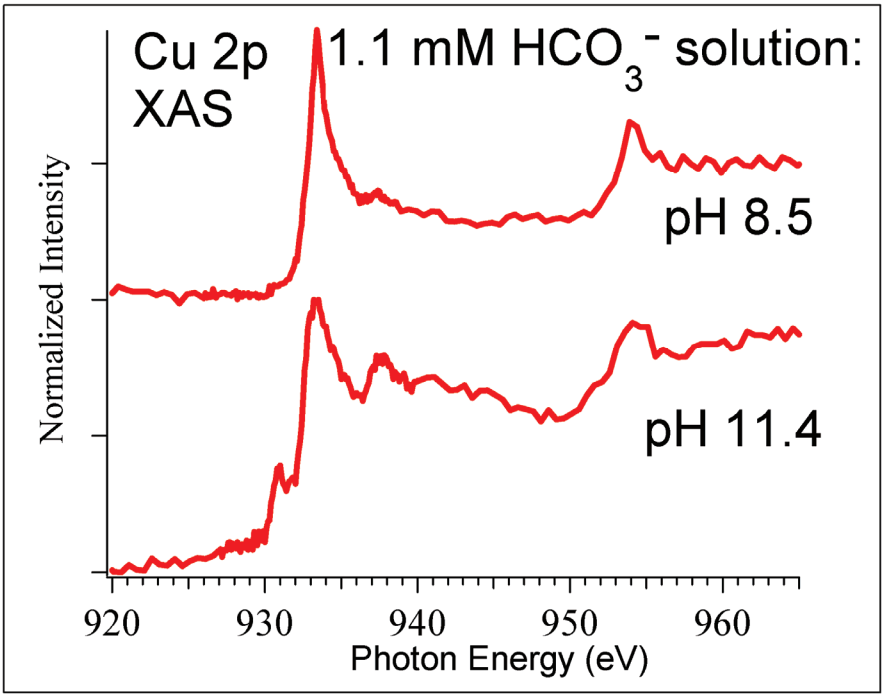

Fig. 6. Cu 2p XA spectra of 100Å thick copper film in liquid cells with 1.1 mM HCO_3^- solutions in MQ water with different pH

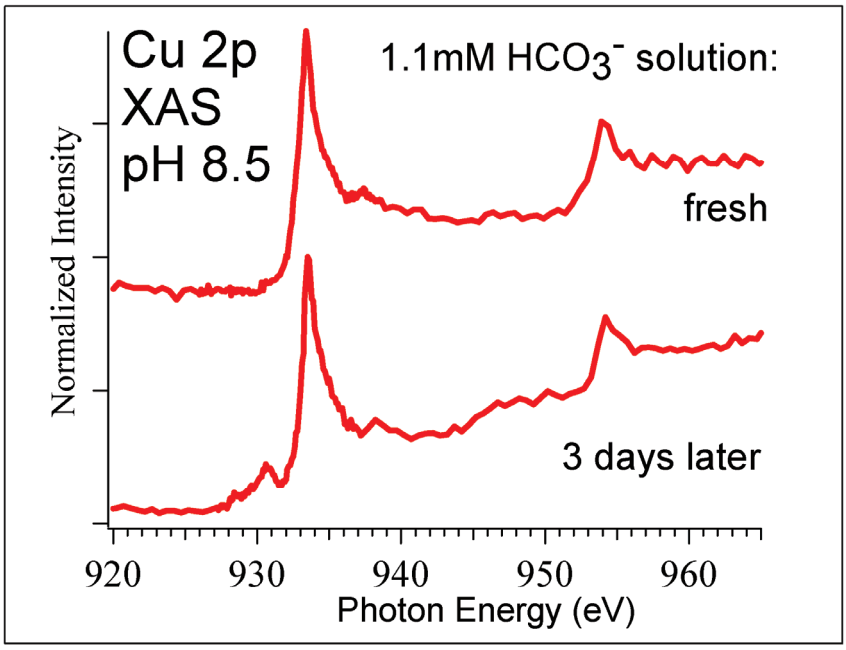

Fig.7. Dependence of Cu 2p XA spectra of 100Å thick copper film in liquid cells on the exposure time to the 1.1 mM HCO_3^- solution in MQ water.

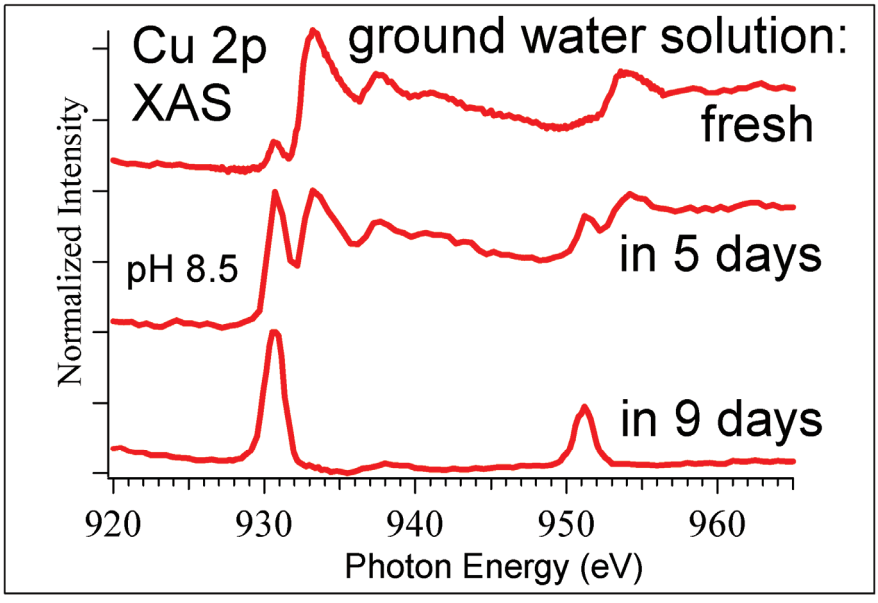

Fig.8 Dependence of Cu 2p XA spectra of 100Å thick copper film in liquid cells on the exposure time to ground water solution.

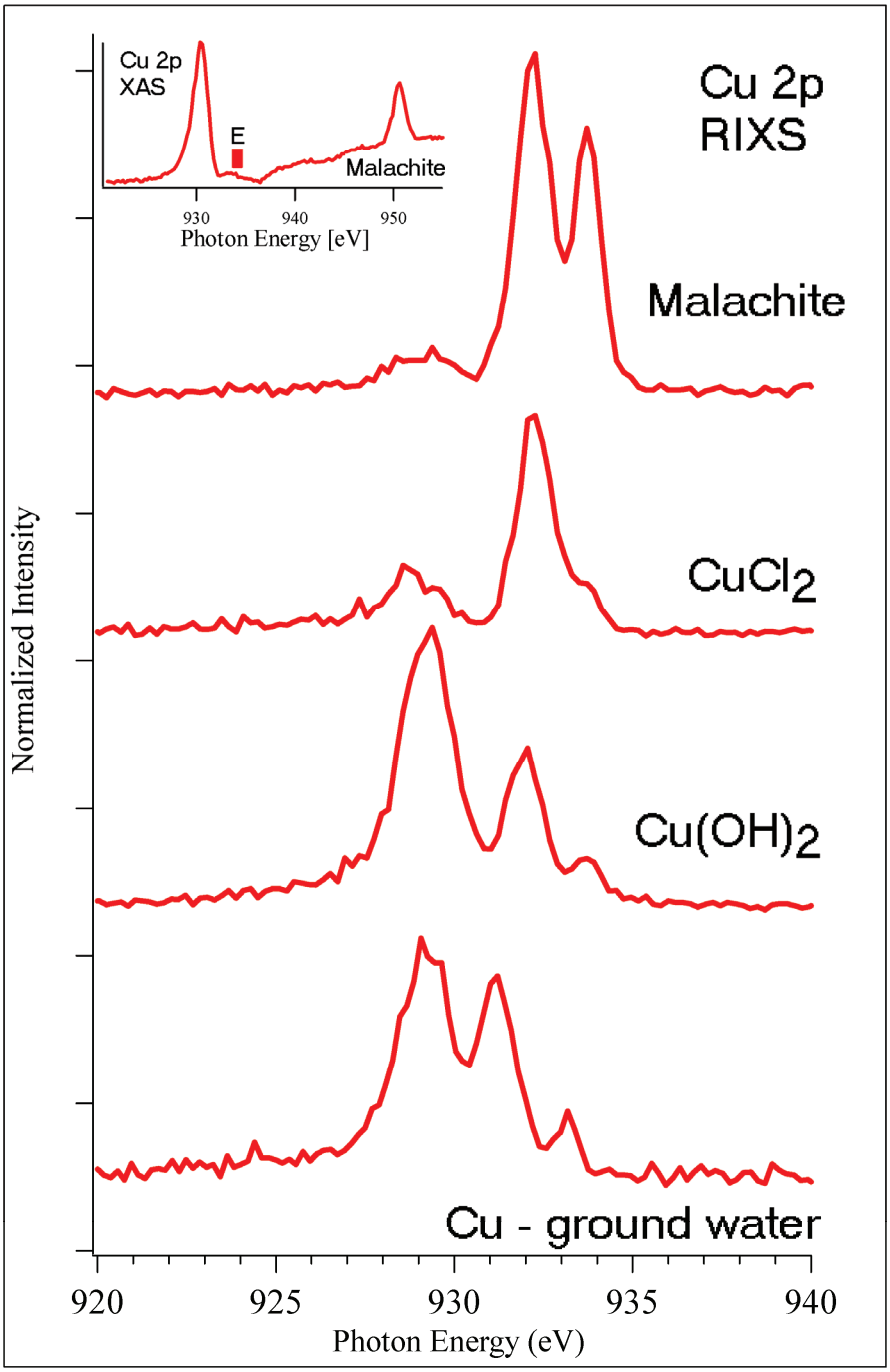

Fig. 9. RIXS spectra of $CuCl_2$, $Cu(OH)_2$,malachite $Cu_2(CO_3)_2(OH)_2$ and 100Å thick copper film in liquid cell with groundwater solution recorded at the excitation energy indicated in the top panel of XA spectrum.

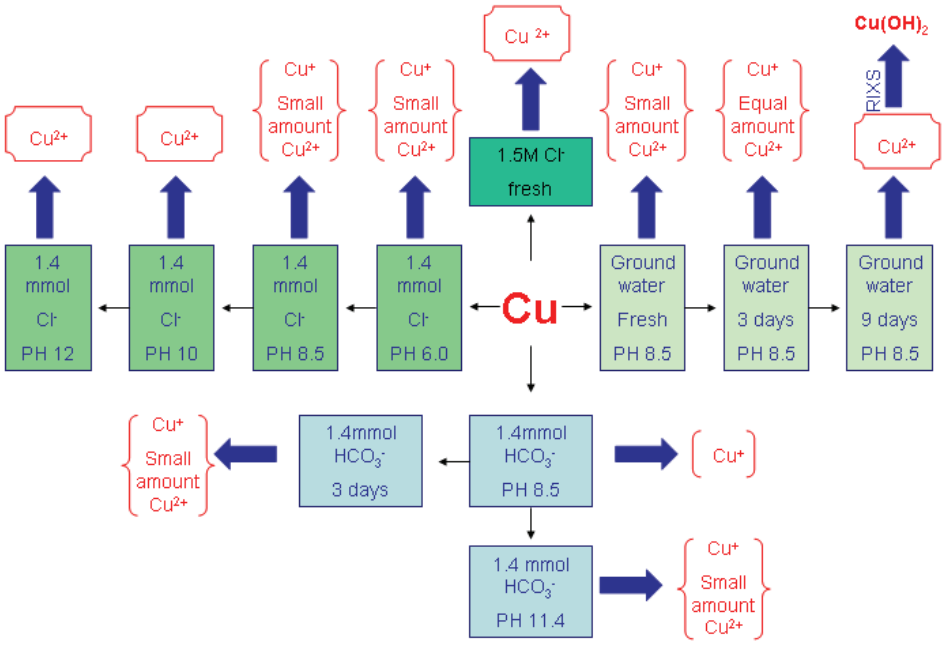

Fig. 10. Schematic summary of the copper corrosion processes in different solutions.

Paper IX

Suppression of Copper Corrosion in Groundwaters Observed by In-situ X-ray Absorption Spectroscopy

K.O. Kvashnina[1*], S.M. Butorin[1], A. Modin[1], I. Soroka[1], M. Marsellini[1], J.-H. Guo[2], L. Werme[1,3] and J. Nordgren[1]

[1] *Department of Physics, Uppsala University, Box 530, 751 21 Uppsala, Sweden*
[2] *Advanced Light Source, Lawrence Berkeley National Laboratory, Berkeley, CA 94720, USA*
[3] *SKB, Stockholm, Sweden*

Copper is a widely used industrial metal for electrical wiring, piping, air conditioning tubing and roofing. The properties of copper, which make it suitable for these applications, include high electrical and thermal conductivity, easy fabrication and installation, ready availability, and high recyclability. However, the question of copper corrosion is still open for discussions. This study illustrates how the damage from copper corrosion can be reduced, by modifying the chemistry of copper surface environment. The surface modification of oxidized copper films induced by chemical reaction with Cl^-, SO_4^{2-} and HCO_3^- ions in aqueous solutions was monitored by *in-situ* x-ray absorption spectroscopy, The results show that corrosion of copper can be significantly reduced by adding even a small amount of sodium bicarbonate (normal baking soda). For example, copper alloys corrode quickly in chloride solution, whereas the same solution containing 1.1mM HCO_3^- prevent the corrosion processes of copper films.

The problem of copper corrosion, that occurs randomly and affects many areas in our life, has been noticed for decades. However, it cause is still not fully understood. Copper tube is usually used as piping material for installation systems in most countries. The corrosion of copper pipe may occur when water is in contact with the pipe for a period of time. Currently, there is no guaranteed remedial treatment for copper corrosion other than to replace the affected section of copper pipe with alternative material. There is a plenty of information available about specific corrosion problems[1-4] or about detecting corrosion processes[5,6], but no effective natural solution has been found to inhibit or suppress the corrosion.

X-ray absorption spectroscopy (XAS) can be used to determine the oxidation state for different type of copper compounds [7-9], which makes it a promising technique for studying corrosion processes. A discussion of whether copper is monovalent or divalent is relevant for the studies of corrosion processes because it is commonly considered that a

corrosion product layer formed on copper surface consists of an inner layer of Cu_2O and an outer layer of Cu(II) oxides or other Cu(II) compounds, depending on the composition of the aqueous solution in contact with copper. The extent of corrosion status can, therefore, be detected by the oxidation state of copper; i.e. by the presence or absence of a divalent copper signal. Thus, fully corroded copper will give a strong divalent copper signal in the X-ray Absorption (XA) spectrum. The relative stabilities of Cu(I) and Cu(II) signals depend very strongly on the nature of the species present in the water solutions.

In this study, Cu 2p XAS was employed to study the chemical reactions of 100Å thick Cu films with Cl^-, SO_4^{2-} and HCO_3^- ions in aqueous solution. Our results demonstrate that the rate of the corrosion can be reduced by modifying the chemistry of the copper surface environment.

We utilized liquid cells with different concentration of chlorine, sulfate and carbonate ions in ultra-pure deionized water (MQ) for the in-situ studies. A schematic picture of the cell is shown in Fig.1. The plastic cell (made from PEEK polymer) was about 20 mm in diameter and 4 mm thick, which holds a small volume (~4μL) of liquid. X-rays penetrated through a silicon nitride (Si_3N_4) membrane window. The size of the used membrane was 1 mm x 1 mm and it was held by a 10 mm x 10 mm Si frame, which was attached to the cell. On the other side of the 100 nm Si_3N_4 windows 100Å copper films were deposited in order to study the chemical reactions between copper and various solutions. The spectral shape of the Cu 2p absorption edge and the chemical shift of main absorption line served as a tool in monitoring the changes during the reaction.

The Cu 2p absorption spectra were measured on beam-line 7.0[10] at the Advanced Light Source of Lawrence Berkeley National Laboratory, which equipped with a spherical grating monochromator, with a resolution of 200 meV at the Cu $2p_{3/2}$ peak of

CuO (~931eV). XA spectra were recorded in Total Fluorescence Yield (TFY) mode under high vacuum conditions (~10^{-10}Torr).

First, we examined the 100 Å copper thin film deposited on the Si_3N_4 window by XAS. It is evident from Fig. 2 that both oxidized and metallic copper is present in the film on the window membrane. Cu_2O has predominantly d^{10} configuration with a small mixture of d^9 character and only the final state $2p^5 3d^{10} 4s^1$ can be reached, which gives rise to the main peak at 933.3 eV. There is also a small peak at ~930.8 eV, which shows the presence of Cu^{2+} impurities and, thus, indicates that further oxidation of copper has taken place. Metallic copper is represented by characteristic satellite structures in the 938 – 942 eV range and higher background.

All copper objects begin to corrode as soon as they come into contact with air. In dry air, a very thin layer of copper oxides forms on the copper surface. This process is sometimes refereed to as "toning" and it usually protects the object from further oxidation[4]. However, at higher moisture levels or in moist environments impurities from the air, ground and sea, can cause further corrosion, resulting in that the corrosion processes often do not stop with toning, especially not for objects buried in the ground. Acids and salts present in the ground and sea attack the metal. It is proposed that corrosion of copper in wet environment is controlled by availability of oxygen and the availability of groundwater components at the copper surface. Typical content of various ions in synthetic groundwater (modified allard) is given in Table 1.

Na^+	Ca^{2+}	Mg^{2+}	K^+	SO_4^{2-}	Cl^-	HCO_3^-
52.5mg/L	5.1mg/L	0.7mg/L	3.9mg/L	9.6mg/L	48.8mg/L	65.0mg/L

Table 1. Groundwater composition

We utilized liquid cells with groundwater and ultra-pure MQ water with different concentrations of chloride and carbonate ions for the in-situ studies. First, the corrosion behavior of copper in groundwater solution was investigated. In order to do this, one drop

(~4μL) of groundwater solution was accommodated in the liquid cell and in direct contact with the copper film on Si_3N_4 window. The Cu 2p XA spectrum of the film exposed to the solution for 1 hour (Fig. 2) shows mainly contribution of Cu^+ with a small admixture from divalent copper at the lower energy. It is obvious that the intensity of the Cu(II) signal from the copper exposed to the groundwater (see Table1), decreases in comparison with the Cu(II) signal from the deposited copper film on the back side of Si_3N_4 membrane.

In general, copper metal corrosion in groundwater can lead to products such as cuprous chloride (CuCl), cupric chloride ($CuCl_2$), cuprous oxide (Cu_2O), and the green- and blue-colored cupric carbonates, malachite ($Cu_2(OH)_2CO_3$), and azurite ($Cu_3(OH)_2(CO_3)_2$)[11]. The most damaging corrosion occurs when chlorine ion comes into contact with copper film and, unfortunately, chlorine ion is quite common in the ground and in marine environments. Fig. 3 illustrates what happens in just a 5 days time with 10 mm thick copper slab in a 1.5M Cl^- in water solution. The copper surface is covered with patches of pale green powder material.

We suggest, as have many others, that Cl^- is the most aggressive species for the copper in groundwater composition. We measured Cu 2p XAS for the film in a liquid cell with 1.4 mM Cl^- ion solution. For this solution we mixed 100ml of MQ water with 8.18 mg of NaCl in powder form and then adjusted pH to 8.5, i.e. the pH in the groundwater, by adding a small amount of sodium hydroxide NaOH. The resulting Cl^- ion concentration was similar to that usually found in groundwaters (see Table1). Fig. 2 shows the XA spectrum of the film exposed for 1 hour to the water solution contining Cl^- ion. The main line of the spectrum is at energy ~ 933.3 eV and corresponds to monovalent copper species. The peak at ~ 930.8 eV is due to Cu^{2+} contribution. We

found that the intensity of this Cu^{2+} peak varied for the different studied solutions. Fig. 2 also shows Cu 2p XAS taken from the copper film in the liquid cell, containing 1.1mM HCO_3^- ions in the MQ water solution. For this solution we mixed 100ml of MQ water with 9.24mg of sodium bicarbonate $NaHCO_3$. The resulting HCO_3^- concentration is similar to that in goundwaters. pH in that case was also adjusted to 8.5 using hydrochloric acid HCl. In the TFY spectrum at the Cu 2p edge recorded after 1 hour exposure of the Cu film to the solution, one can see that the peak at lower energy corresponding to the divalent copper species is almost absent.

The first step in the electrochemical corrosion of copper and copper alloys in chloride solutions is the production of cuprous ions. These ions are then combined with the chlorine ions in solutions to form cuprous chloride as a major component of the corrosion layer:

$$Cu \rightarrow Cu^+ + e$$

$$Cu^+ + Cl^- \rightarrow CuCl$$

When cuprous chloride CuCl is very unstable compound and continue to corrode chemically by reaction between cuprous chloride and oxygen (which are hydrolyzed) to form hydrochloric acid and basic cupric chloride[12]:

$$4CuCl + 4H_2O + O_2 \rightarrow CuCl_2 \cdot 3Cu(OH)_2 + 2HCl$$

These reactions continue until no metal remains. This chemical corrosion process was confirmed here by XAS. We prepared a liquid cell with 1.5M of Cl^- desolved in MQ water, which is similar to the Cl^- concentration in marine environment. Fig. 4 shows the presence of divalent copper species on the investigated copper film. The ground state of

divalent copper in oxide can be described as a mixture of $3d^9$ and $3d^{10}\underline{L}$ character [7], where $\underline{L}$ stands for a hole in the O 2p band. The main peak at 930.8 eV in the XA spectrum corresponds to the $2p^5 3d^{10}$ final state. This state gives a single line without multiplet splittings because the *d* shell is full. Our data indicate that in solutions with Cl^- content approaching that of sea water, the copper was fully corroded due to the high Cl^- concentration.

By comparing spectra for different concentration (Fig. 4) we conclude that strong complex formation of $CuCl_2$ on the copper surface occurs at high Cl^- concentration. We believe that the difference between seawater (Fig.4) and groundwater (Fig.2) is caused by the difference in Cl^- concentrations, pH value[13,14] and the presence of carbonate ion in groundwater solution. These factors are affecting the copper corrosion processes the most.

The pH value of the water solution influences the corrosion process. According to the Pourbaix diagram for copper at room temperature[15,16], Cl^- in small concentrations can form strong complexes with divalent copper at higher pH. The stability of divalent copper species, compared to monovalent, increases for pH higher than 8.5[3,13]. This effect appears to be particularly strong at pH=10 (see Fig. 5). The Cu 2p XA spectrum was measured from a copper film exposed to a 1.4 mM Cl^- solution in liquid cell for 1 hour. The pH value of the solution was adjusted to 10 by adding a small amount of sodium hydroxide NaOH. The data reveal almost fully corroded copper in this case.

It was suggested that the presence of carbonate ions may lead to a decreasing the amount of divalent copper, in accordance with previous observations[17]. Adeloju and Duan [18] suggest that the increased protectiveness is a consequence of pH buffering by HCO_3^-, which stabilizes the Cu_2O film rather than leads to the formation of basic cupric

carbonate species. In order to understand how corroded copper will respond to the carbonate treatment we added to the above described solution (1.4 mM Cl^- with pH 10.0) 1.1 mM HCO_3^-, which is exactly the same concentration as in the groundwater. A good example of a conflict between corrosion and reduction of copper corrosion rates are presented in Fig. 5. The Cu 2p XA spectrum displays sensitivity to the presence of carbonate ions. The monovalent copper signal is clearly observed in this spectrum, which indicates that in a solution already containing 1.4mM Cl^- with pH 10.0, the copper film was not corroded at all in the presence of 1.1 mM HCO_3^- (normal baking soda).

Our results are not surprising since the sodium sesquicarbonate (equal amount of Na_2CO_3 and $NaHCO_3$) treatment has been the standard chemical treatment used by antiquaries in order to clean cuprous chloride formed on copper surfaces[12,19]. There are three different treatments available to clean chloride contaminations: sodium sesquicarbonate, sodium carbonate and benzotriazole[19-21]. These three alternatives can remove cuprous chlorides, but these chemical techniques do not strip the corrosion layer. Although initially the sodium sesquicarbonate treatment seems to be ideal for the antiquaries, since they do not need to remove the outer green patina layers while the cuprous chloride is removed. The normal concentration for this chemical treatment is a 5% solution of sodium sesquicarbonate[21], which is higher then what we used for sodium bicarbonate.

Small amount of baking soda in the significantly strong solution, which immediately corrode copper surface, can prevent the corrosion process of copper in aquaeous environments. Understanding how copper will respond to carbonate treatment was of main interest during our investigation. Our suggestion was proven by in-situ analysis of liquid cells with different concentration of chloride and carbonate ions in de-

ionized water. Corrosion of copper has been observed in waters with high Cl^- concentration as well as with low Cl^- concentration but at high pH. The groundwater composition was considered as "non-corrosive" due to the presence of carbonate ions and near neutral pH value. By present experiments we also showed that the corrosion damage can be reduced if a small amount of carbonate is introduced into a solution.

Acknowledgements

We would like to thank Kaja Ollila and Hans Nilsson for making groundwater solution. This work was financially supported by the Swedish Nuclear Fuel and Waste Management Co. (SKB), by the Swedish Research Councill and Göran Gustafsson Foundation for Research in Natural Sciences and Medicine. The ALS work was supported by the Director, Office of Science, Office of Basic Energy Sciences, and Biosciences of the U.S. Department of Energy at Lawrence Berkeley National Laboratory under contract No. DE-AC02-05CH11231.

* - Corresponding author: Kristina Kvashnina, Uppsala University, Department of Physics, Box 530, 75121, Uppsala, Sweden, t. (+46)18-4713540, f. (+46)18-471-3524, Kristina.Kvashnina@fysik.uu.se

References

[1] Stuart Lyon, Nature, Vol. 407, 406-407, 2004
[2] J. Hernandez, P. Wrschka and G.S. Oehrlein, J. Electrochem. Soc. 148, G389-G397 (2001)
[3] I. Betova, B. Beverskog, M. Bojinov, P. Kinnunen, K. Makela, S.-O. Petersson, T. Saario, Electrochem. And Solid State Lett. 6 (4), B19-B22 (2003)
[4] H. Chan, C. Takoudis, M. Weaver, J. Phys.Chem. B 1999, 103, 357-365
[5] F. U. Renner, A. Stierle, H. Dosh, D.M. Kolb, T-L. Lee, J. Zegenhagen, Nature Vol 439, 707-709, 2006
[6] M. Stratmann and M. Rohwerder, Nature 410, 420 (2001)
[7] G. van der Laan, R.A.D. Pattrick, C.M.B. Henderson and D.J. Vaughan, J. Phys.Solids 53, 9, 1185-1190 (1992)
[8] G. van der Laan, C.Westra, C. Haas, G.A. Sawatzky, Phys.Rev. B 23, 4369 (1981)
[9] M. Grioni, J. B. Goedkoop, R. Schoorl, F. M. F. de Groot, and J. C. Fuggle, F. Schäfers and E. E. Koch, G. Rossi, J.–M. Esteva, and R. C. Karnatak, Phys. Rev. B 39, 1541–1545 (1989)
[10] T. Warwick, P.Heimann, D. Mossessian, W. McKinney, H. Padmore, Rev. Sci. Instrum. 66 (1995) 2037.
[11] R. J. GettensMineral Alteration Products on Ancient Metal Objects. In *Recent Advances in Conservation*, pp. 89-92. Butterworths, London, 1963
[12] Oddy, W. A., and M. J. Hughes. 1970. The Stabilization of Active Bronze and Iron Antiquities by the Use of Sodium Sesquicarbonate. *Studies in Conservation* 15:183-189.
[13]U. Bertocci, D.R. Turner, Encyclopedia of Electrochemistry of the Elements, Vol. II, p-p 383-497, 1974
[14] D. Thomans, R-H. Sun, J. Electrochem. Soc. 138, 3235, 1991
[15] M. Pourbaix, PhD Thesis, Unversite Libredes Bruxelles (1945), M. Pourbaix, 1966. *Atlas of Electrochemical Equilibria in Aqueous Solutions*. Pergamon Press, New York
[16] B. Beverskog, I. Puigdomenech, J. Electrochem. Soc., Vol 144, N10, 1997
[17] S.B. Ribotta, M.E. Folquer, J.R. Vilche, Corrosion 51 (1995) p. 682.
[18] S.B. Adeloju and Y.Y. Duan, Br. Corros. J., 29 (1994) p. 315.
[19] H. J. Plenderleith,, and A. E. A. Werner. 1971. *The Conservation of Antiquities and Works of Art*. Oxford University Press.
[20] H. J. Plenderleith, 1956. *The Conservation of Antiquities and Works of Art*. Oxford University Press

[21] T.D. Weisser, 1987. The Use of Sodium Carbonate as a Pre-Treatment for Difficult-to-Stabilize Bronzes. In *Recent Advances in the Conservation and Analysis of Artifacts,* edited by J. Black, pp. 105-108. Summers Schools Press, London.

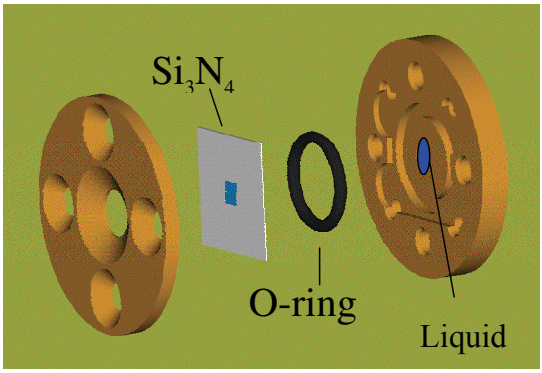

Fig. 1. Schematic drawing of liquid cell

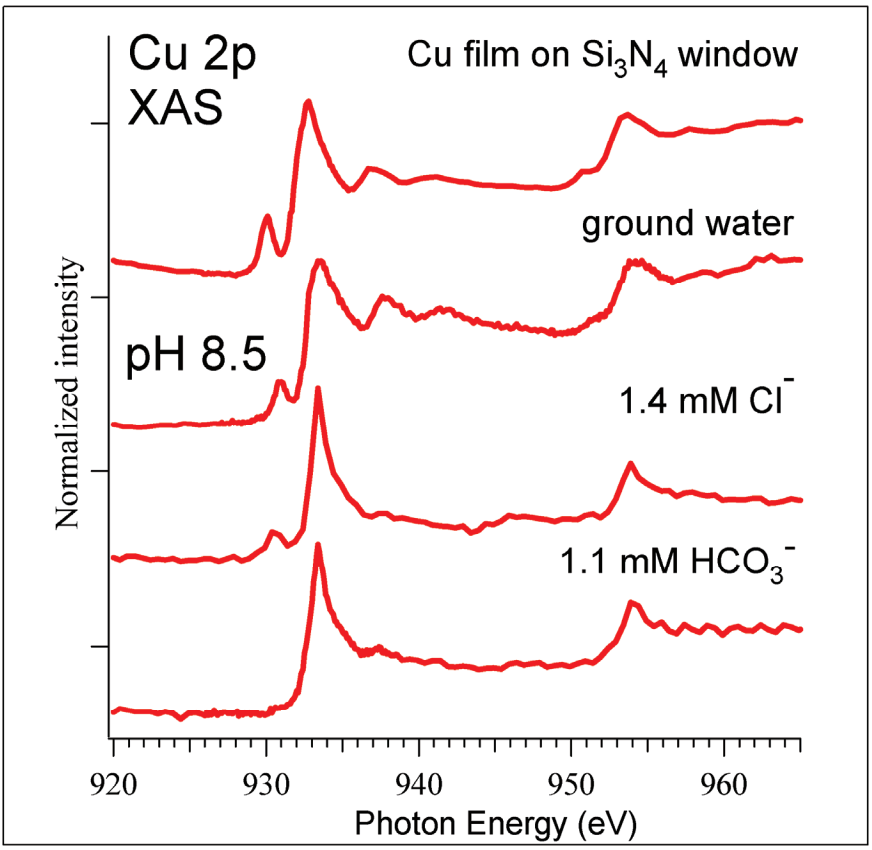

Fig. 2. Cu 2p X-ray absorption spectrum of the copper film deposited on the back side of the Si_3N_4 window before any contact with solutions and Cu 2p XA spectra of copper film in the liquid cell after 1 hour exposure to the synthetic ground water solution, the 1.4 mM Cl^- in ultra-pure deionized water (MQ) and the 1.1 mM HCO_3^- solution in MQ water. pH for all solution was adjusted to 8.5.

Fig. 3. 10mm thick copper slabs exposed to 1.5M Cl^- solution in a deionized water after 5 days.

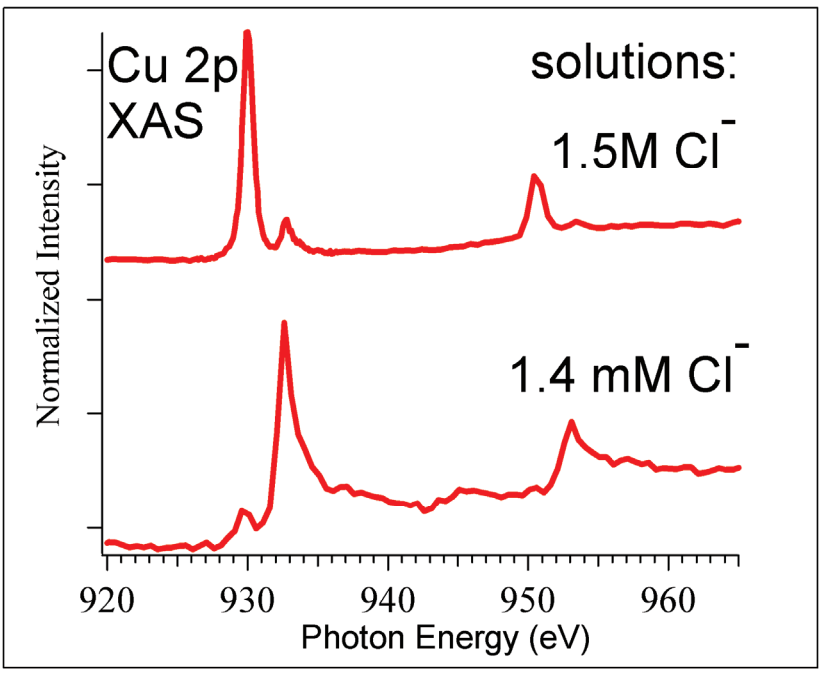

Fig. 4. Cu 2p x-ray absorption spectra of the copper film in the liquid cell after 1 hour exposure to 1.5M Cl^- and with 1.4 mM Cl^- solution in MQ water respectively.

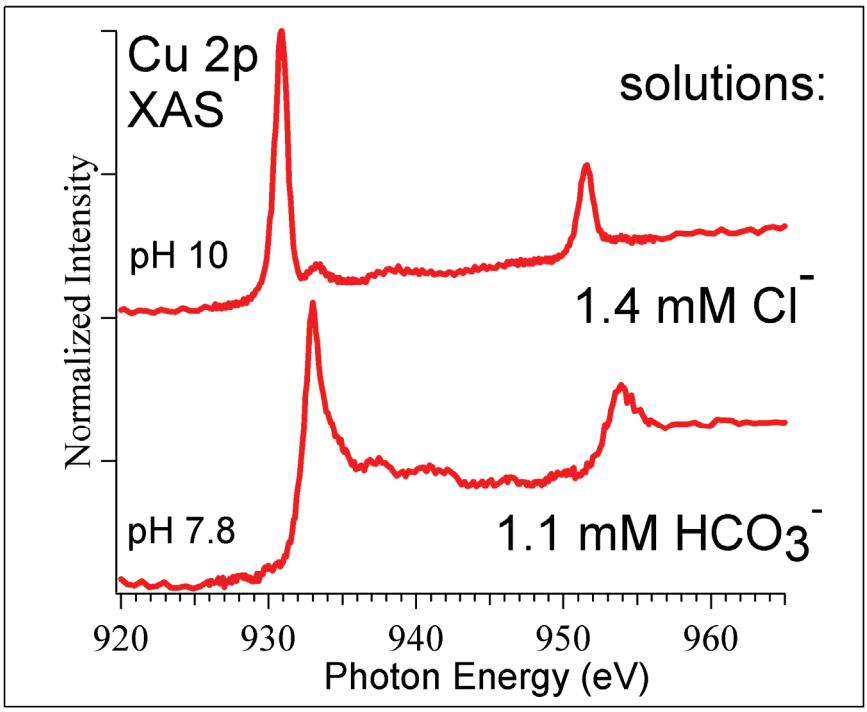

Fig. 5. Cu 2p X-ray absorption spectrum of the copper film (top) in the liquid cell exposed for 1 hour to the 1.4 mM Cl^- solution in MQ water and increased pH up to 10 by means of NaOH. Cu 2p X-ray absorption spectrum of the copper film (bottom) with the same exposure to the above described solution but with added 1.1 mM HCO_3^- ions.